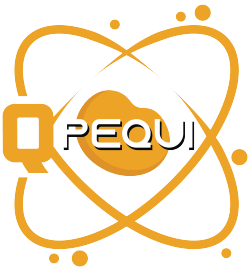

Federal University of Goiás

Institute of Physics

Quantum Pequi Group

Asymmetry and Entropy Production in Nonequilibrium Quantum Systems: The LMG Model under Dynamical Quantum Phase Transitions.

PhD in Physics

Andesson Brito Nascimento

Goiânia, February 2026

Brazil

"*O homem, guiado pelo medo, escolhe muitos refúgios, nas montanhas, nas florestas, nos bosques, nos mangueirais e nos templos.*

Mas estes não são refúgios seguros. Porque tomando este tipo de refúgio a pessoa não se liberta do sofrimento."

Dhammapada

"*À Francisca e João, Maria José e Henrique, meus avós.*"

Agradecimentos

Aos meus pais, Sandra e Antonio, que empregaram todo o esforço possível para que eu pudesse ter todas as condições de estudar, pensar e me desenvolver como cidadão. Ao meu irmão, Andrey, que dividiu a infância, adolescência e hoje divide essa vida acadêmica comigo. Amo vocês.

A todos os familiares que contribuíram na minha formação e que sempre me incentivaram e me apoiaram nessa trajetória. Aos meus avós, que construíram a base dessa família por meio de muito esforço e trabalho.

À Keity, minha companheira há 10 anos. Não é possível expressar o tamanho da sua contribuição para essa tese e para meu processo de doutoramento. Desde o dia em que nos conhecemos, você ouve eu falar do doutorado e sempre foi a maior incentivadora. Agradeço pelos dias de felicidade e de companheirismo, mas também agradeço pela paciência nos momentos mais difíceis desse processo. Só nós sabemos o quanto isso custou. Eu te amo! Que nossa vida seja cada dia mais feliz.

Ao meu orientador, Lucas Céleri, que aceitou me orientar em 2014, aceitou novamente em 2018, quando não pude dar andamento ao doutorado e, pela terceira vez, em 2021, para cumprir esta etapa acadêmica. Muito além da orientação, fica meu agradecimento pelas conversas sobre mundo, sobre vida acadêmica e pela disponibilidade e dedicação total aos seus alunos. Você contribuiu muito para meu crescimento pessoal e profissional.

Aos colegas de pós-graduação e do grupo QPequi, por todos os dias compartilhados nas salas de estudo, reuniões de grupo e fora delas. Nossas amizades fazem a pós-graduação mais leve e divertida. Em especial, aos amigos mais próximos, Pedro, Ronaldo, Gabriel, Débora e Marcelo que partilharam de muitos momentos bons e de muitos atropelos durante esse período. Quero ver todos nós doutores e felizes.

Aos membros da banca examinadora, pelas contribuições dadas, comentários e sugestões que ajudaram a aprimorar este trabalho.

À Universidade Federal de Goiás, em especial ao Programa de Pós-Graduação em Física (PPGF–UFG) e ao Instituto Federal Goiano, pelo suporte institucional e pelas condições oferecidas para a realização desta pesquisa no Brasil.

Por fim e tão importante quanto, a todas as professoras e professores, servidoras e servidores da educação que tive a oportunidade de encontrar durante meus 35 anos de formação. Desde a primeira vez que entrei em uma sala de aula essas pessoas contribuem para o que sou hoje. Valorizemos os profissionais da educação!

Abstract

The nonequilibrium dynamics of many-body quantum systems has attracted increasing attention due to the emergence of dynamical phenomena with no equilibrium counterpart, such as dynamical quantum phase transitions (DQPTs). In this thesis, we investigate the interplay between entropy production, symmetry, and dynamical criticality in isolated quantum systems driven far from equilibrium. We use the Lipkin–Meshkov–Glick (LMG) model as a paradigmatic platform, as it allows for an analysis of finite-size effects and symmetry sectors. Sudden quenches of the system parameters are considered, and dynamic criticality is identified through the Loschmidt echo and its associated rate function, as well as through a dynamical order parameter. Entropy production is quantified via a geometric approach based on the Bures angle, providing a lower bound to the irreversible entropy generated during the unitary dynamics, while asymmetry is characterized using measures associated with collective spin operators, enabling a dynamical analysis of this quantity during symmetry restoration induced by DQPTs. We show that the time-averaged entropy production displays clear signatures in the vicinity of the dynamical critical point, reflecting enhanced irreversibility induced by the nonequilibrium dynamics. In addition, we demonstrate that quantum asymmetry provides a robust indicator of DQPT, capturing the dynamical restoration of the underlying $\mathbb{Z}_2$ symmetry during the evolution. Finally, we show that the location of these signatures depend on the anisotropy parameter, highlighting its central role in dynamical critical behavior of the system.

Keywords: Dynamical Criticality; Entropy Production; Asymmetry.

Contents

List of Figures

List of Tables

Chapter 1

Introduction

The study of quantum systems driven far from equilibrium has revealed a variety of dynamical phenomena that are outside the scope of equilibrium statistical mechanics [1, 2]. In contrast to equilibrium phase transitions, which are characterised by non-analyticities in thermodynamic potentials, nonequilibrium dynamics does not admit a universal classification scheme. As a consequence, the identification of qualitatively distinct dynamical regimes remains an open and active problem.

In this context, sudden quenches in isolated quantum systems have emerged as a setting to investigate how complex dynamical regimes arise from unitary time evolution. Depending on the quench protocol and on the parameters of the system, the resulting dynamics may exhibit qualitatively distinct behaviours, suggesting the existence of different dynamical regimes separated by critical conditions.

Within this framework, dynamical quantum phase transitions (DQPTs) have emerged as an important framework to identify and analyse qualitative changes in nonequilibrium quantum dynamics. Unlike equilibrium phase transitions, DQPT are not defined through singularities in free energies, but instead through non-analytic features in time-dependent quantities, such as the Loschmidt echo and its associated rate function [1–3], also called type-II DQPT, or through abrupt changes in long-time dynamical properties characterised by dynamical order parameters [4–7], known as type-I DQPT. Since their introduction, DQPTs have been extensively studied both theoretically and experimentally [8–10], revealing connections between dynamical criticality, coherence, and symmetry in quantum systems.

An important question is to determine which physical quantities are capable of capturing these dynamical distinctions in a meaningful and robust way. In particular, it is natural to ask how changes in the dynamical regime are reflected in the way a quantum system explores its state space during time evolution, and whether such changes can be identified through quantities that probe global features of the evolving quantum state. This question constitutes the main motivation for the present work.

In our work, we investigate DQPT from two complementary perspectives. The first is based on nonequilibrium thermodynamics and focusses on entropy production as a measure of irreversibility. The second is based on symmetry considerations and explores the role of asymmetry as a quantitative indicator of how coherence and symmetry evolve dynamically. Although these two approaches originate from different conceptual frameworks, they both probe how the system spreads and reorganises in the space of quantum states under nonequilibrium dynamics.

Entropy production is a central concept in thermodynamics, whose positivity guarantees the irreversibility of physical processes, as established by the second law [11]. Originally formulated within classical thermodynamics, the notion of entropy production has been consistently extended to the quantum domain through tools from quantum information theory, allowing irreversible behaviour to be quantified even in isolated or strongly nonequilibrium quantum systems [12–14]. In this sense, entropy production provides a powerful framework for characterising nonequilibrium processes and their degree of irreversibility.

A particularly fruitful development in this direction has been the formulation of the entropy production in geometric terms. In [15], geometric concepts were introduced into thermodynamics by associating a metric structure with the space of thermodynamic states, enabling entropy variations to be related to distances between probability distributions. In the quantum regime, this geometric perspective naturally leads to the use of statistical distances between quantum states. The Wootters' length provides a geometric measure of the distance between pure states [16]. However, for mixed states, the Bures distance naturally arises as a generalization [17].

Based on these ideas, in [18, 19], it was shown that the Bures angle establishes a direct connection between the geometric separation of quantum states and entropy production, leading to lower bounds on irreversibility for arbitrarily far-from-equilibrium quantum evolutions. Within this framework, entropy production can be interpreted as a measure of how rapidly and how strongly the system departs from its corresponding equilibrium reference state in the space of quantum states.

This geometric formulation is particularly relevant in the context of DQPTs, since these transitions are intrinsically related to nonequilibrium dynamics. Since DQPTs are characterised by qualitative changes in system dynamics, entropy production provides a natural quantity to probe how dynamical criticality affects irreversibility and the exploration of the space of system's states during time evolution [1, 2].

Complementary to the thermodynamic perspective provided by entropy production, symmetry considerations play a fundamental role in the understanding of both equilibrium and nonequilibrium quantum phenomena. Symmetries impose

constraints on the dynamics of physical systems and are deeply connected to conservation laws and the structural properties of quantum states. In the quantum domain, symmetries are associated not only with invariance under transformations but also with the presence or absence of coherence between the eigenstates of the symmetry generators, establishing a direct link between the principles of symmetry and quantum information [20].

Within this framework, asymmetry provides a quantitative way to characterise how a quantum state departs from invariance under a given symmetry. In the context of resource theories, asymmetry is associated with coherence relative to a symmetry group [21, 22], and several measures have been proposed to quantify this property [23–26]. Such measures capture information beyond the expectation values of the symmetry generators, making them useful in the analysis of nonequilibrium quantum dynamics [20].

Recent studies of DQPT have highlighted that symmetry plays a central role in dynamical critical phenomena. The complementary notions of DQPT, types I [4, 27, 28] and Type-II [29–31], formulations are commonly employed in the literature to characterise dynamical critical behaviour, providing complementary perspectives on the same underlying phenomenon.

From this perspective, asymmetry measures offer a promising framework for probing dynamical criticality from the point of view of the structure of the quantum state. Since dynamical phase transitions are accompanied by qualitative changes in the way the system explores its Hilbert space and in the role played by symmetry-related sectors, asymmetry provides a natural quantity to investigate how coherence and symmetry properties evolve during nonequilibrium dynamics. This motivates the use of asymmetry as a diagnostic tool for dynamical quantum phase transitions, complementing thermodynamic indicators such as entropy production.

A paradigmatic system in which the interplay between dynamical criticality and symmetry can be explored is the Lipkin-Meshkov-Glick (LMG) model [32–34]. This fully connected spin model exhibits both permutation symmetry and a discrete $\mathbb{Z}_2$ symmetry [35, 36], and has long served as a model for studies of quantum phase transitions. More recently, it has been shown that the LMG model also displays clear signatures of dynamical quantum phase transitions under sudden quenches [1, 7, 8, 27, 37]. The dynamical restoration of $\mathbb{Z}_2$ symmetry plays a central role in this behaviour, making the model particularly suitable for a symmetry-based analysis.

In this work, we use the LMG model as a platform to investigate how DQPT manifest themselves through entropy production and asymmetry measures. Although our analysis is carried out for a specific model, the quantities employed are not model-dependent: entropy production and asymmetry are defined in general

terms and probe universal features of nonequilibrium quantum dynamics. As such, the insights obtained here are expected to be relevant beyond the particular system considered.

This thesis is organised as follows: in Chapter 2, we present a brief discussion of classical phase transitions and quantum phase transitions (QPT), aiming to establish the foundation for defining and understanding dynamical quantum phase transitions, discussed at the end of the chapter. Chapter 3 is devoted to entropy and entropy production. We introduce these concepts, starting from its classical definition and extending to the quantum definition via von Neumann entropy. Additionally, in this chapter, we discuss a key result for our work: the entropy production in an arbitrarily out-of-equilibrium quantum evolution.

In Chapter 4, we dedicate ourselves to the study of asymmetry as a framework for characterising the symmetry properties of quantum states. We begin by introducing symmetry transformations and their action on quantum systems, discussing the distinction between symmetry-invariant and symmetry-breaking states. Within this framework, asymmetry is interpreted as a manifestation of coherence with respect to a given symmetry group. We then present the asymmetry measure employed throughout this thesis, discussing its main properties and physical interpretation.

The Chapter 5 is dedicated to the presentation of the Lipkin–Meshkov–Glick (LMG) model, which serves as the central physical platform for the analysis carried out in this thesis. We introduce the Hamiltonian of the model and discuss its main features. Particular attention is paid to the symmetry properties of the model, including the permutation symmetry and the discrete $\mathbb{Z}_2$ symmetry, which play a crucial role in its equilibrium and nonequilibrium behaviour.

Within this framework, we review the occurrence of DQPTs in the LMG model. These transitions are characterised using two complementary approaches: type-II DQPTs, identified through non-analyticities in the Loschmidt echo and its associated rate function following a sudden quench, and type-I DQPTs, characterised by the behaviour of a dynamical order parameter defined as the long-time average of the collective magnetization.

In Chapter 6 we present and discuss the main results obtained in this work. This chapter is divided into two parts, each corresponding to one of the articles published during the development of this thesis [38, 39].

In Part I, we investigate the behavior of entropy production in the LMG model that undergoes a DQPT. To this end, we employ a geometric formulation of entropy production based on the Bures angle, which allows us to express a lower bound for entropy production in terms of a distance in the space of quantum states.

This approach enables a direct analysis of how dynamical criticality influences irreversibility and the rate at which the system departs from its reference equilibrium state.

Part II is devoted to the analysis of symmetry properties of the quantum state during the post-quench dynamics. In this part, we apply the asymmetry measures introduced in Chapter 4 to the LMG model, focussing on the generators associated with the rotation group. This choice is particularly relevant, as one of these generators is directly related to the $\mathbb{Z}_2$ symmetry that is dynamically restored at the DQPT.

Finally, Chapter 7 presents our conclusions. We summarise the main results obtained, discuss their physical implications, and outline possible directions for future research to extend the present analysis. The thesis concludes with the list of references used throughout this work.

Chapter 2

Dynamical Quantum Phase Transition

We begin our work with a discussion of phase transitions. The objective of this chapter is to start from the well-developed and extensively studied concept of phase transitions in classical systems, described in terms of the thermodynamic parameters of the system, and arrive at the definition of dynamical quantum phase transitions, which are formulated by analogy with classical transitions.

To achieve this, we will first provide a brief review of classical phase transitions, covering their main concepts. Next, we will discuss the idea of quantum phase transitions, which share similarities with classical transitions but are driven exclusively by quantum fluctuations. Finally, we will address dynamical quantum phase transitions, which, in essence, have a different nature from the first two, as they occur in systems evolving out of equilibrium.

Readers already familiar with the concept of classical and equilibrium quantum phase transitions may begin reading this work from section 2.3, if they so wish, without any loss of comprehension regarding the concept of DQPT, which is the central topic of this chapter.

2.1 Classical Phase Transition

The phenomenon of phase transition can be easily observed in nature. Almost no one has not noticed that an ice cube is melting when left on a surface exposed to a temperature above $0\,^{\circ}\mathrm{C}$. Similarly, one can observe the wax of a candle melting when heated by the flame and then solidifying again as it drips and cools.

We can think of the phase of a substance as the form in which it presents itself. Water is the most common example in our daily lives, as it can easily appear in three different forms: solid water (commonly called ice), liquid water, and gaseous water (water vapour). Moreover, we can transition between these phases by inducing certain changes in the system.

In a more pragmatic sense, the phase of a physical system can be characterised by its properties[1]. For example, water in its solid state exhibits certain characteristics that classify it as a specific physical state: the ability to resist compression, shear forces, and the inability to flow can be cited as defining traits of this substance in its solid form. However, liquid water, although it shares the ability to resist compression[2], does not offer significant resistance to shear forces, and has the ability to flow.

Another important example, which sometimes goes unnoticed in our daily lives, is the ferromagnetic-to-paramagnetic phase transition. Here, a given material can transition from a ferromagnetic phase, where the spins of the material are aligned and point in the same direction, thus ensuring a certain magnetization, to a paramagnetic phase, where the spins of the material point in various random directions, leading to the material's overall magnetization to vanish. This transition can also occur due to heating, just as in the case of water's phase transition. The reverse transition is also possible, and the technique behind it is widely used in magnet production. Certain paramagnetic materials can be turned into ferromagnetic materials by subjecting them to intense magnetic fields for a specific period.

Indeed, phases of matter can be characterised by their properties, and thus we can understand phase transitions as phenomena that drive a physical system from one state, in which it possesses certain properties associated with the structural ordering of the substance at that moment, to another with a different ordering, leading to a change in the system's physical properties. The transformation of ice into liquid water can be seen as a structural change in which water molecules, initially arranged in a crystalline structure with strong intermolecular bonds, transition to a different molecular organisation with weaker bonds, losing the structure it had in its solid form. This change can occur due, for example, to the injection of heat into the system or due to a variation in the pressure to which the substance is subjected.

Both the phase transitions of water and the transition of ferromagnetic materials are examples of classical phase transitions, which occur at finite temperatures and are driven by thermodynamic fluctuations. In the following subsections, we will discuss and classify classical phase transitions. Specifically, we will address the two main types: First-Order Phase Transitions and Continuous Phase Transitions.

[1] Namely compressibility, molar heat capacity, and molar potentials

[2] It does have compressibility, but its compressibility is very low compared to gases and is closer to that of solids; Many authors classify liquid water as "practically incompressible," and for this reason, we consider here that this phase resists compression.

2.1.1 First-Order Classical Phase Transition

To begin the discussion on classical phase transitions, let us introduce the concept of a phase diagram. Figure 2.1 presents the pressure-temperature (PT) phase diagram of water. In this diagram, the stable phases of water are represented by the regions separated by solid lines, which indicate the coexistence points between phases. A specific point on the diagram, such as the point i, represents the substance at a given pressure and temperature (p_i, T_i), corresponding to the phase associated with that pair (in the example shown in the figure, the liquid phase).

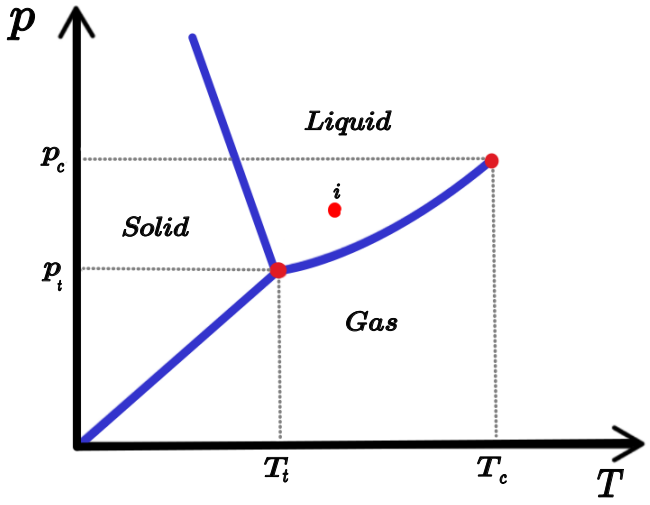

FIGURE 2.1: Phase diagram of water. Figure based on reference [40].

We can observe in Figure 2.1 that a phase transition can occur when the state point crosses a coexistence line. For example, if we take a portion of water at pressure p_i and temperature T_i and increase its temperature beyond the boiling point, the point moves from the liquid-phase region to the liquid-gas coexistence line and, after some time, transitions into the gas-phase region. A transition that occurs by crossing a coexistence line, like the one described above, is classified as a *First-Order Phase Transition* [40, 41].

The phase change discussed here can be analysed through the behaviour of the extremum of a thermodynamic potential as we cross the critical value of the parameter responsible for the transition (in this case, temperature). Taking the Gibbs free energy as the thermodynamic potential, the stable state of a physical system will be the one that minimises the Gibbs potential. Therefore, in a situation like the one illustrated in Figure 2.2, the system has a stable minimum, the global minimum, and another minimum where the system is not in its stable state, the local minimum, but which still has a nonzero probability of being visited due to thermodynamic fluctuations.

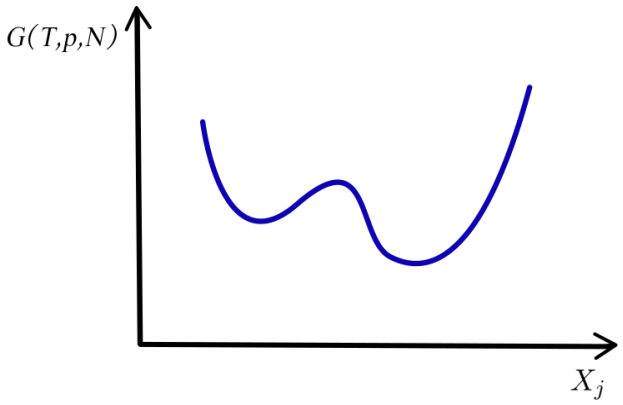

FIGURE 2.2: Gibbs potential as a function of an extensive parameter X_j of the system. Figure based on reference [41].

Each minimum is associated with a value of the property X_j, which represents any extensive parameter of the system, in this case, the volume. Notice that the volume corresponding to the stable phase of the substance, which it will assume in its equilibrium state, corresponds to the minimum on the right in the graph. Therefore, in equilibrium, the substance will have a high molar volume or, equivalently, a low density.

As we vary the temperature, the shape of the Gibbs potential changes, shifting both the local and the global minima. Figure 2.3 illustrates the situation in which the minima invert.

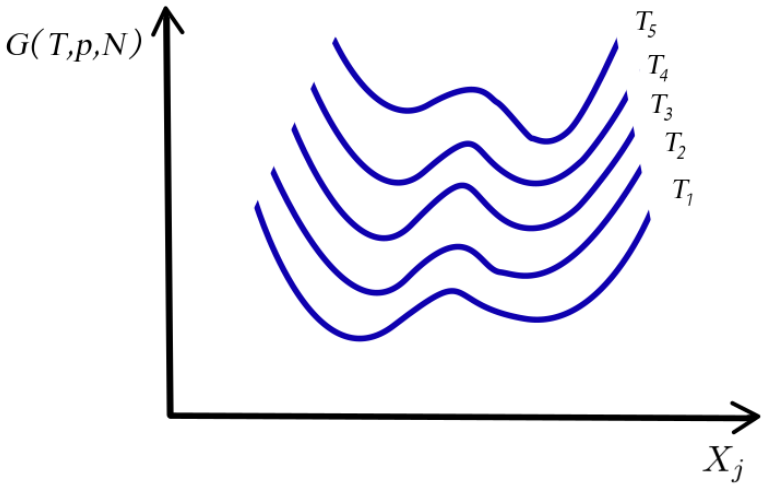

FIGURE 2.3: Gibbs potentials as functions of an extensive parameter X_j of the system for different temperatures. Figure based on reference [41].

Temperature variation affects the stability of the physical state. Note that as we decrease the temperature, moving from T_5 to T_1, the system transitions from

a stable state, where the global minimum was on the right (with a larger molar volume), to a state where stability is reached for a smaller molar volume, with the global minimum now on the left. Also, observe that at T_4, the minima are equal, which means that at this temperature the system does not have a unique value for the extensive parameter corresponding to the stable phase. This marks the phase transition temperature between the states.

For example, in water condensation, the initial stable state—the gaseous phase—has a larger molar volume, which corresponds to the minimum on the right for T_5 in Figure 2.3. As the temperature decreases, a slight reduction in the molar volume of the equilibrium phase occurs, which can be interpreted as a thermal contraction of the substance.

When the transition temperature T_4 is reached, both minima are equivalent, which means that the substance remains stable at both higher and lower molar volume values. In this situation, we have a coexistence of phases, which corresponds to a point on the liquid-gas coexistence line in the diagram shown in Figure 2.1. At this temperature, the system undergoes a First-Order Phase Transition. For temperatures lower than T_4, the system inverts the minimum values, making the most stable state the one with lower molar volume and higher density, corresponding to liquid water.

It is evident that the molar volume is discontinuous at the transition, which is directly associated with the non-analytic points in the thermodynamic potential under consideration in first-order phase transitions. We can take this as a characteristic of classical first-order phase transitions: *In first-order phase transitions, thermodynamic potentials are non-analytic, causing a discontinuity in their first derivatives with respect to intensive parameters* [41].

Mathematically, the minimum of the molar Gibbs free energy $g = g(T, p)$, which indicates the stable phase of the substance in terms of temperature, is given by the lower surface of the envelope shown in Figure 2.4.

Notice that in Figure 2.4, the Gibbs potentials for the three phases are plotted as functions of temperature. However, the minima of these potentials, which define the most stable phase, depend on the system's temperature. In region (I), the minimum corresponds to the potential associated with the solid phase. In region (II), at higher temperatures, the minimum corresponds to the Gibbs potential of the liquid phase. If we further increase the temperature, we reach the region (III), where the minimum corresponds to the potential of the gas phase. Therefore, the effective Gibbs potential of the substance, shown in Figure 2.5, has two non-analytic points corresponding to the two phase transitions the system can undergo [41].

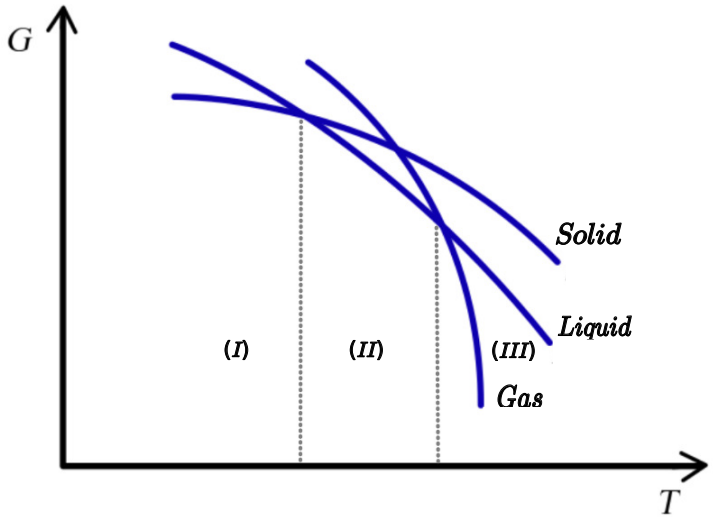

FIGURE 2.4: Representation of the Gibbs potentials of the three phases (solid, liquid, and gas) as a function of temperature. Figure based on reference [41].

We can analyse the consequences of this non-analyticity by considering the differential form of the molar Gibbs potential [42]:

$$dg = -sdT + vdp, \tag{2.1}$$

where s is the molar entropy and v is the molar volume:

$$\left(\frac{\partial g}{\partial T}\right)_p = -s \quad ; \quad \left(\frac{\partial g}{\partial P}\right)_T = v. \tag{2.2}$$

Since at the transition temperatures, the effective Gibbs potential exhibits non-analyticities, equations (2.2) show that the molar entropy s and molar volume v undergo abrupt changes when the system transitions from one state to another, becoming discontinuous at the transition points. These discontinuities in the first derivatives of the Gibbs potential (which can be extended to all thermodynamic potentials), caused by the non-analyticities of the potential at phase transition points, characterise first-order classical phase transitions.

The presence of these discontinuities results in a finite difference between the entropy and molar volume values of the phases at the transition point [42]:

$$\Delta s \equiv s_2 - s_1 = -\frac{\partial(\Delta g)}{\partial T} > 0 \tag{2.3}$$

$$\Delta v \equiv v_2 - v_1 = \frac{\partial(\Delta g)}{\partial p} > 0 \tag{2.4}$$

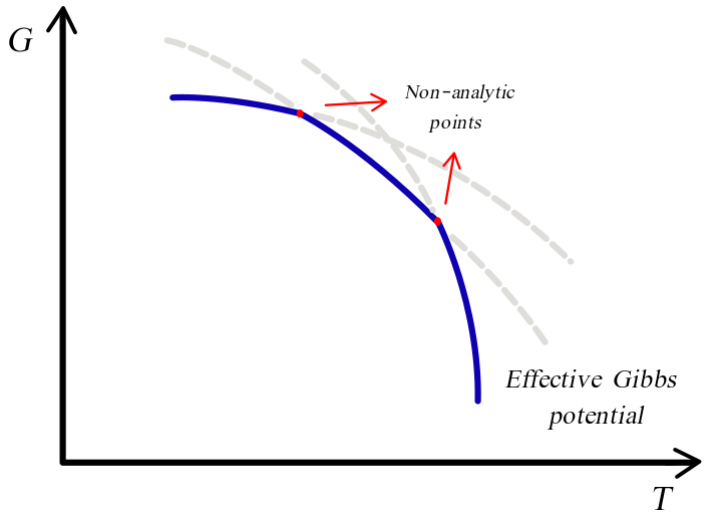

FIGURE 2.5: Lower envelope of the Gibbs potentials. Figure based on reference [41].

This characteristic will be further explored when we define the *Order Parameter*.

2.1.2 Continuous Classical Phase Transition

Continuing our discussion, we begin to analyse continuous phase transitions from the perspective of the Gibbs free energy behaviour of the system, as we did in the previous section.

Figure 2.6 presents a segment of a phase coexistence curve in the PT diagram. We can observe the change in the minima of the Gibbs free energy, as discussed in Section 2.1.1, when crossing the curve, leading to discontinuity in the system's extensive parameters, characterising a first-order phase transition.

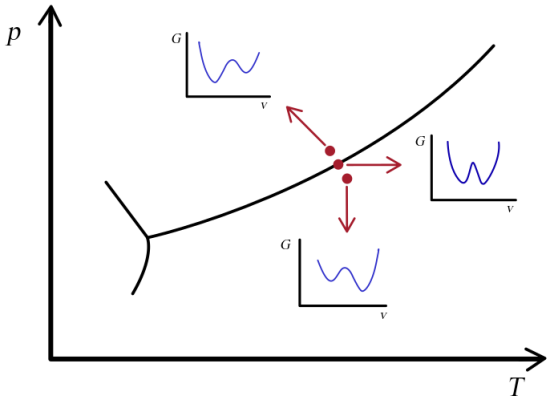

FIGURE 2.6: Inversion of the global minimum of the Gibbs potential when crossing the critical line. Figure based on reference [41].

We might ask what happens to the shape of the Gibbs free energy as we move towards the end of the critical line in the phase diagram. In other words, what happens to the competition between the global minima of the Gibbs free energy as we move from point A to point D in Figure 2.7?

Figure 2.7 shows the behaviour of G as we move along the coexistence line until we reach the point D, known as the *critical point*. The Gibbs potential changes its behaviour, transitioning from having two competing minima separated by a barrier (point A), indicating phase coexistence during the transition, to having a single minimum (point D), represented by the curve at temperature T_D [41].

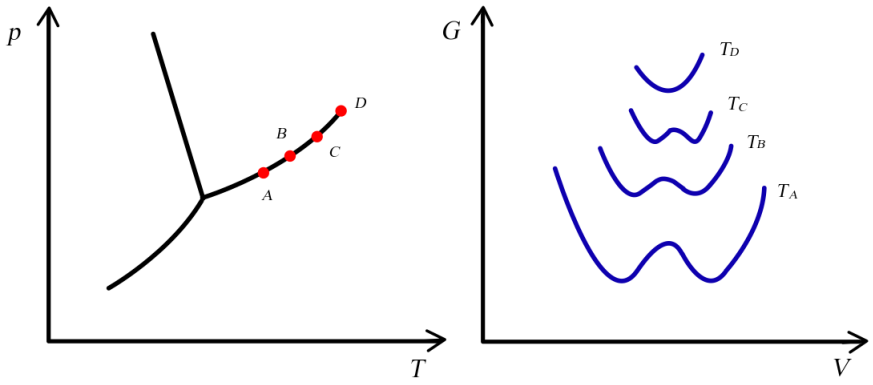

FIGURE 2.7: (Left) Points along the liquid-gas coexistence line. (Right) Gibbs potential shape for each point shown in the left graph. Figure based on reference [41].

In terms of the first derivatives of the potential, as we approach the critical point, the differences given in equations (2.3) and (2.4) decrease, both approaching zero at the critical point. That is, when the phase transition occurs beyond this point, we no longer observe discontinuities in the external parameters. For this reason, transitions occurring in this region of the phase diagram are classified as *continuous phase transitions*.

Unlike the abrupt and discontinuous changes observed in first-order transitions, continuous transitions are characterised by smooth and gradual changes in system properties as an external condition, such as temperature or pressure, is varied beyond the critical transition point.

We can again consider the example of the liquid-gas transition of water. If the system is at a temperature or pressure higher than the critical values[3], a smooth phase transition occurs, where the coexistence between the liquid and gas phases is not observed at any specific moment of the transition. The molar volume of the substance (and its density) does not undergo an abrupt change, making it impossible to diagnose the transition through these quantities.

[3]For water: $T_c \approx 650K$ and $p_c \approx 22MPa$ [40]

In the PT phase diagram, as shown in Figure 2.1, the continuous transition occurs without crossing the phase coexistence line. Instead, there is a critical region where the system's properties change gradually. Near the critical point, interesting phenomena are observed, such as the divergence of *generalized susceptibilities* (specific heats, compressibilities, magnetic susceptibilities, etc.), which are related to the system's response to small perturbations in its thermodynamic variables (temperature and pressure, in the case of the Gibbs potential) [41]. These divergences are directly associated with failures in the stability criteria of the thermodynamic potential.

To better understand this, we examine Figure 2.8, which shows the behaviour of the Gibbs free energy as we move beyond the critical region, projected onto the phase coexistence curve. In addition to the convergence of the minima into a single one, we can observe the flattening of the potential minimum near the transition criticality. This flattening corresponds to a failure in the stability criteria [41], which can be expressed as:

$$\begin{aligned} &\left(\frac{\partial^2 g}{\partial T^2}\right)_p < 0 \quad ; \quad \left(\frac{\partial^2 g}{\partial p^2}\right)_T < 0 \\ &\left(\frac{\partial^2 g}{\partial T^2}\right)_p \left(\frac{\partial^2 g}{\partial p^2}\right)_T - \left(\frac{\partial^2 g}{\partial T \partial p}\right)^2 > 0 \end{aligned} \tag{2.5}$$

These relations reflect the concavity of the Gibbs potential and, consequently, the stability of the system.

The flattening observed in Figure 2.8 represents a failure of these requirements. In fact, all three stability criteria fail simultaneously, causing α, κ_T, and c_p, which are associated with the second derivatives of the thermodynamic potential[4] to diverge simultaneously near the critical point [41]. For this reason, in some literature, this transition is referred to as a *second-order phase transition.*

Once again using the water transition as an example, when a phase transition is imposed near T_c and p_c, we observe an opalescence effect (a phenomenon that gives fluids a milky appearance). This effect results from large fluctuations in the molar volume of the substance (and its density), leading to an increased absorption of incident light. This effect disappears when the system is taken just a few Kelvins above or below the critical temperature T_c [41].

[4]Considering the Gibbs potential: $c_p = -T\left(\frac{\partial^2 g}{\partial T^2}\right)_p$, $\alpha = \frac{1}{V}\left(\frac{\partial^2 g}{\partial T \partial p}\right)$, and $\kappa_T = -\frac{1}{V}\left(\frac{\partial^2 g}{\partial p^2}\right)_T$

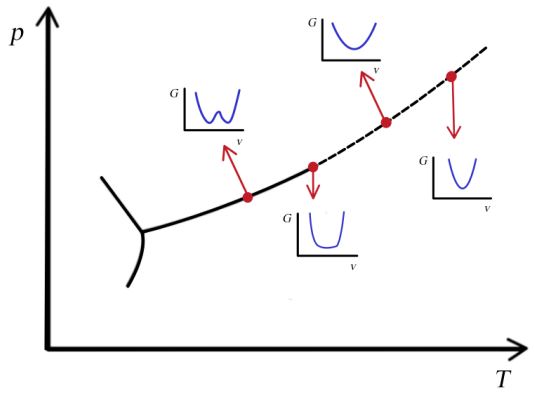

FIGURE 2.8: Behaviour of the Gibbs potential beyond a continuous transition. Figure based on reference [41].

2.1.3 Landau's theory of phase transition

The introduction of the concept of *order parameter*, proposed by Lev Landau in 1937, marked a significant advance in the study of phase transitions. Essentially, Landau suggested analysing critical transitions by expanding the free energy of the system in powers of a parameter, the order parameter, around the critical point of the system.

This parameter can take nonzero values in one phase (the ordered phase, where the system's symmetry is broken) and zero values in another (the disordered phase, where the symmetry is preserved) [40]. The order parameter of a transition is directly related to the specific system under consideration. Table 2.1 presents some examples of critical transitions and their corresponding order parameters.

System	Order Parameter	Symmetry Broken
Ferromagnet	Magnetization	Rotational Invariance and time reversal
Antiferromagnet	Staggered magnetization	Rotational Invariance and time reversal
Coexisting liquid-gas	Density difference	Spatial homogeneity
Superfluid	Condensate wave function	Global gauge invariance

TABLE 2.1: Order Parameters and Symmetry Breaking in Different Systems. Table based on reference [42].

Two order parameters from the table are particularly noteworthy: the density difference for the liquid-gas transition and the magnetization for the transition in a ferromagnetic system.

Starting with the liquid-gas transition, in Section 2.1.1 – equations (2.3) and (2.4) – we associated the discontinuity in both entropy and molar volume with first-order phase transitions, which occur when crossing the phase coexistence line. Thus, in

this type of transition, the differences Δs, Δv, and consequently $\Delta\rho$ (the density difference between phases) take finite values. Later, in Section 2.1.2, we discussed how these differences vanish as we move along the coexistence curve toward the critical point.

This behaviour can be interpreted within Landau's theory of continuous phase transitions. The density difference between phases, defined as:

$$\Delta\rho = \rho_l - \rho_g, \tag{2.6}$$

is a natural parameter to describe the liquid-gas transition [40]. For temperatures below the critical temperature ($T < T_c$), the liquid and gas phases have different densities, leading to a nonzero $\Delta\rho$. However, at the critical point ($T = T_c$), the distinction between phases disappears and the density difference vanishes continuously, characterising a continuous phase transition.

Thus, the density difference between phases serves as an order parameter for the liquid-gas transition, since it distinguishes the liquid phase from the gas phase and varies continuously until it vanishes at the critical point. This behaviour reflects the smooth nature of continuous phase transitions.

Another notable order parameter is magnetisation in ferromagnetic systems in the absence of an external field [40]. Below a critical temperature T_c, the magnetization takes nonzero values, indicating a phase in which the material's spins are predominantly aligned in the same direction—an ordered phase in which the rotational symmetry of the system is broken. As the temperature increases, thermal fluctuations become stronger, progressively reducing the order and thus the magnetization. At $T = T_c$, the magnetization vanishes, marking the transition to a disordered phase where rotational symmetry is restored.

Next, we explore Landau's mathematical description. Taking into account an order parameter γ, we expand the Gibbs free energy around the critical point as [40]:

$$g(T,p;\gamma) = g_0(T,P)+g_1(T,p)\gamma+g_2(T,p)\gamma^2+g_3(T,p)\gamma^3+g_4(T,p)\gamma^4+\dots. \tag{2.7}$$

Since we assume analyticity near the critical point and that γ remains small due to the continuity of the transition [43], higher-order terms beyond the fourth power can be neglected.

The equilibrium value of γ is found by minimising $g(T,p;\gamma)$:

$$\frac{\partial g}{\partial\gamma}(T,p;\gamma) = g_1(T,p) + 2g_2(T,p)\gamma + 3g_3(T,p)\gamma^2 + 4g_4(T,p)\gamma^3 = 0. \tag{2.8}$$

which leads to:

$$g_1(T,p) + \gamma(2g_2(T,p) + 3g_3(T,p)\gamma + 4g_4(T,p)\gamma^2) = 0. \tag{2.9}$$

Since the coefficients g_n are arbitrary functions of T and p, the coefficient $g_1(T,p)$ must necessarily be zero for equation (2.9) to have solutions. Setting $g_1(T,p) = 0$, we obtain two possible solutions: $\gamma = 0$ and $\gamma \neq 0$.

Let us analyse the consequences of these solutions. The minimisation condition for $g(T,p;\gamma)$ is given by:

$$\frac{\partial^2 g}{\partial \gamma^2}(T,p;\gamma) = 2g_2(T,p) + 6g_3(T,p)\gamma + 12g_4(T,p)\gamma^2 > 0. \tag{2.10}$$

For the solution $\gamma = 0$, associated with the disordered phase, equation (2.10) produces the condition $2g_2(T,p) > 0$, which is valid only if $g_2(T,p)$ is positive.

On the other hand, for the solution $\gamma \neq 0$, associated with the ordered phase, neglecting the coefficient $g_4(T,p)$ due to the smallness of γ near the critical region, we obtain from (2.9):

$$\begin{aligned} 2g_2(T,p) + 3g_3(T,p)\gamma &= 0, \\ \gamma &= -\frac{2g_2(T,p)}{3g_3(T,p)}. \end{aligned} \tag{2.11}$$

Substituting (2.11) into (2.10), we get:

$$\frac{\partial^2 g}{\partial \gamma^2}(T,p;\gamma) = -2g_2(T,p) > 0. \tag{2.12}$$

Thus, for (2.12) to hold, which means that $g(T,p;\gamma)$ is a minimum, $g_2(T,p)$ must be negative when choosing the solution $\gamma \neq 0$.

This implies that the function $g_2(T,p)$ changes sign as the system passes through the critical temperature T_c, being positive for $T > T_c$ and negative for $T < T_c$. The function $g_2(T,p)$ is assumed to be nonsingular at the critical point [41].

Landau proposed expressing g_2 in the form: $g_2(T,p) = c(T - T_c)$, where c is a constant. Note that this choice preserves the behaviour of $g_2(T,p)$ as we cross the critical temperature.

With this, we can rewrite the expansion given by (2.7), already considering $g_1(T,p) = 0$:

$$g(T,p;\gamma) = g_0(T,P) + c(T - T_c)\gamma^2 + g_3(T,p)\gamma^3 + g_4(T,p)\gamma^4, \tag{2.13}$$

which, at the critical point, takes the form:

$$g_c(T_c, p; \gamma) = g_0(T_c, P) + g_3(T_c, p)\gamma^3 + g_4(T_c, p)\gamma^4, \tag{2.14}$$

thus, the minimisation condition, considering equation (2.14), becomes:

$$\frac{\partial^2 g_c}{\partial \gamma^2}(T_c, p; \gamma) = 6g_3(T_c, p)\gamma + 12g_4(T_c, p)\gamma^2. \tag{2.15}$$

From (2.15), we conclude that if $g_3(T_c, p) = 0$, in order to satisfy the minimum condition $\frac{\partial^2 g_c}{\partial \gamma^2}(T_c, p; \gamma) > 0$, we must have $g_4(T_c, p) > 0$. If this value is positive at the critical point, it must remain so in the surrounding region.

We therefore have almost all the solutions for the coefficients of equation (2.7). We are missing only the solution for the coefficient $g_3(T, p)$. Here, we have two possibilities: $g_3(T, p) \neq 0$ or $g_3(T, p) = 0$. We will consider the latter, due to the interest in associating the description made here with the discussion in the previous sections.

Once the choice $g_3(T, p) = 0$ is made, with the remaining coefficients obtained and considering Landau's assumption that the coefficient $g_4(T, p)$ is practically constant near the critical point, we can write the expansion of the Gibbs free energy around the critical point of the system as:

$$g(T, p; \gamma) = g_0(T, p) + c(T - T_c)\gamma^2 + g_4\gamma^4. \tag{2.16}$$

Let us note that equation (2.16) can exhibit two distinct behaviours, depending on the sign of the coefficient accompanying the term γ^2. For $c(T - T_c) > 0$, equivalent to $T > T_c$, we have the behaviour shown on the left in Figure 2.9, where the Gibbs potential has only one minimum. On the other hand, when $c(T - T_c) < 0$, equivalent to $T < T_c$, the Gibbs potential develops a bifurcation of the minima, as shown on the right in Figure 2.9. The reader may recall these behaviours from the discussions on first-order and continuous transitions presented in the previous sections. Landau's theory recovers the results discussed there, as well as the characteristic continuity of the first derivatives of the potential with respect to the intensive parameters and the discontinuity of the second derivatives.

For example, calculate the molar entropy s and the specific heat at constant pressure c_p. These are given by:

$$s = -\frac{\partial g}{\partial T} \quad ; \quad c_p = -T\left(\frac{\partial^2 g}{\partial T^2}\right)_p. \tag{2.17}$$

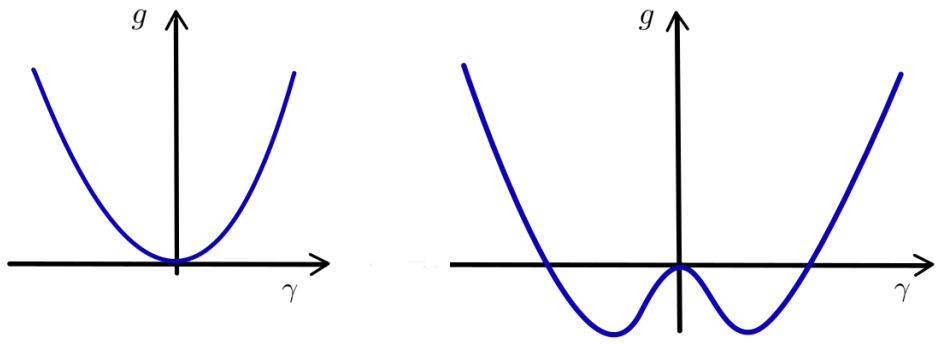

FIGURE 2.9: Behaviour of the expansion of g in powers of γ around the critical point. Figures based on references [40, 41].

Thus, considering equation (2.16) near the critical point and neglecting fourth-order terms, the molar entropy is given by:

$$s(T,p) = s_0(T,p) - c\gamma^2, \tag{2.18}$$

where $s_0 = -\frac{\partial g_0(T,p)}{\partial T}$. To analyse the behaviour of $s(T,p)$, let us express it in terms of temperature.

Applying the renormalisation condition in terms of γ to equation (2.16):

$$\frac{\partial g(T,p;\gamma)}{\partial \gamma} = 2c(T-T_c)\gamma + 4g_4\gamma^3 = 0 \tag{2.19}$$

we obtain two solutions:

$$\gamma^2 = \frac{-c(T-T_c)}{2g_4} \tag{2.20}$$

and

$$\gamma = 0. \tag{2.21}$$

Recalling that the order parameter behaves differently in each phase, we can state that the behaviour given by (2.21) is associated with the phase where $T > T_c$. Therefore, in this regime, from (2.18), we have:

$$s(T,p) = s_0(T,p). \tag{2.22}$$

On the other hand, for the regime $T < T_c$, the valid solution is the one associated with a nonzero γ. In this case, substituting (2.20) into (2.18), we obtain:

$$s(T,p) = s_0 + \frac{c^2(T-T_c)}{2g_4} \tag{2.23}$$

The behaviour of $s(T, p)$ is shown in Figure 2.10 (left). Notice that at the critical point, the function $s(T, P)$ remains continuous, since for $T = T_c$, equation (2.23) reduces to (2.22).

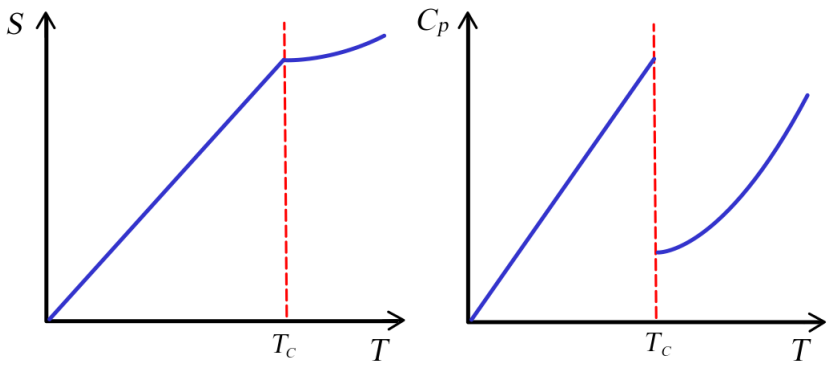

FIGURE 2.10: Continuity of entropy and discontinuity of specific heat at the critical point T_c. Figure based on reference [44].

The specific heat for each phase can be obtained directly from equations (2.22) and (2.23), considering that $c_p = -T\left(\frac{\partial^2 g}{\partial T^2}\right)_p = T\left(\frac{\partial s}{\partial T}\right)_p$.

Thus, in the disordered phase ($T > T_c$), we have $c_p(T) = c_{p0}$. Meanwhile, in the ordered phase ($T < T_c$), we obtain:

$$c_p(T) = c_{p0} + T\frac{c^2}{2g_4} \tag{2.24}$$

Unlike molar entropy, this function exhibits a discontinuity at the critical point $T = T_c$, as represented in Figure 2.10.

In addition to the specific heat at constant pressure, the specific heat at constant volume c_v and other generalised susceptibilities also exhibit discontinuities, which characterise continuous phase transitions [43].

2.1.4 Critical exponent, universality, correlation length

The definition of the order parameter, combined with the fact that various susceptibilities diverge at the critical point, motivates the definition of a set of *critical exponents*, which describe the behaviour of these quantities in critical regions.

We have a set of four fundamental critical exponents that can be defined for the critical region $|T - T_c| \to 0$ and $h \to 0$ (for the case of magnetic systems), where h is the external magnetic field. Let us briefly discuss each of these exponents. For a more detailed treatment, we refer to [41–43, 45].

Critical exponent α

This exponent is associated with the molar heat capacity, C[5], which is a quantity that diverges at the critical point, just like the specific heat discussed in the previous section. We can express the dependence of the singular part of the heat capacity[6] as:

$$C \sim (T - T_c)^{-\alpha}. \tag{2.25}$$

Critical exponent γ

The γ exponent is associated with generalised susceptibilities: $\kappa_T = \left(\frac{\partial v}{\partial p}\right)_T$, compressibility for fluids and $\chi_T = \mu_0 \left(\frac{\partial I}{\partial h}\right)_T$, magnetic susceptibility of the system, for magnetic systems, where I is the system's magnetic moment. Similarly, the singular part of these quantities follows:

$$\kappa_T \quad \text{or} \quad \chi_T \sim (T - T_c)^{-\gamma}. \tag{2.26}$$

Critical exponent β

The β exponent is associated with the behaviour of the order parameter along the coexistence curve. Considering the molar volume difference Δv for fluids and the magnetization I for magnetic systems, we can express the temperature dependence as:

$$\Delta v \quad \text{or} \quad I \sim (T - T_c)^{\beta}. \tag{2.27}$$

Critical exponent δ

The critical exponent δ is associated with the relationship between the order parameter and its corresponding intensive parameter along the critical isotherm ($T = T_c$). For example, for the order parameter given by the magnetic moment I, the intensive parameter associated with the divergence is the applied magnetic field h, leading to:

$$I \sim h^{-\frac{1}{\delta}}. \tag{2.28}$$

[5]There are two heat capacities: for fluids, we have $C_v = T\left(\frac{\partial s}{\partial T}\right)_v$, and for magnetic systems, $C_h = T\left(\frac{\partial s}{\partial T}\right)_h$. However, both behave similarly near the critical point, so we will simplify the notation by adopting C as the heat capacity.

[6]As in the case discussed in the previous section, it is possible to write the heat capacity as $C = C_0 + C_1(T - T_c)^{Exp}$, where the second term is responsible for the divergence of this quantity at the critical temperature and is called the singular part.

For the order parameter given by the difference in the molar volume Δv, the associated intensive parameter is the pressure p:

$$\Delta v \sim (p - p_c)^{-\frac{1}{\delta}}. \tag{2.29}$$

From Landau's theory, using mean-field theory[7], we obtain the following values: $\alpha = 0$, $\gamma = 1$, $\beta = \frac{1}{2}$, and $\delta = 3$ [42, 43].

Correlation Length and Critical Exponent ν

Unlike the exponents α, β, γ and δ, previously defined in terms of thermodynamic quantities, the exponent ν requires concepts derived from statistical physics for its definition, specifically the idea of fluctuation, since it is associated with the divergence of the system's correlation length.

The correlation length ξ is a measure of the range of correlations in a system. In other words, we can understand the correlation length as the distance over which fluctuations in a physical quantity in one part of the system influence another part of the same system [46].

Mathematically, the correlation length ξ is often defined in terms of the correlation function $G(\mathbf{x}, \mathbf{y}) = \langle \phi(\mathbf{x})\phi(\mathbf{y}) \rangle - \langle \phi(\mathbf{x}) \rangle \langle \phi(\mathbf{y}) \rangle$, which describes the correlation between the values of a physical variable ϕ at two points separated by a distance $r = |x - y|$. For $r \gg \xi$, the correlation function typically decays exponentially:

$$G(r) \sim e^{-r/\xi}. \tag{2.30}$$

However, near the system's criticality, the correlation length diverges [42], indicating that the correlations extend throughout the system. This suggests that critical phenomena involve the system as a whole, meaning that fluctuations are no longer confined to a limited region.

As with previous divergences, we can associate a critical exponent ν with the behaviour of the correlation length's divergence in terms of temperature T near the critical temperature T_c:

$$\xi \sim |T - T_c|^{-\nu}. \tag{2.31}$$

From Landau's theory, we obtain $\nu = \frac{1}{2}$ [42].

[7] Mean-field theory is an approximation that replaces local interactions between particles with an effective mean field, simplifying system analysis by disregarding fluctuations. For example, in the case of magnetic interactions, instead of considering the influence of each neighbouring spin individually, it is assumed that each spin experiences an average field generated by the others. We will not further dive into this topic, but we refer to [41, 43, 45] for more details.

Universality	d	n	α	β	γ	δ	ν
Mean Field	all	all	0	$1/2$	1	3	$1/2$
Ising	2	1	0	$1/8$	$7/4$	15	1
Ising	3	1	$0.110(5)$	$0.325(2)$	$1.241(2)$		$0.630(2)$
XY	3	2	$-0.007(6)$	$0.3455(20)$	$1.316(3)$		$0.669(2)$
Heisenberg	3	3	$-0.115(9)$	$0.3645(25)$	$1.386(4)$		$0.705(3)$

TABLE 2.2: Table of critical exponents for different universality classes. d is the system's dimensionality, n is the dimensionality of the order parameter, and α, β, γ, δ, and ν are the critical exponents defined in section 2.1.4. Table adapted from [44].

It should be noted that the critical exponent values obtained from Landau's theory, through mean-field theory, do not match the experimental observations. However, this theory was fundamental in understanding phase transitions, introducing concepts such as the order parameter and the expansion of the free energy, and laying the foundation for more sophisticated approaches.[8]

Universality

The divergence of the correlation length leads us to an interesting scenario. The fact that large regions become correlated implies that details related to the atomic structure of the material are no longer relevant. As a result, long-range correlations dominate the effects in the critical region [41].

One consequence of this is that the critical exponents of different systems assume the same numerical value, with these systems exhibiting the same behaviour in the critical region, near the phase transition. In other words, regardless of the microscopic characteristics of the system, the critical behaviours of systems that share the same exponents are similar. This concept is known as *universality*, and systems that possess the same set of critical exponents are said to belong to the same *universality class*.

The universality class of a system depends only on a few macroscopic characteristics, such as the dimensionality of the system (d), the symmetry of the order parameter, and the range of interactions [41, 42].

In Table 2.2, we can see some universality classes. It is worth noting that the name of each class is assigned according to the simplest system that is attached to it.

[8] The renormalisation group theory (RG), for instance, improves the accuracy of critical exponent calculations, yielding values closer to experimental results. We will not discuss this theory in this text, but we refer to [46] for a better understanding of it.

The mathematical foundation for the development of the universality concept, renormalisation group theory, is not the focus of this text. However, if the reader desires a deeper understanding of the universality phenomenon and how interactions in the system behave with changes in correlation scales, we recommend consulting references [42, 46].

2.1.5 Statistical Physics' Approach

In addition to the approaches discussed in the previous subsections, we can adopt a statistical perspective to analyse classical phase transitions. The *Partition Function* plays an important role in this scenario, with its zeros being associated with the characterisation of the phase transition.

The canonical partition function for a system in thermal equilibrium with a reservoir at temperature T, can be expressed in terms of the system's Hamiltonian [45]:

$$Z = \mathrm{Tr}\big(e^{-\beta H}\big), \tag{2.32}$$

where $\beta = 1/(k_B T)$ is the inverse temperature and k_B is the Boltzmann constant.

From the partition function, we can obtain the state functions of the physical system and, consequently, the thermodynamic quantities of interest. For example, the Helmholtz free energy is defined in terms of the partition function Z as:

$$F = -\frac{1}{\beta} \ln Z, \tag{2.33}$$

and from it we can derive thermodynamic quantities such as pressure $P = -\left(\frac{\partial F}{\partial V}\right)_{T,N}$, entropy $S = -\left(\frac{\partial F}{\partial T}\right)_{V,N}$, and specific heat at constant volume $C_V = -T\left(\frac{\partial^2 F}{\partial T^2}\right)_{V,N}$, for example [40].

In the previous sections, we saw that phase transitions can be characterised by non-analyticities in state functions or their derivatives. As an example, we considered the Gibbs free energy, which exhibits discontinuities in its first derivatives in first-order phase transitions, while in continuous transitions, non-analyticities appear in the second derivatives, such as divergences or discontinuities in the slope.

Considering this, the analysis of phase transitions via the Helmholtz free energy[9] expressed in terms of the partition function becomes interesting. Note that for F to exhibit singularities, the partition function Z must be zero.

[9] We can directly relate the Gibbs and Helmholtz free energies through a Legendre transform: $G(T, p, N) = F(T, V, N) + pV$ [40], so the characteristics under transition can be analysed using the Helmholtz free energy, as well as any thermodynamic potential.

The *zeros of the partition function* occur in the thermodynamic limit and were initially studied in the context of phase transition characterisation by Yang and Lee [47] within the framework of the *grand partition function*[10]. Yang and Lee analysed the distribution of zeros in the complex plane of fugacity[11].

The phase transition occurs in the thermodynamic limit and is characterised when these zeros reach the real axis of fugacity in the complex plane. This phenomenon signals a phase change, since it divides the real axis into two regions, each corresponding to a distinct phase of the system. Therefore, at these critical fugacity points, the system switches from one phase to another. This description will not be explored in depth here; however, the reader can find the development of this idea in references [40, 45].

Fisher expanded the Yang and Lee's approach to the *canonical ensemble*, defining *Fisher zeros*. In Fisher's formulation, instead of analysing the complex fugacity plane, the analysis is conducted in the complex temperature plane.

We can rewrite the partition function (2.32) in terms of the set of eigenvalues $\{E_n\}$ of H:

$$Z = \sum_n e^{-\beta E_n}. \tag{2.34}$$

Considering the possibility that the system exhibits degeneracy in its energy levels, we can rewrite (2.34) in terms of the density of states $\rho(E)$, which counts the multiplicity of energy levels:

$$Z = \sum_n \rho(E_n) e^{-\beta E_n}. \tag{2.35}$$

Assuming that the system has discretised energies $E_n = \epsilon_0 + n\epsilon$, we obtain the following

$$Z = e^{-\beta\epsilon_0} \sum_n \rho_n e^{-\beta n\epsilon} = e^{-\beta\epsilon_0} \sum_n \rho_n z^n, \tag{2.36}$$

where $z \equiv e^{-\beta\epsilon}$. The polynomial form of (2.36) allows us to rewrite the partition function in terms of its roots in the complex plane[12]:

$$Z = e^{-\beta\epsilon_0} \prod_{n=1}^{N} (z - z_n), \tag{2.37}$$

[10] The grand partition function is defined for systems in equilibrium with both heat and particle reservoirs.

[11] This property is associated with the variation in the energy of the system when gaining or losing particles, and the fugacity is defined as $z = e^{\beta\mu}$, so that the grand partition function can be written as $\Gamma(z, \beta) = \sum_N z^N Z(\beta)$ [40].

[12] By the Fundamental Theorem of Algebra, a polynomial of degree N can be factored as a product of its zeros.

where z_n are the complex roots of the partition function.

For finite systems, the zeros of the partition function are distributed in the complex plane and do not touch the real axis, ensuring that Z remains positive and nonzero throughout the real domain. As a consequence, the free energy (2.33) and its derived functions remain analytic. However, in the thermodynamic limit ($N \to \infty$), the zeros can accumulate and reach the real axis, causing Z to vanish at certain critical points. At these points, (2.33) becomes non-analytic, characterising the occurrence of a phase transition [48, 49].

The point where a Fisher zero reaches the real axis is associated with a critical temperature of the system, $T_c = \frac{1}{\beta_c}$. Thus, this point separates two regions on the real temperature axis that are free of real roots. Each region characterises a phase of the system, similar to the behaviour of Yang-Lee zeros.

In the context of this thesis, we will explore an analogous application of this idea in the study of quantum dynamical phase transitions (DQPTs). In this formulation, the dynamical partition function, associated with the Loschmidt Echo, exhibits zeros in complex time, playing a role similar to Fisher zeros in identifying criticality. This connection will be developed in a later section.

2.2 Quantum Phase Transition

Quantum phase transitions, unlike classical transitions, occur exclusively due to quantum fluctuations. Therefore, ensuring that the transition under analysis is indeed a quantum transition requires eliminating the possibility of thermal fluctuations, which means considering the zero-temperature limit $T = 0$ [46, 50].

In this regime, the ground-state energy takes the role of the free energy, which was the quantity analysed in classical phase transitions. Thus, we can study the system simply by analysing the behaviour of the ground state as we vary an external non-thermal parameter of the Hamiltonian, such as an external magnetic field or pressure.

Consider a system described by a Hamiltonian operator $H(g)$, where g is a dimensionless coupling parameter that can be controlled externally. In general, the system behaves smoothly and analytically as a function of g.

However, non-analyticities can arise in the ground state of the system for some value $g = g_c$. For example, the LMG (Lipkin-Meshkov-Glick) model, which will be introduced in Chapter 5, exhibits non-analyticity in the magnetization along a certain direction, associated with symmetry restoration when crossing the critical point (for a critical value of the transverse magnetic field). Thus, the quantum phase

transition is precisely characterised by these non-analyticities in the ground-state energy at $T = 0$.

Such non-analyticities arise in Hamiltonians where g couples only to the conserved quantity [46]:

$$H(g) = H_0 + gH_1, \tag{2.38}$$

with $[H_0, H_1] = 0$, which allows H_0 and H_1 to be diagonalized simultaneously. Hamiltonians of this type are common in spin-chain models, such as the LMG model [32], the transverse-field Ising model [46], and the Dicke model.

Since we can simultaneously diagonalize the components of H, the eigenstates remain independent of g, even though the eigenvalues depend on the external parameter. This results in the possibility of a level crossing at a specific value of g [46].

The crossing between the ground-state energy and the first excited state, as shown in Fig. 2.11 (left), occurs at the critical point $g = g_c$, leading to a non-analyticity in the ground-state energy with respect to g. This is similar to the case discussed in Section 2.1.1, where a shift in the minimum of the Gibbs free energy was observed.

The occurrence of this crossing characterises a *first-order quantum phase transition*, which can occur even in finite-size systems. Furthermore, there are no divergences in the correlation length or any critical singularities [46, 50].

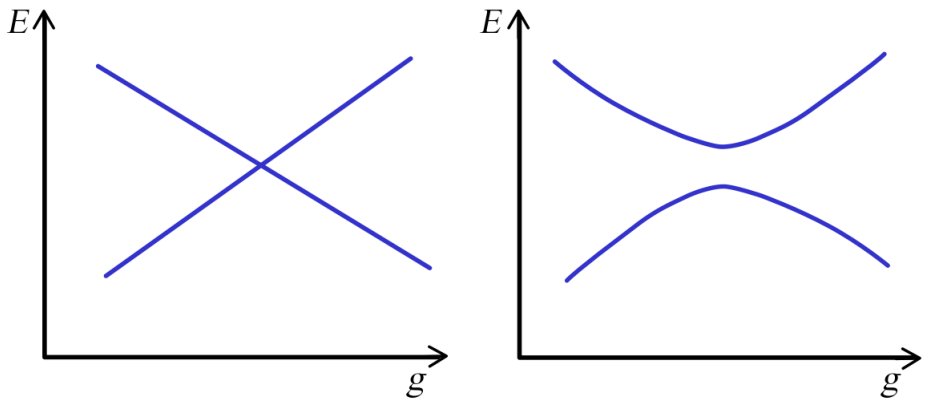

FIGURE 2.11: Crossing (left) and avoided crossing (right) between the ground-state and first excited-state energy levels at $g = g_c$. Figure based on reference [46].

A behaviour like the one shown in Fig. 2.11 (right) can also occur. In this case, there is no exact crossing of the energy level; however, the ground and first excited-state energy levels approach each other as we approach $g = g_c$, with this effect becoming more pronounced as the size of the system increases. Unlike first-order QPTs, the emergence of non-analyticities in the ground-state energy occurs only

in the thermodynamic limit [50]. Transitions with these characteristics are called *continuous quantum phase transitions*.

Continuous transitions, also referred to as *second-order quantum phase transitions*, are characterised by the vanishing of the characteristic fluctuation energy scale Δ above the ground state as the system approaches the critical point. This behaviour allows for their description using critical exponents.

2.2.1 Critical Exponents, Correlation Length, and Energy Scale

The scale Δ can be seen as an energy gap above the ground state, between the ground state and the first excited state. The behaviour of Δ near the point $g = g_c$ is given by [46]:

$$\Delta \sim J \left| g - g_c \right|^{z\nu} , \tag{2.39}$$

where J is the energy scale of the system's coupling and $z\nu$ is a critical exponent. It is evident that the scale Δ decreases as we approach the critical point, becoming zero at $g = g_c$, which characterises a continuous phase transition, as the vanishing of this energy gap leads to a non-analyticity in the ground state.

It should be noted that this behaviour is similar to the one discussed for the physical quantities presented in Section 2.1.4, which also exhibited singular behaviour near the critical point of classical continuous transitions.

Another quantity that exhibits typical behaviour in a QPT is the *characteristic correlation length scale* ξ. Defined in Section 2.1.4, this length scale determines the decay of system correlations at long distances and diverges as we approach the critical point, with the system becoming highly correlated at the phase transition. The divergence of ξ is given by [46, 51]:

$$\xi^{-1} \sim \Lambda \left| g - g_c \right|^{\nu} , \tag{2.40}$$

where Λ is an inverse length scale of the order of the structural spacing of the system, and ν is a critical exponent.

Note that both the energy scale Δ and the inverse correlation length scale ξ^{-1} decay as the system approaches the critical point. Therefore, we can relate these two parameters, obtaining the following relation:

$$\Delta \sim \xi^{-z}. \tag{2.41}$$

Both quantities characterise a QPT through their disappearance at the system's critical point. Although they become zero at the critical point, they do not remain

zero in the disordered phase. Thus, they cannot be strictly considered "order parameters" but rather critical quantities that signal, respectively, the presence or absence of a gap (Δ) and the existence (or lack) of long-range correlations (ξ). In this way, $\Delta \to 0$ and $\xi^{-1} \to 0$ at the critical point indicate the divergence of the characteristic energy and length scales but do not directly represent the symmetry breaking or restoration, which is a fundamental characteristic of the Landau order parameters.

2.2.2 Finite Temperature

Understanding the role of finite temperature in QPTs is relevant since, from an experimental perspective, reaching $T = 0$ is unfeasible. Additionally, even from a theoretical point of view, it is important to analyse how thermal fluctuations affect the quantum scenario near the critical point.

There are two possible scenarios [46, 51]:

(I) The phase transition does not occur for $T > 0$, making the thermodynamic functions analytic with respect to g. In this case, non-analyticity occurs only along the $T = 0$ axis, characterising an exclusively quantum critical point (see Figure 2.12).

(II) There is a continuous phase transition line for $T > 0$, terminating at the quantum critical point at $g = g_c$, in $T = 0$ (see Figure 2.13). In this case, quantum fluctuations compete with thermal fluctuations along the entire transition line.

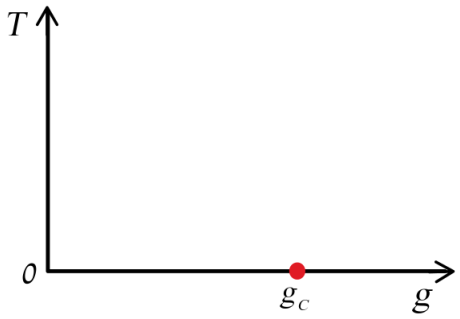

FIGURE 2.12: The critical point exists only at zero temperature. Figure based on reference [46].

In case (I), no phase transition occurs for $T > 0$. The presence of any finite amount of heat makes the thermodynamic quantities analytic in g. Thus, the transition (and criticality) occurs only at $T = 0$, when purely quantum fluctuations dominate while thermal fluctuations vanish.

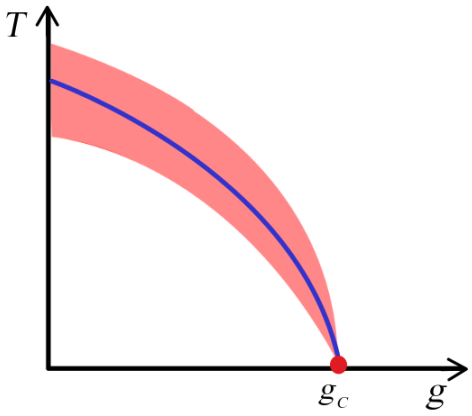

FIGURE 2.13: Phase transition line at $T > 0$ terminating at the quantum critical point. Figure based on reference [46].

For case (II), there is a transition line at $T > 0$, associated with non-analyticities in the free energy. As discussed in Section 2.1.2, classical phase transition theory effectively describes this critical line if thermal fluctuations dominate. However, near the quantum critical point ($T \to 0$ and $g \to g_c$), regions emerge where quantum fluctuations become relevant even at finite temperature, characterising the so-called *quantum critical region*, represented in Figure 2.14 [46].

Energy Scales

To understand the extent to which quantum fluctuations prevail over thermal fluctuations, considering that the transition line ends at the critical point, we analyse the relationship between the two relevant energy scales: the quantum gap Δ (given by 2.39), which measures the smallest excitation above the ground state, and the thermal scale $k_B T$.

Figure 2.14 illustrates this comparison, separating regions where $\Delta > k_B T$ and regions where $\Delta < k_B T$ using a dashed line, where $\Delta = k_B T$.

When $\Delta > k_B T$, thermal excitations cannot promote the system to states above the gap, meaning that quantum fluctuations dominate. In contrast, in the regime where $\Delta < k_B T$, the system is subject to thermal excitations capable of driving it to excited states, even near g_c, characterising the *quantum critical region*. In this region, low-energy quantum fluctuations ($\Delta \to 0$) compete with thermal fluctuations, generating critical behaviour distinct from purely classical transitions.

Thus, although purely quantum transitions strictly occur at zero temperature, even at finite temperatures, it is possible to identify critical behaviours strongly influenced by quantum criticality. In these regimes, low-energy quantum fluctuations

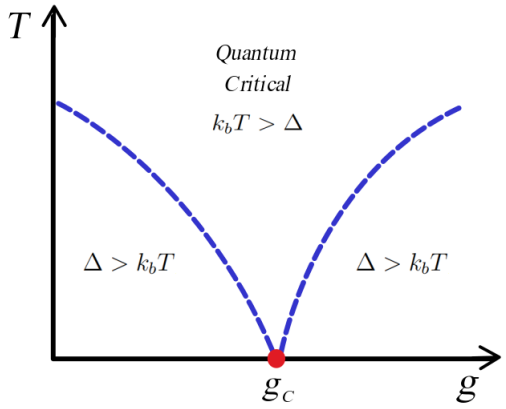

FIGURE 2.14: Regions where Δ and k_BT dominate. Figure based on reference [46].

remain relevant and compete with thermal fluctuations, resulting in critical properties that still carry the signature of the quantum critical point, even though they are not exclusively quantum transitions [46].

2.3 Dynamical Quantum Phase Transition

The transitions discussed in the previous sections share similarities in their descriptions and can be approached using well-established concepts in equilibrium physics. They are analysed through definitions of free energy, partition functions, and other parameters derived from equilibrium statistical physics. However, when dealing with systems evolving out of equilibrium, it is not possible to define such quantities, making it impossible to describe them using this framework.

In this section, we will discuss a method for characterising the *Dynamical Quantum Phase Transition* (type-II DQPT), based on the works of M. Heyl [1, 2], who introduced this phase transition concept. This method is grounded in the concept of the Loschmidt Echo and the Fisher zeros associated with this function, drawing parallels to the framework developed for equilibrium transitions. In addition, we present the dynamical order-parameter approach (type-I DQPT), where the transition is identified through qualitative changes in long-time averaged observables [4, 7, 27].

2.3.1 Non-equilibrium protocol

Since DQPTs are phenomena arising from non-equilibrium evolutions, before proceeding with their formal definition, we must introduce the concept of *quantum quench*, which will be the non-equilibrium protocol used.

The protocol consists of a system prepared in an initial state $|\psi_0\rangle$, which is an eigenstate of the Hamiltonian $H_0 = H(\lambda_0)$, where λ_0 is the initial parameter associated with a variable system parameter λ. At time t, a sudden change occurs in λ:

$$\lambda : \lambda_0 \longrightarrow \lambda_f, \tag{2.42}$$

such a change is called a *quantum quench*.

For example, if the parameter λ is an external magnetic field, the quench is equivalent to a very rapid alteration of this field, induced by an external agent, in such a way that the change can be considered instantaneous.

Consequently, the system's Hamiltonian also undergoes a change:

$$H_0 \longrightarrow H = H(\lambda_f). \tag{2.43}$$

The evolution of the initial state, governed by the post-quench Hamiltonian H, allows the system to undergo real-time quantum dynamics, with the evolved state given by:

$$|\psi(t)\rangle = e^{-iHt} |\psi_0\rangle . \tag{2.44}$$

This evolution is non-trivial in most cases, considering that $|\psi_0\rangle$ is generally not an eigenstate of H [1].

This will be the protocol used in our calculations, which will be presented in Chapter 5. Now, let us move on to the definitions of the quantities used in identifying the DQPT.

2.3.2 Loschmidt Amplitude and Loschmidt Echo

We begin by defining the *Loschmidt Amplitude*, which is a central quantity in the study of DQPTs [1, 52]. Being the overlap between the initial state $|\psi_0\rangle$ and the state evolved by the post-quench Hamiltonian $|\psi(t)\rangle$, given by (2.44), it can be written as:

$$\mathcal{G}(t) = \langle\psi_0|\psi(t)\rangle = \langle\psi_0| e^{-iHt} |\psi_0\rangle . \tag{2.45}$$

The Loschmidt amplitude can be understood as a "deviation" of the evolved state from the initial state or as a probability amplitude for the evolved state to return to the initial state [1, 2].

The probability associated with $\mathcal{G}(t)$ is called the *Loschmidt Echo*,

$$\mathcal{L}_e(t) = |\mathcal{G}(t)|^2 = |\langle\psi_0| e^{-iHt} |\psi_0\rangle|^2 \tag{2.46}$$

and can be interpreted as the probability that the system, at each instant t, is projected onto the initial state of the system, that is, a probability of returning to the initial state manifold [1].

The use of these quantities in the identification of DQPTs arises from the possibility of drawing analogies with the quantities applied to the identification of classical phase transitions, such as the partition function and free energy.

2.3.3 Partition Function, Fisher Zeros, and Rate Function

The Loschmidt amplitude, as well as the Loschmidt echo, exhibit functional dependence on the number of degrees of freedom N, particularly for large N [1, 52]. This behaviour suggests an analogy with the equilibrium partition function.

To understand this connection, we first rewrite the Loschmidt amplitude by extending it to the complex time plane, considering $z = t - i\tau$:

$$\mathcal{G}(z) = \langle\psi_0| e^{-iHz} |\psi_0\rangle . \tag{2.47}$$

When z is purely imaginary, i.e., $z = -i\tau$, we can rewrite the amplitude as:

$$\mathcal{G}(-i\tau) = \langle\psi_0| e^{-H\tau} |\psi_0\rangle . \tag{2.48}$$

This expression is equivalent to a boundary partition function, which corresponds to an equilibrium partition function with fixed boundary states at $|\psi_0\rangle$ [52].

Due to this analogy, we can analyse the dynamical behaviour using the Fisher zeros formalism. In this way, we can characterise the dynamical phase transition by analogy with the classical transition described by Fisher zeros [1].

Fisher Zeros

In 2.1.5, we introduced Fisher zeros as a generalisation of Yang-Lee zeros, analysing the roots of the partition function in the complex temperature plane.

In the construction presented in 2.1.5, the partition function was represented as a polynomial in terms of a complex variable associated with temperature. To establish an analogy here, let us rewrite equation (2.47) considering $H = \sum_n E_n |n\rangle\langle n|$, where E_n are the eigenvalues and $\{|n\rangle\}$ are the eigenstates of H:

$$\mathcal{G}(z) = \sum_n e^{-iE_n z} |\langle n|\psi_0\rangle|^2. \tag{2.49}$$

Equation (2.49) is similar to that obtained in (2.35). This similarity suggests that we can factorise this function in terms of its roots, analogously to the procedure applied in the previously mentioned section.

Using the Weierstrass factorisation theorem[13], we can express the generalised Loschmidt amplitude in factored form [1]:

$$\mathcal{G}(z) = e^{-\beta\epsilon_0} \prod_{n=1}^{N} (z - z_n), \tag{2.50}$$

where z_n correspond to the roots of the Loschmidt amplitude in the complex time plane.

For finite systems, the zeros are distributed away from the real-time axis, ensuring that the amplitude never vanishes. However, in the limit $N \to \infty$, the zeros can accumulate and cross the real-time axis, leading to critical points where the Loschmidt amplitude becomes zero.

Rate Function

Continuing the analogy, just as we relate the partition function to the free energy in classical systems, we can define the rate function associated with the Loschmidt amplitude

$$g(z) = -\lim_{N\to\infty} \frac{1}{N} \ln \mathcal{G}(z). \tag{2.51}$$

This function plays a role analogous to the free energy per particle in equilibrium phase transitions. Therefore, we also define the rate function associated with the Loschmidt echo in real-time, returning to our initial definition of $\mathcal{L}_e$,

$$\lambda(t) = -\lim_{N\to\infty} \frac{1}{N} \ln \mathcal{L}_e(t). \tag{2.52}$$

Both (2.51) and (2.52) characterise the system's evolution in the thermodynamic limit and allow us to identify dynamical transition points when they exhibit non-analyticities. These non-analyticities are associated with the Fisher zeros of the Loschmidt amplitude in the complex plane and the Loschmidt echo, occurring when the Fisher zeros reach the real-time axis in the complex time plane [29].

The connection with Fisher zeros makes this approach robust for studying DQPTs, as it provides a well-defined mathematical criterion for the occurrence of the transition, analogous to the treatment of equilibrium phase transitions via Fisher zeros in the partition function.

[13] The Weierstrass factorisation theorem states that any entire function (a function analytic over the entire complex plane) can be expressed as an infinite product involving its zeros, generalising the fundamental theorem of algebra.

Type-II DQPT Definition

We can now formally define the occurrence of a DQPT. A DQPT occurs when the rate function $\lambda(t)$ exhibits nonanalyticalities at specific times t_c. These non-analyticities are directly associated with Fisher zeros reaching the real-time axis in the thermodynamic limit, which are discretely linked to the zeros of the Loschmidt echo [1, 2].

The time dependence of the rate function means that the transition is guided solely by time, characterising the DQPT as a phase transition in time. In Figure 2.15, we illustrate a typical behaviour of the rate function $\lambda(t)$ in a situation where criticality occurs at a critical time t_c. The observed kink indicates non-analyticity and characterises the occurrence of a DQPT.

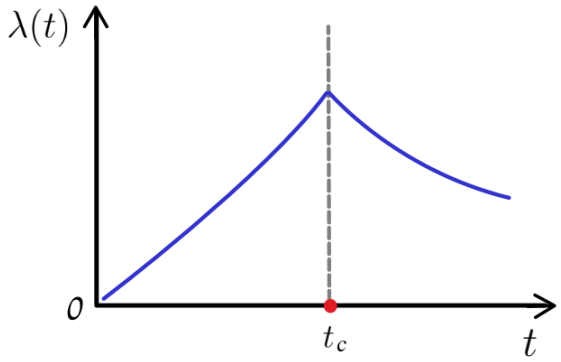

FIGURE 2.15: Rate function as a function of time for a system undergoing a DQPT at t_c. Figure based on reference [1].

This behaviour is analogous to that found in second-order equilibrium phase transitions, reinforcing the interpretation of DQPTs as critical transitions in time. DQPTs occur on transient time scales, meaning that they take place on timescales much shorter than the system's thermalization time. Therefore, they are phenomena independent of the system reaching equilibrium.

2.3.4 Order Parameter and Type-I DQPT

Another way of characterising DQPT consists in the analysis of a *parameter of dynamical order*, which marks the transition and is referred to as DPT-I when described in this way. This characterisation follows the Landau definition of an order parameter for classical phase transitions, presented in Sec. 2.1.3.

In out-of-equilibrium systems, dynamical phases naturally present oscillations in physical observables, a direct consequence of the dynamical character of the evolution. Qualitatively distinct behaviours are then observed in different phases, below or above the dynamical critical point [7]. For instance, physical quantities can oscillate around a nonzero average value in one phase and around zero in another.

In this context, the dynamical order parameter is defined as the long-time average of an observable, such as a component of the collective spin [27]:

$$\overline{\langle J_i \rangle} = \lim_{T\to\infty} \frac{1}{T} \int_0^T dt \, \langle J_i(t) \rangle. \tag{2.53}$$

where $\langle J_i(t) \rangle = \langle \psi(t) | \, J_i \, | \psi(t) \rangle$ is the expectation value with respect to the time-evolved state $|\psi(t)\rangle$. This quantity is finite in the dynamically ordered phase, the one with broken-symmetry, and vanishes in the disordered one, with restored symmetry, thus capturing the non-equilibrium transition [4, 28, 53].

As an illustrative example, in the Lipkin-Meshkov-Glick model, the dynamical order parameter corresponds to the magnetization along a specific direction. Starting from an initial ferromagnetic state, quenches below the critical point lead to oscillations around a nonzero average value, whereas quenches above the critical point drive the system into a phase where the average magnetization vanishes. A more detailed discussion and graphs of this case will be presented later in Section 5.3, in this thesis.

Chapter 3

Entropy Production

This chapter aims to explore the concept of entropy production in nonequilibrium systems. We begin with a brief discussion of the classical concepts of entropy and its relationship to thermodynamic irreversibility. Next, we address entropy and its production within the framework of information theory, defining it in the quantum context and constructing entropy production for more general scenarios of quantum evolution. Finally, we express entropy production in terms of the distinction between the initial and evolved states, a result that will be of great importance for the continuation of this work.

3.1 What is Entropy?

In any physical process, changes in the quantities involved will inevitably occur throughout its course. In processes that take place in finite time, entropy will flow between systems. However, unlike other quantities such as energy or the number of particles, entropy can be irreversibly produced, meaning that it does not satisfy a "continuity equation" [54].

Entropy is a fundamental quantity in thermodynamics and statistical physics. In classical thermodynamics, it emerges as a state function introduced in the form of postulates, restricting certain processes by requiring its maximisation for a closed system to reach equilibrium.

Unlike other state functions—such as internal energy, enthalpy, Helmholtz free energy, and Gibbs free energy—which have direct interpretations related to a system's energy content and useful work, entropy lacks an immediate intuitive interpretation. Although these state functions offer a clear understanding of concepts such as total energy, available work, and heat exchange at constant pressure or volume, entropy is initially abstract.

In the context of statistical physics, entropy is associated with the number of accessible microstates of a system under given constraints [41]. This perspective provides a more intuitive explanation, linking entropy to the concept of disorder:

systems evolve by maximising entropy, reaching states with the highest number of accessible microstates.

In the classical context, the change in entropy of a system S is defined by Clausius as [54, 55]:

$$\Delta S_s \geq -\sum_i \frac{Q_i}{T_i} \tag{3.1}$$

where ΔS_s is the variation in system entropy, Q_i is the heat reversibly exchanged between the system and the reservoir i during the process, and T_i is the temperature of the reservoir i. Here, by convention, we adopt $Q_i > 0$ when heat flows from the system to the reservoir i. Note that if $\sum_i Q_i > 0$, the entropy variation of the system will be negative; however, this does not violate any thermodynamic laws, since entropy is not decreasing globally, but rather in a specific part of the universe.

The definition (3.1) is based on the idea of an interaction between the system and the thermal reservoirs, associated with the concept of variation in entropy between the initial and final states of the process under analysis, rather than an intrinsic characteristic of the system.

However, one of the fundamental postulates of thermodynamics states that:

> "The entropy of any system vanishes in state for which $(\partial U/\partial S)_{V,N_1,N_2,\cdots,N_r} = 0$" [41].

That is, the entropy of any system tends to zero in states where $T \to 0$, giving us the idea of an absolute value of the entropy. This postulate is related to what became known as the *Nernst Theorem* and was later formalised as the *Third Law of Thermodynamics* [41].

The Nernst Theorem states that the entropy variation in reversible isothermal processes tends to zero as the system's temperature approaches absolute zero $T \to 0$:

$$\lim_{T\to 0} \Delta S = 0. \tag{3.2}$$

Meanwhile, the Third Law of Thermodynamics, attributed to Planck, is slightly more general, asserting that the absolute entropy of systems with a single fundamental (non-degenerate) state tends to zero in the limit $T \to 0$:

$$\lim_{T\to 0} S = 0. \tag{3.3}$$

Although the Nernst Theorem and the Third Law impose a lower bound on entropy, assigning it an absolute reference, in the context of classical thermodynamics, entropy remains abstract, being defined in terms of variation and lacking a concrete physical interpretation [41].

A more concrete understanding of entropy arises with statistical mechanics through Boltzmann's formulation. In this context, entropy is directly related to the number of accessible microstates of the system Ω and is defined as the logarithm of this quantity [40, 41]:

$$S = k_B \ln \Omega, \tag{3.4}$$

where k_B is the Boltzmann constant.

In Boltzmann's formulation, all microstates are considered to have the same probability of occupation, a valid assumption for ergodic systems[1] in thermal equilibrium. Statistical mechanics describes that a macroscopic system, characterised by parameters such as total energy, volume, and number of particles, can be distributed among various possible microstates.

The total number Ω is determined by the macroscopic constraints imposed on the system. Changing at least one of these constraints, such as volume or total energy, allows access to new microstates, increasing Ω. This change directly results in an increase in the system's entropy, as described by equation (3.4) [40]. However, out-of-equilibrium, the equiprobability assumption may not hold, requiring more general and appropriate descriptions for entropy.

Therefore, statistical interpretation relates the entropy to the number of accessible microstates, which justifies why, in thermodynamic equilibrium, it reaches its maximum value: states with larger Ω are more probable [41]. This probabilistic view underlies the irreversibility described by the second law, as systems tend to evolve spontaneously toward configurations of higher entropy (with greater Ω). In irreversible processes, such as free expansion, the entropy variation quantifies the departure from equilibrium, illustrating the statistical basis of dissipation in both macroscopic and microscopic systems.

3.2 Entropy production

Given the concept of entropy and its interpretation in the context of classical thermodynamics and statistical mechanics, we can now move on to the idea of entropy production and its relation to irreversibility and the second law of thermodynamics.

[1] An ergodic system is one in which, after a sufficiently long time, the system's representative point comes arbitrarily close to any point on the energy surface; In other words, the system's trajectory "explores" the entire accessible phase region, ensuring that time averages of physical quantities coincide with ensemble averages [42].

3.2.1 Systems in Equilibrium and Nonequilibrium

Thermodynamics is based on the concept of *thermodynamic equilibrium*, a condition in which the macroscopic properties of the system remain constant over time, determined exclusively by intrinsic factors, without the influence of externally applied conditions [41]. In equilibrium, we describe the system using state functions and extensive and intensive variables, as well as the principle of entropy maximisation.

Formally, equilibrium states can be characterised by the following postulate:

> **Postulate I** - There exist particular states (called equilibrium states) of simple systems that, macroscopically, are characterized completely by the internal energy U, the volume V, and the mole numbers N_1, N_2, $\cdots$, N_r of the chemical components [41].

And also via entropy maximisation:

> **Postulate II** - There exists a function (called the entropy S) of the extensive parameters of any composite system, defined for all equilibrium states and having the following property: The values assumed by the extensive parameters in the absence of an internal constraint are those that maximize the entropy over the manifold of constrained equilibrium states [41].

However, for out-of-equilibrium systems, such as those subjected to temperature gradients or particle flows, traditional thermodynamic tools become inadequate. In these conditions, the dynamic description and entropy production are essential to understand deviations from equilibrium and the resulting fluxes.

For example, systems operating in out-of-equilibrium regimes, such as non-equilibrium steady states (*NESS*), maintain constant energy and entropy fluxes, even though the total entropy variation in the system may be zero $\left(\frac{dS_s}{dt} = 0\right)$. Such states are characterised by a constant and nonzero entropy production, allowing a detailed analysis of the irreversibility of the processes involved [54].

Furthermore, phenomena such as *Dynamical Quantum Phase Transitions* (DQPT) occur purely in the out-of-equilibrium regime. These transitions, discussed in Section 2.3, highlight the importance of temporal dynamics in the analysis of out-of-equilibrium quantum systems and show how concepts like the *Loschmidt Echo* can complement the traditional thermodynamic approach.

This distinction between equilibrium and out-of-equilibrium systems emphasises the importance of entropy production, establishing it as an essential tool for quantifying irreversibility and understanding phenomena in different dynamical regimes.

3.2.2 Definition

To introduce the idea of entropy production, we will use the definition of entropy given by Clausius, presented in equation (3.1). This definition expresses the second law of thermodynamics as an inequality which is saturated only for reversible processes. In these cases, we have:

$$\Delta S_s = -\sum_i \frac{Q_i}{T_i} \tag{3.5}$$

That is, for reversible processes, the entropy variation of the system is determined only by the heat flow between the system and the thermal reservoirs. This flow contributes exclusively to the global entropy balance, without generating irreversibilities. In other words, for a reversible process, the entropy variation of the system occurs due to the heat flow out of the system $Q_i > 0$, which generates a negative entropy flow from the perspective of the system, $\Delta S_s < 0$, or due to the heat flow into the system $Q_i < 0$, which generates a positive entropy flow, $\Delta S_s > 0$ [54].

On the other hand, for irreversible processes, the equality is not satisfied. In such situations, the entropy variation of the system exceeds the entropy flow as a result of heat exchange. This excess entropy quantity is called *entropy production* Σ and reflects the irreversibility of the process.

Rewriting equation (3.1), we can define Σ as:

$$\Sigma = \Delta S_s + \sum_i \frac{Q_i}{T_i} \geq 0, \tag{3.6}$$

which indicates the non-negativity of entropy production, $\Sigma \geq 0$, reaching zero only when the system undergoes a reversible transformation. In other words, entropy production quantifies the departure from equilibrium and is a characteristic of the thermodynamic process rather than an intrinsic property of the system, as entropy is. The further from equilibrium the process occurs, the higher the value of Σ [54].

Thus, entropy production not only quantifies the irreversibility of thermodynamic processes but also provides a basis for understanding and analysing nonequilibrium systems.

For processes that evolve over time, it is useful to consider the entropy production rate $\dot{\Sigma}$, which expresses the time variation of the entropy production. This quantity allows us to analyse irreversibility in dynamical systems:

$$\dot{\Sigma} = \frac{d\Sigma}{dt}. \tag{3.7}$$

Considering definition (3.6) and writing the total entropy flux as $\phi_s = \sum_i \frac{Q_i}{T_i}$, with the convention $\phi_s > 0$ for the entropy flow out of the system, meaning the system's entropy decreases while the reservoir's entropy increases, we can write:

$$\dot{\Sigma} = \frac{dS_s}{dt} + \dot{\phi}_s \geq 0. \tag{3.8}$$

$\dot{\Sigma}$, therefore, is a balance between the time rates of variation in entropy in the system and the entropy flow between the system and the reservoir.

In terms of entropy variation in the system, we have:

$$\frac{dS_s}{dt} = \dot{\Sigma} - \dot{\phi}_s. \tag{3.9}$$

Note that the time variation of the entropy in the system depends on the difference between the entropy production rate $\dot{\Sigma}$, which is always positive, and the rate at which this entropy flows into or out of the system $\dot{\phi}_s$.

The case of *NESS*, mentioned above, is particularly interesting since we have $\dot{\Sigma} = \dot{\phi}_s$, leading to a zero entropy variation in the system over time $\frac{dS_s}{dt} = 0$. The constant rates of entropy production and entropy flux characterise this condition and differentiate it from equilibrium, which occurs when both entropy production and entropy flux cease entirely, i.e. $\dot{\Sigma} = \dot{\phi} = 0$[54].

The second law of thermodynamics can then be formalised in terms of these two definitions: entropy production, given by (3.6), and entropy production rate, via (3.8), ensuring that total entropy production is always non-negative ($\Sigma \geq 0$ and $\dot{\Sigma} \geq 0$).

3.3 The Role of Entropy Production

Having established the fundamentals of entropy production and its relationship with irreversibility, we can analyse some examples in which this concept plays a fundamental role. Furthermore, we will explore the extension of this concept to quantum systems, formulated via informational entropy. This section is based on reference [54].

To begin, let us analyse the operation of a heat engine, a classic example that directly connects this concept to the limits imposed by the second law of thermodynamics.

3.3.1 Heat Engine

Let us consider a system s continuously interacting with two thermal reservoirs at different temperatures, T_h and T_c, with $T_h > T_c$. In addition, the system interacts with an external agent capable of extracting or performing work on s. Here, we adopt the convention $W > 0$ for the work done on the system, along with the convention previously adopted for heat flow.

The first and second laws of thermodynamics, in terms of the time rate of change of the system's internal energy $\frac{dU_s}{dt}$ and the entropy production rate $\dot{\Sigma}$, can be expressed as [54]:

$$\frac{dU_s}{dt} = \dot{W} - \dot{Q}_h - \dot{Q}_c, \tag{3.10}$$

and

$$\dot{\Sigma} = \frac{dS_s}{dt} + \frac{\dot{Q}_h}{T_h} + \frac{\dot{Q}_c}{T_c} \tag{3.11}$$

where $\dot{Q}_h$ and $\dot{Q}_c$ are the rates at which heat flows between the system and the reservoirs at T_h and T_c, respectively.

When operating for a sufficiently long time, the steady-state condition $\left(\frac{dU_s}{dt} = \frac{dS_s}{dt} = 0\right)$ is reached [54]. Under this condition, equations (3.10) and (3.11) can be rewritten as follows:

$$\dot{W} = \dot{Q}_h + \dot{Q}_c, \tag{3.12}$$

and

$$\dot{\Sigma} = \frac{\dot{Q}_h}{T_h} + \frac{\dot{Q}_c}{T_c} \tag{3.13}$$

Using the above equations, we can express the efficiency $\eta = \frac{\dot{W}}{\dot{Q}_h}$ as follows:

$$\begin{aligned} \eta &= 1 + \frac{\dot{Q}_c}{\dot{Q}_h}, \\ &= 1 - \frac{T_c}{T_h} + \frac{T_c}{\dot{Q}_h}\dot{\Sigma}, \\ &= \eta_c + \frac{T_c}{\dot{Q}_h}\dot{\Sigma}, \end{aligned} \tag{3.14}$$

where $\eta_c = 1 - \frac{T_c}{T_h}$ is the Carnot efficiency.

Since $\dot{Q}_h < 0$, the second term in equation (3.14) is always non-positive, as the second law ensures $\dot{\Sigma} \geq 0$. Thus, from equation (3.14), we conclude that the efficiency of a heat engine is always lower than the Carnot efficiency because of a term proportional to the entropy production rate. The two efficiencies are equal only when the processes are reversible $\dot{\Sigma} = 0$. Therefore, the less entropy that is generated in the involved processes, the closer the system is to Carnot efficiency.

Since Carnot's statement of the second law of thermodynamics is given by [54]:

> "The efficiency of any quasi-static or reversible cycle between two heat reservoirs depends only on the temperatures of the reservoirs themselves, and is the same, regardless of the working substance. An engine operated in this way is the most efficient possible heat engine using those two temperatures".

We conclude that as the entropy production increases because of irreversibility in the heat engine cycle, the efficiency decreases relative to the Carnot efficiency. Thus, entropy production serves as a quantitative measure of the degree of irreversibility of the system.

Furthermore, entropy production in the cycle dictates two important rules. First, considering a single reservoir in contact with the system, taking $\dot{Q}_c = 0$, from equations (3.12) and (3.13) we obtain:

$$\dot{W} = \dot{Q}_h \tag{3.15}$$

and

$$\dot{\Sigma} = \frac{\dot{Q}_h}{T_h}, \tag{3.16}$$

therefore, from (3.15) and (3.16), we have:

$$\dot{\Sigma} = \frac{\dot{W}}{T_h} \geq 0. \tag{3.17}$$

Notice that, in order to maintain the non-negativity condition of entropy, we necessarily have $\dot{W} \geq 0$, meaning that work must be injected into the system, as described by the Kelvin-Planck statement of the second law of thermodynamics [54]:

> "It is impossible to devise a cyclically operating device, the sole effect of which is to absorb energy in the form of heat from a single thermal reservoir and to deliver an equivalent amount of work."

Finally, if we consider $\dot{W} = 0$, from (3.12), we obtain $-\dot{Q}_c = \dot{Q}_h$. Then, equation (3.13) can be rewritten as:

$$\dot{\Sigma} = \dot{Q}_c \left(\frac{1}{T_c} - \frac{1}{T_h} \right) \geq 0, \tag{3.18}$$

which indicates that, due to the conditions $\dot{\Sigma} \geq 0$ and $T_h > T_c$, heat must necessarily flow from the hot reservoir to the cold reservoir. This consequence can be summarised by the Clausius statement of the second law of thermodynamics [54]:

> "Heat can never pass from a colder to a warmer body without some other change, connected therewith, occurring at the same time."

Considering the same example, we can introduce another possibility of exchange between the system and the reservoirs. Suppose now that the system is allowed to exchange particles with both the hot and cold reservoirs, given by N_h and N_c, respectively. Again, we adopt the convention that flows leaving the reservoir are positive, $N_i > 0$. Assuming that no work is involved, the first law can be rewritten as [54]:

$$\frac{dU_s}{dt} = -\dot{Q}_h - \dot{Q}_c + \mu_h \dot{N}_h + \mu_c \dot{N}_c. \tag{3.19}$$

Notice that two new terms, dependent on the chemical potentials μ and the particle fluxes $\dot{N}$, also contribute to the system's energy variation.

Taking into account the steady-state case again, $\frac{dU_s}{dt} = \frac{dS_s}{dt} = 0$, and due to particle conservation, $\dot{N}_h = -\dot{N}_c$, we can rewrite equation (3.19) as:

$$\dot{Q}_h = -\dot{Q}_c + (\mu_h - \mu_c)\dot{N}_h. \tag{3.20}$$

Notice that only in the case where $\mu_h = \mu_c$ do we obtain the condition $\dot{Q}_h = -\dot{Q}_c$.

Using equations (3.11) and (3.20), we can express the entropy production rate as:

$$\dot{\Sigma} = \dot{Q}_c \left(\frac{1}{T_c} - \frac{1}{T_h} \right) + \dot{N}_h \frac{\mu_h - \mu_c}{T_c}. \tag{3.21}$$

In equation (3.21), if we consider equal chemical potentials, we recover the case discussed above. On the other hand, if we assume equal temperatures $T_h = T_c$, we obtain the following relation:

$$\dot{\Sigma} = \dot{N}_h \frac{\mu_h - \mu_c}{T_c} \geq 0, \tag{3.22}$$

therefore, if $\mu_h > \mu_c$, we necessarily have that particles flow from the reservoir with the higher chemical potential to the system, $\dot{N}_h > 0$, and consequently, from the system to the reservoir with the lower chemical potential, $\dot{N}_c < 0$.

We can conclude that the existence of generalised forces, or thermodynamic affinities, such as temperature and chemical potential gradients, drive the system towards equilibrium, generating conjugate fluxes, such as heat and particle flows. Entropy production, described as the sum of the products between these affinities and the associated fluxes, as indicated in equation (3.21), is a direct reflection of the departure from equilibrium. At equilibrium, the thermodynamic forces vanish, leading to cessation of conjugate fluxes and, consequently, entropy production [54].

This example illustrates the direct relationship between entropy production and irreversibility and how they impose practical limitations on energy conversion efficiency. Entropy production emerges as a tool for quantifying irreversibility in physical processes and connects the statements of the second law—Carnot, Kelvin-Planck, and Clausius—within a unified framework. Whether by limiting the efficiency of a heat engine, restricting the extraction of work from a single reservoir, or imposing the natural direction of heat and particle flow, entropy production plays a fundamental role in enforcing these fundamental restrictions.

3.3.2 Entropy and information

Beyond its fundamental importance in macroscopic systems, entropy plays a crucial role in information theory. Shannon entropy is essential to describe a probabilistic system, as it quantifies the amount of information it contains. Moreover, this idea can be generalised to quantum systems, where von Neumann entropy fulfils this role. These approaches connect the statistical description of macroscopic systems with the quantum foundations of information, expanding the scope of the entropy concept.

Let us explore this connection by first presenting the classical formulation of informational entropy and then extending it to the quantum domain, laying the groundwork for a deeper understanding of its relationship with irreversibility and entropy production.

Informational entropy

In the context of classical information theory, Shannon [56] introduced the concept of informational entropy as a measure of the *average information content* associated with the random emission of a source.

To better understand Shannon's definition, consider a random variable X associated with a source that can produce different outcomes x_i, with probabilities p_i. The amount of information associated with a single event x_i is defined as [57]:

$$I(x_i) = -\log_2(p_i). \tag{3.23}$$

This quantity, $I(x_i)$, measures the *surprise* when observing the result of a random experiment [57], that is, how much information is gained when measuring the event. Note that a highly probable event ($p_i \to 1$) yields a small value of $I(x_i)$, indicating little information or surprise, while an unlikely event ($p_i \to 0$) provides a larger amount of information about the system. A certain event ($p_i = 1$) does not result in surprise or information, which means $I(x_i) = 0$.

Shannon then proposed quantifying the information contained in the random variable X as a weighted average of the information associated with all possible events. *Shannon entropy* is defined as [57, 58]:

$$H(X) = H(p_1, \cdots, p_n) = -\sum_i p_i \log_2 p_i. \tag{3.24}$$

Shannon entropy represents the average amount of information contained in the random variable X and can be understood as a measure of the uncertainty associated with the possible values of X before observation, or the amount of information acquired after knowing them [58]. Thus, for the case of a single event, the amount of information is associated with the probability of the event occurring. For a source with probabilities close to 1, the value of $H(X)$ will be small. For unlikely events, with probabilities close to zero, we obtain higher values of $H(X)$[2].

It is possible to establish a connexion between the Shannon entropy, equation (3.24), and the Boltzmann entropy, equation (3.4), through the concept of maximisation of entropy. To do this, let us examine which probability distributions maximise expression (3.24) under conditions $(i) \sum_i p_i = 1$ (probability normalisation) and $(ii) \langle U \rangle = \sum_i p_i E_k$ (fixed average energy).

Using the method of Lagrange multipliers to maximise the functional $H(X)$ for condition (i), we have:

$$\mathcal{L} = -\sum_i p_i \log p_i + \lambda \left(\sum_i p_i - 1 \right), \tag{3.25}$$

where λ is the Lagrange multiplier.

Differentiating $\mathcal{L}$ with respect to p_i and λ, we obtain:

$$\frac{\partial \mathcal{L}}{\partial p_i} = -\log p_i - 1 + \lambda = 0, \tag{3.26}$$

$$\frac{\partial \mathcal{L}}{\partial \lambda} = \sum_i p_i - 1 = 0. \tag{3.27}$$

We can then write:

$$\log p_i = \lambda - 1, \tag{3.28}$$

which, when exponentiated[3], becomes:

$$p_i = e^{\lambda - 1}, \tag{3.29}$$

[2] For events with zero probability $p_i = 0$, it is assumed that $0 \log_2 0 \equiv 0$.

[3] It is assumed that $\log x \equiv \ln x$

thus, substituting (3.29) into (3.27), we obtain:

$$\sum_i e^{\lambda-1} = 1, \tag{3.30}$$

since $e^{\lambda-1}$ is independent of i, we have $\sum_i e^{\lambda-1} = Ne^{\lambda-1} = 1$, where N is the number of possible outcomes of the random variable X. Therefore, from (3.29) and (3.30), we get:

$$p_i = \frac{1}{N}. \tag{3.31}$$

The probability distribution that maximises Shannon entropy under the condition $\sum_i p_i = 1$ is the equiprobable distribution (3.31). This result directly connects to the definition of the Boltzmann entropy for systems in thermal equilibrium, where all accessible microstates are equally probable. In the context of thermodynamics, this maximisation characterises the microcanonical ensemble, which describes isolated systems with fixed total energy and no energy exchange with the environment. Thus, the conceptual connection between information theory and statistical physics naturally emerges when maximising Shannon entropy.

Including restriction (ii), the Lagrange functional $\mathcal{L}$ takes the form:

$$\mathcal{L} = -\sum_i p_i \log p_i + \lambda\left(\sum_i p_i - 1\right) + \beta\left(\langle U\rangle - \sum_i p_i E_i\right), \tag{3.32}$$

where β is the Lagrange multiplier associated with the additional constraint.

The derivative of $\mathcal{L}$ with respect to p_i in this case is:

$$\frac{\partial \mathcal{L}}{\partial p_i} = -\log p_i - 1 + \lambda - \beta E_i = 0. \tag{3.33}$$

Rewriting:

$$\log p_i = \lambda - 1 - \beta E_i. \tag{3.34}$$

Exponentiating both sides, we obtain:

$$p_i = e^{\lambda-1}e^{-\beta E_i}. \tag{3.35}$$

Here, we can use the result obtained previously for the restriction (i): $e^{\lambda-1} = \frac{1}{N}$. Thus, we have:

$$p_i = \frac{e^{-\beta E_i}}{N}. \tag{3.36}$$

For comparison purposes, we can redefine the normalisation factor N by introducing Z as the canonical partition function:

$$Z = \sum_i e^{-\beta E_i}. \tag{3.37}$$

Therefore, the probability distribution that maximises $H(X)$, considering conditions (i) and (ii), is:

$$p_i = \frac{e^{-\beta E_i}}{Z}. \tag{3.38}$$

By associating $\beta^{-1} = k_b T$, we can say that equation (3.38) represents the probability distribution associated with microstates i in a system in contact with a reservoir at temperature T [40].

By introducing the constraint of fixed average energy $\langle U \rangle = \sum_i p_i E_i$, maximisation of entropy leads to the canonical distribution (3.38). In this case, we consider the canonical ensemble, which describes systems in thermal equilibrium with a reservoir at temperature T, allowing energy exchange [40]. These results highlight the broad applicability of informational entropy by demonstrating its connection to the foundations of statistical physics and its role in describing systems in thermal equilibrium.

Substituting (3.38) into (3.24):

$$\begin{aligned} H(X) &= -\sum_i \frac{e^{-\beta E_i}}{Z} \log \frac{e^{-\beta E_i}}{Z}, \\ &= -\sum_i \frac{e^{-\beta E_i}}{Z} \left(-\beta E_k - \log Z\right), \\ &= \beta \sum_i \frac{e^{-\beta E_i}}{Z} E_i + \log Z \sum_i \frac{e^{-\beta E_i}}{Z}. \end{aligned} \tag{3.39}$$

Identifying the average energy as $\langle U \rangle = \sum_i \frac{e^{-\beta E_i}}{Z} E_i$ and using the condition $\sum_i \frac{e^{-\beta E_i}}{Z} = 1$, we obtain:

$$H(X) = \beta \langle U \rangle + \log Z. \tag{3.40}$$

which can be rewritten as:

$$-k_b T \log Z = \langle U \rangle - k_b T H(X). \tag{3.41}$$

Notice that, up to constants and the base of the logarithm, equation (3.41) is similar to the Helmholtz free energy expression, $F = U - TS$, where S is the thermodynamic entropy. Therefore, equation (3.24) indeed possesses the characteristics of an

entropy [59].

3.3.3 Quantum Entropy

In quantum mechanics, the lack of knowledge about the physical state of a system is intrinsically related to the probabilistic description provided by the density matrix ρ. Thus, we can consider the natural extension of quantifying the uncertainty associated with the quantum state, using the ideas presented so far.

Taking into account a system represented by the density matrix ρ, which contains information on the probabilities associated with each possible measurement outcome, the entropy $S(\rho)$ of the state is defined as [57, 58]:

$$S(\rho) = -\operatorname{Tr}(\rho \log \rho). \tag{3.42}$$

Equation (3.42) is known as the *von Neumann entropy* or *quantum entropy* and quantifies the degree of uncertainty or "lack of knowledge" about the system described by the state ρ. Similarly to Shannon entropy, von Neumann entropy provides a measure of the average amount of information required to describe the system's state, but now adapted to the quantum context.

If the density operator can be expressed as a spectral decomposition, with p_i being the non-negative eigenvalues of ρ, satisfying $\sum_i p_i = 1$, and $\{|i\rangle\}$ being the associated orthonormal eigenvectors:

$$\rho = \sum_i p_i \, |i\rangle\langle i| \tag{3.43}$$

then von Neumann entropy reduces to:

$$S(\rho) = -\operatorname{Tr}\left(\sum_i p_i \, |i\rangle\langle i| \log \sum_j p_j \, |j\rangle\langle j| \right). \tag{3.44}$$

Since ρ is a diagonal matrix, we obtain: $\log \rho = \log\left(\sum_j p_j \, |j\rangle\langle j|\right) = \sum_j (\log p_j) \, |j\rangle\langle j|$. Thus:

$$\begin{aligned} S(\rho) &= -\operatorname{Tr}\left(\sum_i p_i \, |i\rangle\langle i| \sum_j (\log p_j) \, |j\rangle\langle j| \right), \\ &= -\operatorname{Tr}\left(\sum_{i,j} p_i \log p_j \, |i\rangle \, \langle i|j\rangle \, \langle j| \right). \end{aligned} \tag{3.45}$$

Since the set $\{|i\rangle\}$ is necessarily orthonormal, we obtain:

$$\begin{aligned} S(\rho) &= -\operatorname{Tr}\left(\sum_{i,j} p_i \log p_j \, |i\rangle\langle j| \, \delta_{ij}\right), \\ &= -\operatorname{Tr}\left(\sum_{i} p_i \log p_i \, |i\rangle\langle i|\right), \\ &= -\left(\sum_{i} p_i \log p_i \, \langle i|i\rangle\right), \\ &= -\sum_{i} p_i \log p_i. \end{aligned} \tag{3.46}$$

Therefore, von Neumann entropy reduces to Shannon entropy for systems represented by diagonal density matrices. These systems lack quantum coherence and thus possess a purely classical probability distribution.

The Von Neumann entropy is therefore broader than the Shannon entropy, which is a particular case. Quantum entropy (3.42) accounts for both classical uncertainties and quantum uncertainties present in the system [57].

3.3.4 Properties

Let us now examine some properties of von Neumann entropy. These properties can be found in references [57, 58].

Property 1: Non-Negativity. Quantum entropy $S(\rho)$ is non-negative for any density operator ρ:

$$S(\rho) \geq 0. \tag{3.47}$$

Proof. Using the spectral decomposition of ρ, equation (3.43), we can express von Neumann entropy as:

$$S(\rho) = -\sum_{i} p_i \log p_i.$$

The terms $-p_i \log p_i$ are non-negative for all i, since $0 \leq p_i \leq 1$, and therefore $\log p_i \leq 0$. Thus:

$$S(\rho) \geq 0. \tag{3.48}$$

The validity of this proof applies to any density operator ρ, regardless of whether it exhibits coherence or not. This is because von Neumann entropy is entirely determined by the eigenvalues of ρ, which remain invariant under basis transformations [58]. Off-diagonal terms do not affect the eigenvalues, and therefore, even if

the state possesses coherence, the quantum entropy remains unchanged. Hence, $S(\rho) \geq 0$ is a general property of quantum entropy.

Property 2: Minimum Value. The minimum value of quantum entropy is zero, and it occurs when the density operator represents a pure state.

Proof. Assuming $p_i = 1$ and $p_j = 0$, $\forall j \neq i$ in equation (3.46), we obtain: $S(\rho) = -1 \log 1 - \sum_{i \neq j} 0 \log 0$. Since, by convention, $0 \log 0 \equiv 0$, we get $S(\rho) = 0$ for the given pure state.

This aligns with the physical interpretation of quantum entropy: in a pure state, the information gained from measuring the system is zero, as it is fully defined without any statistical mixture.

Formally, this is related to the fact that the density matrix of pure states has rank equal to 1, indicating that only one eigenvalue is nonzero.

Property 3: Maximum Value. The maximum value of quantum entropy is $\log d$, where d is the system's dimension. This value occurs for the maximumly mixed state:

$$\rho = \frac{I}{d}. \tag{3.49}$$

Proof. Considering the state (3.49), the eigenvalues of ρ are uniform and equally probable: $p_i = \frac{1}{d}$, $\forall i$. Substituting these values into the von Neumann entropy expression (3.46), we obtain:

$$\begin{aligned} S(\rho) &= -\sum_{i=1}^{d} \frac{1}{d} \log \frac{1}{d}, \\ &= -d \frac{1}{d} \log \frac{1}{d}, \\ &= -\log \frac{1}{d} = \log d. \end{aligned} \tag{3.50}$$

Therefore, the maximum quantum entropy value, $\log d$, is reached for the maximally mixed state.

Unlike **Property 2**, where the absence of uncertainty leads to a minimum entropy, here the entropy reaches its maximum value due to a complete lack of knowledge about the state of the system. The maximally mixed state implies that all probabilities associated with different eigenvalues are equal, similar to the microcanonical ensemble case presented in the previous section.

Property 4: Concavity. Let $\rho_i \in D(\mathcal{H})$ and p_i be the probability distribution associated with ρ_i. Quantum entropy is concave in the density operator, meaning

that:

$$S(\rho) \geq \sum_i p_i S(\rho_i), \tag{3.51}$$

where $\rho = \sum_i p_i \rho_i$.

Proof. To prove (3.51), let us consider an auxiliary system B, whose state space has an orthonormal basis $\{|i\rangle\}$ in space $\mathcal{H}_B$, associated with the index i of the operators ρ_i. The joint state ρ_{AB}, with $\rho_A \equiv \sum_i p_i \rho_i \in \mathcal{H}_A$, is given by:

$$\rho_{AB} \quad = \sum_i p_i \rho_i \otimes |i\rangle\langle i| \,. \tag{3.52}$$

Calculating entropies $S(\rho_A)$ and $S(\rho_B)$:

$$S(\rho_A) = S\left(\sum_i p_i \rho_i\right), \tag{3.53}$$

and

$$S(\rho_B) = S\left(\sum_i p_i \, |i\rangle\langle i|\right) = H(p_i). \tag{3.54}$$

Computing the joint entropy $S(\rho_{AB})$:

$$\begin{aligned} S(\rho_{AB}) &= -\operatorname{Tr}\left(\rho_{AB} \log \rho_{AB}\right) \\ &= -\operatorname{Tr}\left(\sum_i p_i \rho_i \otimes |i\rangle\langle i| \log \left(\sum_j p_j \rho_j \otimes |j\rangle\langle j|\right)\right). \end{aligned} \tag{3.55}$$

which can be rewritten as:

$$S(\rho_{AB}) = -\sum_{ij} p_i \operatorname{Tr}\left(\rho_i \otimes |i\rangle\langle i| \log \left(p_j \rho_j \otimes |j\rangle\langle j|\right)\right). \tag{3.56}$$

Again, using the orthonormality of bases $\{|i\rangle\}$ and $\{|j\rangle\}$ to eliminate a summation:

$$\sum_{ij} p_i \operatorname{Tr}\left(\rho_i \otimes |i\rangle\langle i| \log \left(p_j \rho_j \otimes |j\rangle\langle j|\right)\right) = \sum_i p_i \operatorname{Tr}\left(\rho_i \otimes |i\rangle\langle i| \log \left(p_i \rho_i \otimes |i\rangle\langle i|\right)\right). \tag{3.57}$$

Thus, we obtain:

$$S(\rho_{AB}) = -\sum_i p_i \operatorname{Tr}\left(\rho_i \otimes |i\rangle\langle i| \log \left(p_i \rho_i \otimes |i\rangle\langle i|\right)\right), \tag{3.58}$$

Using $\log(p_i\rho_i \otimes |i\rangle\langle i|) = \log(p_i\rho_i) \otimes |i\rangle\langle i|$, we get

$$\begin{aligned} S(\rho_{AB}) = & - \sum_i p_i \operatorname{Tr}(\rho_i \otimes |i\rangle\langle i| \, (\log p_i + \log \rho_i) \otimes |i\rangle\langle i|), \\ = & - \sum_i p_i \left[\operatorname{Tr}(\rho_i \otimes |i\rangle\langle i| \log p_i \otimes |i\rangle\langle i|)\right. \\ & + \left. \operatorname{Tr}(\rho_i \otimes |i\rangle\langle i| \log \rho_i \otimes |i\rangle\langle i|)\right]. \end{aligned} \tag{3.59}$$

Using property $\operatorname{Tr}[(A \otimes B)(C \otimes D)] = \operatorname{Tr}(AC)\operatorname{Tr}(BD)$, we obtain the following:

$$S(\rho_{AB}) = -\sum_i p_i \left[\operatorname{Tr}(\rho_i \log p_i)\operatorname{Tr}(|i\rangle\langle i| \, |i\rangle\langle i|) + \operatorname{Tr}(\rho_i \log \rho_i)\operatorname{Tr}(|i\rangle\langle i| \, |i\rangle\langle i|)\right], \tag{3.60}$$

since $\operatorname{Tr}(|i\rangle\langle i| \, |i\rangle\langle i|) = 1$ and $\operatorname{Tr}(\rho_i \log p_i) = \log p_i \operatorname{Tr}(\rho_i) = \log p_i$, we get:

$$\begin{aligned} S(\rho_{AB}) &= -\sum_i p_i \left(\log p_i + \operatorname{Tr}(\rho_i \log \rho_i)\right), \\ &= -\sum_i p_i \log p_i - \sum_i p_i \operatorname{Tr}(\rho_i \log \rho_i), \\ &= H(p_i) + \sum_i p_i S(\rho_i). \end{aligned} \tag{3.61}$$

Substituting (3.53), (3.54), and (3.61) into the subadditivity property of entropy, $S(\rho_{AB}) \leq S(\rho_A) + S(\rho_B)$, we obtain:

$$H(p_i) + \sum_i p_i S(\rho_i) \leq S\left(\sum_i p_i \rho_i\right) + H(p_i), \tag{3.62}$$

which results in equation (3.51).

The expression (3.51) can be understood as a measure of the influence of the additional uncertainty arising from the mixing. The inequality reflects that the uncertainty about the mixed state ρ is not just a simple average of the uncertainties of the component states ρ_i, but also includes the additional uncertainty associated with the lack of knowledge about which state ρ_i was chosen in the mixture. This extra uncertainty arises from the probability distribution p_i and is related to the ignorance about the index i [58].

Property 5: Isometric Invariance. Let $\rho \in D(\mathcal{H})$ and $U : \mathcal{H} \to \mathcal{H}'$ be isometry. The quantum entropy is invariant under isometries, meaning that:

$$S(\rho) = S(U\rho U^\dagger). \tag{3.63}$$

Proof. The eigenvalues of a density operator are invariant under isometries. We can write:

$$U\rho U^\dagger = U\left(\sum_i p_i \left|i\right\rangle\!\left\langle i\right|\right)U^\dagger, \tag{3.64}$$

$$= \sum_i p_i \left|\phi_i\right\rangle\!\left\langle\phi_i\right|, \tag{3.65}$$

where $\{|\phi_i\rangle\}$ is an orthonormal basis such that $U|i\rangle = |\phi_i\rangle$. Thus, since entropy depends only on the eigenvalues, it remains invariant under isometric transformations.

3.3.5 Quantum Relative Entropy and Quantum Mutual Information

In this section, we define two important quantities associated with quantum entropy. However, before introducing these definitions, we first present the concepts of *kernel* and *support* of an operator.

Kernel

The kernel of an operator is the subspace formed by its eigenvectors with zero eigenvalues [58]. Given an operator $A \in \mathcal{L}(\mathcal{H}, \mathcal{H}')$, where $\mathcal{L}(\mathcal{H}, \mathcal{H}')$ is the space of all linear operators mapping vectors from $\mathcal{H}$ to $\mathcal{H}'$, the kernel of A, $\ker(A)$, is defined as [57]:

$$\ker(A) = \{|\psi\rangle \in \mathcal{H} \mid A|\psi\rangle = 0\}, \tag{3.66}$$

Thus, the kernel of the operator A is a subspace of the Hilbert space $\ker(A) \subseteq \mathcal{H}$.

Support

The support of an operator is the subspace formed by the operator's eigenvectors with nonzero eigenvalues [58]. Given an operator $A \in \mathcal{L}(\mathcal{H}, \mathcal{H}')$, the support of A, $\sup(A)$, is defined as [57]:

$$\sup(A) = \{|\psi\rangle \in \mathcal{H} \mid \exists\ |\phi\rangle \in \mathcal{H} \ \text{ with } \ A|\phi\rangle = |\psi\rangle\}. \tag{3.67}$$

The support is also a subspace of the Hilbert space, $\sup(A) \subseteq \mathcal{H}$, and by definition it is orthogonal to its kernel [57]:

$$\sup(A) = \ker(A)^\perp = \{\,|\psi\rangle \in \mathcal{H} \mid \ \langle\psi|\phi\rangle = 0,\ \forall\ |\phi\rangle \in \ker(A)\}\,. \tag{3.68}$$

Thus, we can write: $\mathcal{H} = \sup(A) \oplus \ker(A)$.

Now, we are ready to define *quantum relative entropy* and *quantum mutual information.*

Quantum Relative Entropy

Given two states represented by the density matrices $\rho \in \mathcal{H}$ and $\sigma \in \mathcal{H}$, the relative quantum entropy of ρ with respect to σ is defined as [58]:

$$S(\rho \parallel \sigma) = \mathrm{Tr}(\rho \ln \rho) - \mathrm{Tr}(\rho \ln \sigma), \tag{3.69}$$

provided that the condition

$$\sup(\rho) \subseteq \sup(\sigma), \tag{3.70}$$

is satisfied. Otherwise, $S(\rho \parallel \sigma) = +\infty$ [57].

Condition (3.70) ensures that the subspace of $\mathcal{H}$ where ρ acts non-trivially is also "accessible" to σ. In other words, if ρ allows the possibility that the system being in some state $|\psi\rangle$, then σ must also allow this possibility. Otherwise, if $\ker(\rho)$ has a non-trivial intersection with $\sup(\sigma)$—that is, if there exists a state $|\chi\rangle$ with a nonzero probability for ρ but a zero probability for σ—the term $\mathrm{Tr}(\rho \ln \sigma) \to -\infty$, leading to $S(\rho \parallel \sigma) \to +\infty$. Therefore, condition (3.70) ensures that $S(\rho \parallel \sigma)$ is well-defined and finite [57, 58].

The quantum relative entropy is non-negative[4], and it equals zero only when $\rho = \sigma$. Moreover, it is not a symmetric quantity and does not satisfy the triangle inequality. Thus, it cannot be considered a true metric in the strict mathematical sense. However, it can be interpreted as a measure of "distinction" between two density matrices in the state space [54].

Quantum Mutual Information

Consider two subsystems A and B, described by the density operators ρ_A and ρ_B, respectively. The quantum mutual information between A and B, denoted by $\mathcal{I}_{\rho_{AB}}(A : B)$, is defined as [54, 58]:

$$\mathcal{I}_{\rho_{AB}}(A : B) = S(\rho_A) + S(\rho_B) - S(\rho_{AB}) = S(\rho_{AB} \parallel \rho_A \otimes \rho_B), \tag{3.71}$$

where $S(\rho) = -\mathrm{Tr}(\rho \ln \rho)$ is the von Neumann entropy and $S(\rho_{AB} \parallel \rho_A \otimes \rho_B)$ is the relative quantum entropy between ρ_{AB} and the state of the product $\rho_A \otimes \rho_B$.

Thus, $\mathcal{I}_{\rho_{AB}}(A : B)$ quantifies the information shared between parts of the system, which is lost when the bipartite system is separated or when access to one of

[4] $S(\rho \parallel \sigma) \geq 0$, also known as Klein's inequality [58].

its parts is removed [58]. Therefore, it also serves as a measure of both classical and quantum correlations existing between the two parts of the system [57].

3.3.6 Entropy Production in Quantum Dynamics

We will continue our discussion by analysing entropy production in the context of dynamic quantum systems. To this end, we will discuss the approach presented in [11], which considers systems strongly coupled to finite reservoirs. This approach is of great importance in understanding entropy production in this context, as it relates irreversibility to system-reservoir correlations that develop during the dynamics of the composite system.

In addition to being consistent with the second law of thermodynamics, the formulation in [11] provides a deeper understanding of irreversibility in out-of-equilibrium systems.

To derive the results from [11], let us consider a system S, represented by the state $\rho_s(t)$, in contact with N finite thermal reservoirs r, described by $\rho_r(t)$. Initially, we assume that the reservoirs are in thermal states:

$$\rho_r(0) = \rho_r^{th} = \frac{\exp\left(-\beta_r H_r\right)}{Z_r}, \tag{3.72}$$

where H_r is the Hamiltonian, $\beta_r = \frac{1}{T_r}$ is the inverse temperature, and Z_r is the canonical partition function, all referring to the reservoir. We assume that H_r is time-independent.

The system and the reservoirs are coupled at time $t = 0$, and the initial density operator of the composite system can be written as:

$$\rho(0) = \rho_s(0) \prod_r \rho_r(0). \tag{3.73}$$

This coupling occurs due to the activation of an interaction potential $V(t)$ between the system and the reservoirs. Initially, we assume that the system and the reservoirs do not share any correlations (classical or quantum), allowing us to write equation (3.73). The correlations develop during the evolution of the composite system $\rho(t)$, which follows the Liouville equation for the total Hamiltonian [11]:

$$H(t) = H_s(t) + \sum_r H_r + V(t). \tag{3.74}$$

Our interest lies in the evolution of the system and in the characterisation of the irreversibility of this process. Therefore, let us consider the entropy of the system

$S(\rho_s(t))$:

$$S(\rho_s(t)) = -\operatorname{Tr}_s \rho_s(t) \log \rho_s(t), \tag{3.75}$$

where $\rho_s(t) = \operatorname{Tr}_r \rho(t)$ is the reduced state.

It is important to note that the evolution of the composite system $\rho(t) = U\rho(0)U^\dagger$ does not modify the entropy due to the unitarity of the process, given **Property 5**, which means that $S(\rho(0)) = S(\rho(t))$. However, when considering only the evolution of the system, which behaves as an open system, we can no longer assume that the process is unitary. As a result, we expect that $S(\rho_s(t)) \neq S(\rho_s(0))$ [11].

Thus, we can understand that disregarding the degrees of freedom of the environment ensures the irreversibility of the process [54].

Starting from the invariance of the entropy of the composite system:

$$\begin{aligned} S(\rho(t)) &= S(\rho(0)), \\ -\operatorname{Tr}(\rho(t)\log\rho(t)) &= -\operatorname{Tr}(\rho(0)\log\rho(0)), \end{aligned} \tag{3.76}$$

considering that the system and the reservoir are initially decoupled (3.73) and that the initial states of the reservoirs are given by (3.72), we obtain:

$$-\operatorname{Tr}(\rho(t)\log\rho(t)) = -\operatorname{Tr}(\rho_s(0)\log\rho_s(0)) - \sum_r \operatorname{Tr}\left(\rho_r^{th}\log\rho_r^{th}\right), \tag{3.77}$$

which can be rewritten as:

$$\operatorname{Tr}(\rho(t)\log\rho(t)) - \sum_r \operatorname{Tr}\left(\rho_r^{th}\log\rho_r^{th}\right) = \operatorname{Tr}(\rho_s(0)\log\rho_s(0)) = -S(\rho_s(0)). \tag{3.78}$$

Since the entropy variation of the system is given by $\Delta S(\rho_s) = S(\rho_s(t)) - S(\rho_s(0))$, using (3.78), we have:

$$\Delta S(\rho_s) = -\operatorname{Tr}_s(\rho_s(t)\log\rho_s(t)) + \operatorname{Tr}(\rho(t)\log\rho(t)) - \sum_r \operatorname{Tr}_r(\rho_r^{th}\log\rho_r^{th}), \tag{3.79}$$

Since $\operatorname{Tr}_s[\rho_s(t)\log\rho_s(t)] = \operatorname{Tr}_s[\operatorname{Tr}_r(\rho(t))\log\rho_s(t)] = \operatorname{Tr}[\rho(t)\log\rho_s(t)]$, we obtain:

$$\Delta S(\rho_s) = -\operatorname{Tr}(\rho(t)\log\rho_s(t)) + \operatorname{Tr}(\rho(t)\log\rho(t)) - \sum_r \operatorname{Tr}_r(\rho_r^{th}\log\rho_r^{th}). \tag{3.80}$$

Considering the equality[5]

$$-\operatorname{Tr}(\rho(t)\log\rho_s(t)) = -\operatorname{Tr}\left(\rho(t)\log\left[\rho_s(t)\prod_r \rho_r^{th}\right]\right) + \sum_r \operatorname{Tr}_r(\rho_r(t)\log\rho_r^{th}), \tag{3.81}$$

we can rewrite (3.80) as:

$$\begin{aligned}\Delta S(\rho_s) = &- \operatorname{Tr}\left(\rho(t)\log\left[\rho_s(t)\prod_r \rho_r^{th}\right]\right) + \sum_r \operatorname{Tr}_r(\rho_r(t)\log\rho_r^{th}) \\ &+ \operatorname{Tr}(\rho(t)\log\rho(t)) - \sum_r \operatorname{Tr}_r(\rho_r^{th}\log\rho_r^{th}), \\ = &- \operatorname{Tr}\left(\rho(t)\log\left[\rho_s(t)\prod_r \rho_r^{th}\right]\right) + \operatorname{Tr}(\rho(t)\log\rho(t)) \\ &+ \sum_r \operatorname{Tr}\left[\rho_r(t) - \rho_r^{th}\right]\log\rho_r^{th}.\end{aligned} \tag{3.82}$$

Equation (3.82) can be rewritten as a sum of two independent contributions to the variation of the system's entropy. The first contribution is due to the reversible heat flux:

$$\begin{aligned}\Delta_e S(\rho_s) &= \sum_r \operatorname{Tr}\left[\rho_r(t) - \rho_r^{th}\right]\log\rho_r^{th}, \\ &= \sum_r \operatorname{Tr}\left(\rho_r(t)\log\rho_r^{th}\right) - \sum_r \operatorname{Tr}\left(\rho_r^{th}\log\rho_r^{th}\right).\end{aligned} \tag{3.83}$$

Since $\rho_r^{th} = \frac{e^{-\beta_r H_r}}{Z_r}$, we have:

$$\log\rho_r^{th} = -\beta_r H_r - \log Z_r. \tag{3.84}$$

Thus, equation (3.83) becomes:

$$\Delta_e S(\rho_s) = \sum_r \operatorname{Tr}\left[\rho_r(t)\left(-\beta_r H_r - \log Z_r\right)\right] - \sum_r \operatorname{Tr}\left[\rho_r^{th}\left(-\beta_r H_r - \log Z_r\right)\right].$$

Rewriting,

$$\Delta_e S(\rho_s) = \sum_r \beta_r\left(\operatorname{Tr}\left[\rho_r^{th} H_r\right] - \operatorname{Tr}\left[\rho_r(t) H_r\right]\right) + \sum_r \log Z_r\left(\operatorname{Tr}\rho_r^{th} - \operatorname{Tr}\rho_r(t)\right).$$

[5] To verify this equality, write $\operatorname{Tr}\left(\rho(t)\log\left[\rho_s(t)\prod_r \rho_r^{th}\right]\right) = \operatorname{Tr}(\rho(t)\log\rho_s(t)) + \sum_r \operatorname{Tr}\left(\rho(t)\log\rho_r^{th}\right)$ and use the property $\operatorname{Tr}\left(\rho(t)\log\rho_r^{th}\right) = \operatorname{Tr}_r(\rho_r(t)\log\rho_r^{th})$.

Since $\mathrm{Tr}\,\rho_r(t) = \mathrm{Tr}\,\rho_r^{th} = 1$, due to the normalisation of the density matrices and using the definition of expectation values $\langle A\rangle_t = \mathrm{Tr}[\rho(t)A]$, we obtain:

$$\begin{aligned}\Delta_e S(\rho_s) &= \sum_r \beta_r \left(\langle H_r\rangle_0 - \langle H_r\rangle_t\right), \\ &= \sum_r \beta_r Q_r(t),\end{aligned} \tag{3.85}$$

where $Q_r(t) \equiv \langle H_r\rangle_0 - \langle H_r\rangle_t$.

Equation (3.85) relates the entropy flux to the exchange of energy (heat) between the system and the reservoirs. Note the similarity to the heat exchange term in the expression of classical entropy production (3.6).

The second contribution to the system's entropy variation is given by:

$$\begin{aligned}\Delta_i S(\rho_s) &= -\,\mathrm{Tr}\left(\rho(t)\log\left[\rho_s(t)\prod_r \rho_r^{th}\right]\right) + \mathrm{Tr}(\rho(t)\log\rho(t)), \\ &= S\left(\rho(t) \parallel \rho_s(t)\prod_r \rho_r^{th}\right) \equiv \Sigma,\end{aligned} \tag{3.86}$$

The term represented by (3.86) is associated with the irreversibility of the process in the system's transformation. Noting that, due to the semi-positivity of relative entropy, we have $\Sigma \geq 0$, with equality only when the system and reservoirs are completely uncorrelated at time t. We can interpret the system's entropy production Σ as a measure of how far the joint system state, $\rho(t)$, is from the uncorrelated state $\rho_s(t)\prod_r \rho_r^{th}$ [11][6].

Thus, the entropy variation of the system is written as:

$$\Delta S(\rho_s(t)) = \Sigma + \sum_r \beta_r Q_r(t), \tag{3.87}$$

which provides the thermodynamic relation for the entropy variation of a quantum system evolving out of equilibrium. Moreover, the construction presented here gives us an expression for entropy production, equation (3.86), arising from the evolution of a quantum system in contact with finite reservoirs under strong coupling [11].

Again, it is worth emphasising the similarity with the case discussed at the beginning of this chapter. We note that both in (3.6) and (3.87), the entropy variation in the system is expressed in terms of a contribution associated with a reversible process: energy exchange between the system and the reservoirs, and a contribution associated with an irreversible process: the deviation of the current system

[6] Relate to Mutual Information

state $\rho(t)$ from the initial uncorrelated state in the quantum case.

Entropy and Correlation

We may ask ourselves what the origin of entropy production is in the context presented above. To discuss this point, we note that the sum of the entropies of the reservoirs and the system does not result in the total entropy, i.e. $S(\rho_s(t)) + \sum_r S(\rho_r(t)) \neq S(\rho(t))$. Equality is only obtained when we consider the entropic contribution due to the correlations created during the system's evolution, $S_c(t)$, taking the form:

$$S(\rho(t)) = S(\rho_s(t)) + \sum_r S(\rho_r(t)) + S_c(t), \tag{3.88}$$

Recalling that the system and the reservoir are initially uncorrelated, we have $S_c(0) = 0$.

Since the total system entropy is given by $S(\rho(t)) = -\operatorname{Tr}(\rho(t)\log\rho(t))$, we can rewrite (3.88) from the perspective of the entropy associated with correlation:

$$S_c(t) = -\operatorname{Tr}(\rho(t)\log\rho(t)) - S(\rho_s(t)) - \sum_r S(\rho_r(t)). \tag{3.89}$$

To continue our analysis, let us consider $S\left(\rho(t) \parallel \rho_s(t)\prod_r \rho_r(t)\right) = \operatorname{Tr}\left(\rho(t)\log\rho(t)\right) - \operatorname{Tr}\left(\rho(t)\log\rho_s(t)\prod_r \rho_r(t)\right)$, which can be rewritten as[7]:

$$\begin{aligned} &S\left(\rho(t) \parallel \rho_s(t)\prod_r \rho_r(t)\right) = \\ &= \operatorname{Tr}(\rho(t)\log\rho(t)) - \operatorname{Tr}(\rho(t)\log\rho_s(t)) - \sum_r \operatorname{Tr}(\rho(t)\log\rho_r(t)), \\ &= \operatorname{Tr}(\rho(t)\log\rho(t)) - \operatorname{Tr}_s(\rho_s(t)\log\rho_s(t)) - \sum_r \operatorname{Tr}_r(\rho_r(t)\log\rho_r(t)). \end{aligned} \tag{3.90}$$

Since $S(\rho_s(t)) = -\operatorname{Tr}_s \rho_s(t)\log\rho_s(t))$ and $S(\rho_r(t)) = -\operatorname{Tr}_r \rho_r(t)\log\rho_r(t))$, we obtain:

$$S\left(\rho(t) \parallel \rho_s(t)\prod_r \rho_r(t)\right) = \operatorname{Tr}\rho(t)\log\rho(t) + S(\rho_s(t)) + \sum_r S(\rho_r(t)),$$

[7]Here, we use the property $\operatorname{Tr}_{ab}\rho_{ab}(t) = \operatorname{Tr}_a(\operatorname{Tr}_b \rho_{ab}(t))$ and the fact that $\operatorname{Tr}_s \rho(t) = \rho_r(t)$ and $\operatorname{Tr}_r \rho(t) = \rho_s(t)$.

Compared with (3.89), we arrive at the following:

$$S\left(\rho(t) \parallel \rho_s(t)\prod_r \rho_r(t)\right) = -S_c(t). \tag{3.91}$$

Since $S\left(\rho(t) \parallel \rho_s(t)\prod_r \rho_r(t)\right) \geq 0$, the entropy contained in the correlation is strictly non-positive, $S_c(t) \leq 0$ [11], and can be directly associated with entropy production by equation (3.86) in the thermodynamic limit, where we have $\rho_r(t) = \rho_r^{th}$:

$$-S_c(t) = \Sigma. \tag{3.92}$$

Equation (3.92) can be interpreted as follows: the correlation entropy is the negative of the entropy production in the system when we approximate the reservoirs as ideal reservoirs in the Gibbs state ρ_r^{th} [11].

In addition, we can consider the variations in entropy in the system. Starting from (3.88), we obtain:

$$\Delta S(\rho(t)) = \Delta S(\rho_s(t)) + \sum_r \Delta S(\rho_r(t)) + \Delta S_c(t). \tag{3.93}$$

Since total entropy is invariant under unitary transformation, $\Delta S(\rho(t)) = 0$ (see **Property 5** – subsection 3.3.4), and given that $S_c(0) = 0$ ensures $\Delta S_c(t) = S_c(t)$, we can write:

$$S_c(t) = -\Delta S(\rho_s(t)) - \sum_r \Delta S(\rho_r(t)), \tag{3.94}$$

In the thermodynamic limit, $\Delta S(\rho_s(t))$ can be written in the form of (3.87), resulting in:

$$\begin{aligned} S_c(t) &= -\Sigma - \sum_r \beta_r Q_r - \sum_r \Delta S_r(t), \\ \Sigma + S_c(t) &= -\sum_r \beta_r Q_r - \sum_r \Delta S_r(t), \end{aligned} \tag{3.95}$$

Using equations (3.86) and (3.91), we can rewrite:

$$\begin{aligned}
\Sigma + S_c(t) &= S\left(\rho(t) \parallel \rho_s(t)\prod_r \rho_r^{th}\right) - S\left(\rho(t) \parallel \rho_s(t)\prod_r \rho_r(t)\right), \\
&= -\operatorname{Tr}\left(\rho(t)\log\rho_s(t)\prod_r \rho_r^{th}\right) + \operatorname{Tr}\left(\rho(t)\log\rho_s(t)\prod_r \rho_r(t)\right), \\
&= -\sum_r \operatorname{Tr}_r(\rho_r(t)\log\rho_r^{th}) + \sum_r \operatorname{Tr}_r(\rho_r(t)\log\rho_r(t)), \\
&= \sum_r S\left(\rho_r(t) \parallel \rho_r^{th}\right). \qquad (3.96)
\end{aligned}$$

Therefore, from (3.95) and (3.96), we obtain:

$$\Sigma + S_c(t) = -\sum_r \beta_r Q_r - \sum_r \Delta S_r(t) = \sum_r S\left(\rho_r(t) \parallel \rho_r^{th}\right) \geq 0 \qquad (3.97)$$

since relative entropy is always non-negative.

The result presented by [11] is highly relevant to the study of entropy production, as it is obtained without requiring restrictions on finite systems or weak coupling. The relationship between Σ and system-reservoir correlations provides a unified perspective on irreversibility in quantum systems, emerging from the process to which the system is subject.

The general expression for entropy production (3.86) respects the second law of thermodynamics and enables a connection between microscopic and macroscopic regimes, as it is based on correlations created between the system and the reservoir and, under certain approximations, recovers macroscopic results.

Interpreting it as a measure of the deviation of the current state from the evolved uncorrelated state is essential for studying non-equilibrium systems. This formulation provides a solid foundation for investigating strongly coupled systems and finite reservoirs within the context of quantum thermodynamics.

Landauer's Principle

Landauer's principle is a key practical example of the connection between thermodynamics and information. Initially proposed in the classical context, based on Clausius' inequality (3.1), it provides a bound linking the heat absorbed by a thermal reservoir to the entropy change of a system in contact with it [54]. For a system in contact with a single reservoir, this inequality takes the form:

$$Q \geq -T\Delta S_s, \qquad (3.98)$$

which establishes a lower bound for the heat Q absorbed by the reservoir in a process where the entropy of the system changes by ΔS_s. The fact that this erasure occurs because of the system-reservoir interaction makes the process inherently irreversible, resulting in entropy production associated with the operation.

This relation, proposed by Landauer, can be stated in two different ways [58]:

> "Suppose a computer erases a single bit of information. The amount of energy dissipated into the environment is *at least* $k_B T \ln 2$, where k_B is a universal constant known as *Boltzmann's constant*, and T is the temperature of the environment of the computer."

which considers the energy cost of information erasure, and:

> "Suppose a computer erases a single bit of information. The entropy of the environment increases by *at least* $k_B \ln 2$, where k_B is Boltzmann's constant."

which describes the increase in entropy in the reservoir.

Thus, Landauer's principle states that the logical erasure of a bit of information in a physical system requires the dissipation of a minimum amount of energy as heat into a thermal reservoir. This dissipation can also be interpreted as an increase in the entropy of the reservoir as a result of the heat transfer from the system.

This minimum energy is given by [58]:

$$Q \geq k_B T \ln 2, \tag{3.99}$$

where Q is the minimum heat dissipated in the process, k_B is Boltzmann's constant, and T is the reservoir temperature.

Notably, the required heat dissipation and consequent entropy production imply that the process involved is irreversible. Thus, information erasure in a system is an irreversible process governed by the entropy production rules discussed above. In this sense, Landauer's principle can be understood as a direct consequence of the second law in the form $\Sigma = \frac{Q}{T} + \Delta S_s$ [58].

However, despite its initial formulation in terms of classical thermodynamics, Landauer's principle is general and applies to both classical and quantum systems. The only distinction is that, in the classical case, the entropy involved in the process is the system's thermodynamic entropy, whereas in quantum processes, it is the informational entropy [54].

The fact that entropy production can be generalised in the form (3.87), as proposed by [11], ensures that Landauer's principle is also a consequence of the second

law in the quantum context. Starting from (3.87), we can write [54]:

$$\Sigma = \Delta S(\rho_s(t)) + \sum_r \beta_r Q_r(t). \tag{3.100}$$

Since the second law of thermodynamics ($\Sigma \geq 0$) holds for this form of entropy production, we obtain:

$$\begin{aligned} \Delta S(\rho_s(t)) + \sum_r \beta_r Q_r(t) \geq 0, \\ \Delta S(\rho_s(t)) + \beta Q(t) \geq 0, \end{aligned} \tag{3.101}$$

which, considering a single reservoir, results in an expression analogous to the "classical" Landauer's principle, equation (3.98):

$$Q(t) \geq T\Delta S(\rho_s(t)), \tag{3.102}$$

where $\Delta S(\rho_s(t))$ represents the change in the quantum entropy of the system.

Thus, Landauer's principle can be derived from the entropy production framework introduced in [11], making it a direct consequence of the second law of thermodynamics. Furthermore, obtaining this relation emphasises that the irreversibility of the information erasure process is intrinsically linked to the interaction between the system and the thermal reservoir. The heat dissipation involved in this interaction not only ensures the validity of the second law of thermodynamics but also establishes the entropy production as a direct measure of this irreversibility.

In essence, irreversibility arises from the dynamic correlations established between the system and the reservoir, reinforcing the central role of entropy production in the thermodynamic description of non-equilibrium systems [54].

3.3.7 Nonequilibrium Entropy Production for Driven Quantum Systems

In this section, we derive a microscopic expression for the nonequilibrium mean entropy production of an open driven system weakly coupled to a single reservoir. In addition, we discuss specific cases derived from the general expression. The derivation presented here is based on [60].

Consider a system with a time-dependent Hamiltonian $H(t)$, driven by an external parameter over a finite time interval τ. The system is weakly coupled to a single infinitely large reservoir with which it can exchange energy in the form of heat.

Moreover, the system's initial and final states are not thermally in equilibrium with the reservoir. However, they are in local thermal equilibrium at inverse temperatures β_i and β_f, respectively, allowing us to define thermodynamic quantities. It is important to note that the system does not need to remain near equilibrium throughout the process.

Let us analyse how the system's entropy changes during this process. The assumption of local equilibrium at both the initial and final times allows us to define entropy and internal energy at these instants, and consequently their variations.

The change in system entropy is given by:

$$\Delta S(\rho_s(t)) = \langle \Sigma \rangle + \beta \langle Q \rangle, \tag{3.103}$$

while the variation of internal energy is given by [60]:

$$\Delta U = \langle W \rangle + \langle Q \rangle, \tag{3.104}$$

where $\langle W \rangle$ is the work performed on the system by an external agent.

Note that equation (3.103) is exactly the same as (3.87), in the case where the system is coupled to a single reservoir at inverse temperature β.[8]

From (3.103) and (3.104), we obtain:

$$\begin{aligned} \langle \Sigma \rangle &= \Delta S_s - \beta \langle Q \rangle \\ &= \Delta S_s - \beta \Delta U + \beta \langle W \rangle. \end{aligned} \tag{3.105}$$

The initial and final states of the system are given by the density operators ρ_i and ρ_f:

$$\rho_i = \frac{e^{-\beta_i H_0}}{Z_i}, \tag{3.106}$$

$$\rho_f = \frac{e^{-\beta_f H_\tau}}{Z_f}, \tag{3.107}$$

where H_0 and H_τ are the Hamiltonians at times $t = 0$ and $t = \tau$, and Z_i and Z_f are the initial and final partition functions, respectively.

Using these expressions, we can compute the three terms in equation (3.105). Beginning with the entropy change $\Delta S_s = S_f - S_i$, and using equation (3.42), we obtain:

$$\Delta S_s = -\operatorname{Tr}(\rho_f \ln \rho_f) + \operatorname{Tr}(\rho_i \ln \rho_i). \tag{3.108}$$

[8] The transition to expectation values is justified by fluctuation theorems, which ensure the validity of thermodynamic laws in an average sense, even outside equilibrium; These theorems guarantee that $\langle \Sigma \rangle \geq 0$ and that the mean heat flows $\langle Q \rangle$ obey thermodynamic constraints.

The second term in (3.105), associated with the internal energy variation, can be written as:

$$\begin{aligned}\beta\Delta U &= \beta(U_f - U_i)\\ &= \mathrm{Tr}(\rho_f \beta H_\tau) - \mathrm{Tr}(\rho_i \beta H_0),\end{aligned} \tag{3.109}$$

where we have used the definition of mean energy for a given state: $U_n = \mathrm{Tr}(\rho_n H_n)$ [60].

Now, consider two states in thermal equilibrium with the reservoir: $\rho_0^{th} = \frac{e^{-\beta H_0}}{Z_0}$ is the initial state in thermal equilibrium with the reservoir at inverse temperature β, and $\rho_\tau^{th} = \frac{e^{-\beta H_\tau}}{Z_\tau}$ is the final state under the same condition. Here, $Z_{0(\tau)}$ is the partition function of the system in its initial (final) state. These are the relaxed states corresponding to the initial and final states in local equilibrium —i.e., the states that would be reached if ρ_i and ρ_f were allowed to fully equilibrate with the reservoir.

From ρ_0^{th} and ρ_τ^{th}, we obtain the relations:

$$\begin{aligned}\ln \rho_0^{th} &= \ln\left(\frac{e^{-\beta H_0}}{Z_0}\right),\\ \ln \rho_0^{th} &= -\beta H_0 - \ln Z_0,\\ \beta H_0 &= -\ln \rho_0^{th} - \ln Z_0,\end{aligned} \tag{3.110}$$

and

$$\begin{aligned}\ln \rho_\tau^{th} &= \ln\left(\frac{e^{-\beta H_\tau}}{Z_\tau}\right),\\ \ln \rho_\tau^{th} &= -\beta H_\tau - \ln Z_\tau,\\ \beta H_\tau &= -\ln \rho_\tau^{th} - \ln Z_\tau.\end{aligned} \tag{3.111}$$

Substituting equations (3.110) and (3.111) into (3.109), we obtain:

$$\begin{aligned}\beta\Delta U &= \mathrm{Tr}\big[\rho_f(-\ln \rho_\tau^{th} - \ln Z_\tau)\big] - \mathrm{Tr}\big[\rho_i(-\ln \rho_0^{th} - \ln Z_0)\big],\\ &= -\mathrm{Tr}\big(\rho_f \ln \rho_\tau^{th}\big) - \mathrm{Tr}(\rho_f \ln Z_\tau) + \mathrm{Tr}\big(\rho_i \ln \rho_0^{th}\big) + \mathrm{Tr}(\rho_i \ln Z_0),\\ &= \mathrm{Tr}\big(\rho_i \ln \rho_0^{th}\big) - \mathrm{Tr}\big(\rho_f \ln \rho_\tau^{th}\big) + \ln Z_0\,\mathrm{Tr}(\rho_i) - \ln Z_\tau\,\mathrm{Tr}(\rho_f),\\ &= \mathrm{Tr}\big(\rho_i \ln \rho_0^{th}\big) - \mathrm{Tr}\big(\rho_f \ln \rho_\tau^{th}\big) + \ln Z_0 - \ln Z_\tau,\end{aligned} \tag{3.112}$$

where we used the normalisation of the density operators, $\mathrm{Tr}(\rho_{i,f}) = 1$.

Finally, to obtain the term related to work, we use the definition:

$$\langle W\rangle = \int_0^\tau \mathrm{Tr}(\rho_t \partial_t H_t)dt, \tag{3.113}$$

which relates the average work to the time-dependent expectation value of the system's Hamiltonian variation [60]. This definition was originally proposed in [61].

Note that we are now dealing with the instantaneous state of the system at an arbitrary time during the process. Thus, it is necessary to define an instantaneous equilibrium state associated with ρ_t:

$$\rho_t^{th} = \frac{e^{-\beta H_t}}{Z_t}, \tag{3.114}$$

where H_t and Z_t are the Hamiltonian and the partition function at time t, and β is the inverse temperature of the reservoir.

From (3.114), we obtain H_t:

$$\begin{aligned} \ln \rho_t^{th} &= \ln\left(\frac{e^{-\beta H_t}}{Z_t}\right) \\ \ln \rho_t^{th} &= -\beta H_t - \ln Z_t \\ \beta H_t &= -\ln \rho_t^{th} - \ln Z_t. \end{aligned} \tag{3.115}$$

Taking the time derivative of (3.115):

$$\beta \partial_t H_t = -\partial_t \ln \rho_t^{th} - \partial_t \ln Z_t. \tag{3.116}$$

Using (3.113) and (3.116), we obtain:

$$\begin{aligned} \beta\langle W\rangle &= \beta \int_0^\tau \mathrm{Tr}(\rho_t \partial_t H_t) dt, \\ &= \int_0^\tau \mathrm{Tr}\big[\rho_t(-\partial_t \ln \rho_t^{th} - \partial_t \ln Z_t)\big] dt, \\ &= -\int_0^\tau \mathrm{Tr}\big(\rho_t \partial_t \ln \rho_t^{th}\big) dt - \int_0^\tau \mathrm{Tr}(\rho_t \partial_t \ln Z_t) dt. \end{aligned} \tag{3.117}$$

Since $\int_0^\tau \mathrm{Tr}(\rho_t \partial_t \ln Z_t) dt = \int_0^\tau \mathrm{Tr}(\rho_t) \partial_t \ln Z_t dt = \ln Z_t|_0^\tau$, we obtain:

$$\beta\langle W\rangle = -\int_0^\tau \mathrm{Tr}\big(\rho_t \partial_t \ln \rho_t^{th}\big) dt - \ln Z_\tau + \ln Z_0. \tag{3.118}$$

Finally, combining equations (3.108), (3.112), and (3.118), we obtain from (3.105):

$$\begin{aligned} \langle \Sigma\rangle &= \mathrm{Tr}(\rho_i \ln \rho_i) - \mathrm{Tr}\big(\rho_i \ln \rho_0^{th}\big) - [\mathrm{Tr}(\rho_f \ln \rho_f) - \mathrm{Tr}\big(\rho_f \ln \rho_\tau^{th}\big)] - \int_0^\tau \mathrm{Tr}\big(\rho_t \partial_t \ln \rho_t^{th}\big) dt \\ \langle \Sigma\rangle &= S(\rho_i \parallel \rho_0^{th}) - S(\rho_f \parallel \rho_\tau^{th}) - \int_0^\tau \mathrm{Tr}\big(\rho_t \partial_t \ln \rho_t^{th}\big) dt. \end{aligned} \tag{3.119}$$

Equation (3.119) provides the exact form of the entropy production in a quantum

system weakly coupled to a single thermal reservoir, subjected to an arbitrarily out-of-equilibrium process [60].

For the above derivation, we started from arbitrary states ρ_i and ρ_f, requiring only that they were in local equilibrium so that we could define thermodynamic quantities. We then defined equivalent thermal equilibrium states ρ_0^{th} and ρ_τ^{th} to evaluate the out-of-equilibrium evolution based on the equilibrium evolution. We also introduced an instantaneous equilibrium state ρ_t^{th} associated with the state of the system at any time during the evolution process. Figure 3.1 provides a schematic representation of how we treated evolution.

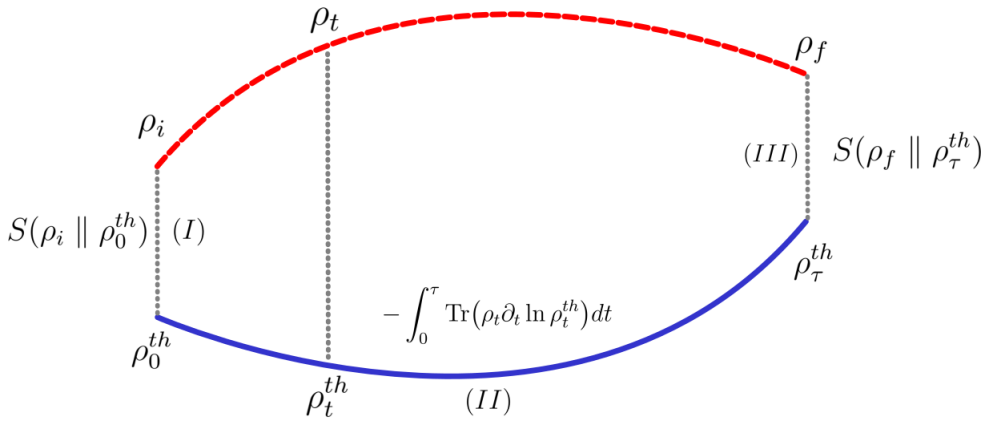

FIGURE 3.1: The figure shows a schematic representation of the equilibrium evolution between the states ρ_0^{th} and ρ_τ^{th} (blue line) and the out-of-equilibrium evolution between the states ρ_0 and ρ_τ (dashed red line). Additionally, the three stages contributing to the entropy production given by (3.119) are highlighted. Figure based on reference [60].

From a practical perspective, equation (3.119) describes the entropy production in the considered process as the sum of the entropy productions in the three stages shown in Figure 3.1:

(I) **Initial Entropy Production:** In this stage, the system transitions from the arbitrary initial state ρ_i to the equivalent thermal state ρ_0^{th}, in equilibrium with the reservoir. This process generates the entropy production described by the relative entropy between the two states:

$$S(\rho_i \parallel \rho_0^{th}) = \mathrm{Tr}(\rho_i \ln \rho_i) - \mathrm{Tr}\big(\rho_i \ln \rho_0^{th}\big). \tag{3.120}$$

This term represents the entropic cost of adjusting the initial system ρ_i to the corresponding thermal state ρ_0^{th} [60].

(II) **Out-of-Equilibrium Evolution:** Once in the initial thermal state ρ_0^{th}, the system evolves under an arbitrary external protocol while remaining in

local equilibrium with the reservoir at all times t. The entropy production in this stage accumulates continuously and is described by the integral term:

$$-\int_0^\tau \mathrm{Tr}\big(\rho_t \partial_t \ln \rho_t^{th}\big)\, dt, \tag{3.121}$$

which measures the "displacement" of the instantaneous thermal state ρ_t^{th} over time.

This stage captures the contribution of irreversibility associated with the evolution process itself, and its magnitude depends on how the system is manipulated during the protocol.

(III) **Final Entropy Production:** Finally, the system transitions from the final thermal state ρ_τ^{th} back to the arbitrary final state ρ_f. As in the first stage, this transition generates entropy production described by the relative entropy:

$$S(\rho_f \parallel \rho_\tau^{th}) = \mathrm{Tr}(\rho_f \ln \rho_f) - \mathrm{Tr}\big(\rho_f \ln \rho_\tau^{th}\big). \tag{3.122}$$

This term reflects the entropic cost of adjusting the system to the final arbitrary state ρ_f [60].

The total entropy production is given by these three contributions, independent of reservoir details, and is valid for arbitrarily out-of-equilibrium intermediate states.

Some considerations, which we will briefly mention, can be made to simplify the expression (3.119). For example, assuming a process in which the system undergoes only relaxation, without performing the work ($\partial_t H_t = 0$), reduces the production of entropies to the term associated with stage (I). Alternatively, considering that the system initially starts in the thermal state $\rho_i = \rho_0^{th}$ and ends in equilibrium with the reservoir, $\rho_f = \rho_\tau^{th}$, results in the production of entropy coming only from the stage (II)[9].

Next, we discuss the case used in our work: a closed system starting from the thermal state.

3.3.8 Closed System

An important constraint will be of great utility for the development of our work. We will consider a closed system, initially in a thermal state $\rho_i = \rho_0^{th}$. Since it is

[9]For more details on these considerations, refer to [60].

closed, the system does not exchange energy as heat with the environment, implying that the production of entropy is exclusively due to the irreversibility associated with the internal transformations of the system. Additionally, the system's evolution will be described by unitary dynamics, ensuring the conservation of von Neumann entropy, $\partial_t S(\rho_t) = 0$. Thus, any observed change in entropy or system dynamics will be attributed exclusively to changes in the internal state rather than dissipative external interactions [60].

As a consequence of this consideration, equation (3.119) simplifies to:

$$\langle \Sigma \rangle = -\int_0^\tau \mathrm{Tr}\big(\rho_t \partial_t \ln \rho_t^{th}\big) dt \tag{3.123}$$

which represents the entropy production associated with stage (II) of the general process presented in Figure 3.1. However, the unitarity of the dynamics allows us to rewrite this equation. Taking the time derivative $\partial_t S(\rho_t \parallel \rho_\tau^{th})$:

$$\partial_t S(\rho_t \parallel \rho_\tau^{th}) = \partial_t \,\mathrm{Tr}(\rho_t \ln \rho_t) - \partial_t \,\mathrm{Tr}\big(\rho_t \ln \rho_t^{th}\big). \tag{3.124}$$

Noting that the first term is precisely the time variation of von Neumann entropy, which is zero, we can rewrite:

$$\begin{aligned} \partial_t S(\rho_t \parallel \rho_\tau^{th}) &= -\partial_t \,\mathrm{Tr}\big(\rho_t \ln \rho_t^{th}\big), \\ &= -\,\mathrm{Tr}\big[\partial_t(\rho_t \ln \rho_t^{th})\big], \\ &= -\,\mathrm{Tr}\big[\partial_t(\rho_t) \ln \rho_t^{th} + \rho_t \partial_t(\ln \rho_t^{th})\big], \\ &= -\,\mathrm{Tr}\big(\rho_t \partial_t \ln \rho_t^{th}\big). \end{aligned} \tag{3.125}$$

Substituting (3.125) into (3.123), we obtain:

$$\begin{aligned} \langle \Sigma \rangle &= \int_0^\tau \partial_t S(\rho_t \parallel \rho_t^{th}) dt = S(\rho_t \parallel \rho_t^{th})|_0^\tau, \\ &= S(\rho_\tau \parallel \rho_\tau^{th}) - S(\rho_0 \parallel \rho_0^{th}). \end{aligned} \tag{3.126}$$

Since we assumed the system is initially in the thermal state, the second term on the right-hand side vanishes, leaving:

$$\langle \Sigma \rangle = S(\rho_\tau \parallel \rho_\tau^{th}) \geq 0. \tag{3.127}$$

Equation (3.127) demonstrates that, for a closed system undergoing unitary dynamics, the production of entropy is determined exclusively by the relative entropy between the final arbitrary state ρ_τ and the equivalent thermal state ρ_τ^{th}. This reflects the irreversibility associated with the internal transformations of the system.

Chapter 4

Asymmetry on Quantum States

The study of asymmetry in quantum systems is motivated by the fact that physical dynamics are often constrained by underlying symmetries. For instance, symmetry under time translations imposes constraints on the energy of the system, while rotational symmetry implies conservation of angular momentum. The asymmetry then quantifies the degree to which a state breaks such symmetries and provides insight into the possible transformations allowed under symmetric dynamics [20].

The goal of this chapter is to explore the concept of asymmetry in quantum systems. We begin with a brief discussion of symmetric transformations and their role in defining invariance under a given symmetry group. Next, we address the informational perspective, where asymmetry is regarded as a resource that enables tasks such as parameter estimation and the establishment of quantum reference frames. Finally, we introduce quantitative measures of asymmetry, which will serve as the main tools for analyzing dynamical symmetry breaking and restoration in the subsequent chapters of this thesis.

4.1 Symmetry Transformations

Consider a physical system evolving under some dynamics. Initially, the system may display certain symmetry properties, such as invariance under rotations around a given axis, parity transformations, or time translations. Transformations can then be applied to this system, which may preserve or break those properties.

Symmetry transformations can be understood as maps that take physical states in the Hilbert space to other states within the same space, preserving the relevant structural features, such as the preservation of the inner product, the physical structure of observables, and the structure of the state space. These maps satisfy properties such as associativity, the existence of an identity transformation, and invertibility. As a consequence, the mathematical framework underlying the description of symmetries is *group theory* [62].

The action of any symmetry transformation is represented by a unitary operator acting on the Hilbert space of the system, and thus such transformations cannot affect the physical properties of the system [63].

An important consequence of this invariance is that, in the absence of an external reference frame[1], states connected by symmetry transformations are operationally indistinguishable. This means that no G-covariant operation, which will be introduced later in this section, can distinguish between a state and its symmetry-transformed versions. In other words, applying a symmetry transformation to the system does not change any physically accessible property. The ability to distinguish between these states would require access to an external reference frame.

The set of symmetry transformations of a physical object forms a group, which must satisfy the following axioms [63, 65]:

- **Closure**: the composition of two symmetry transformations is itself a symmetry transformation of the system.
- **Associativity**: the composition of transformations is associative, reflecting the associativity of the underlying maps acting on the state space.
- **Identity**: the group contains the identity transformation, which leaves the system unchanged.
- **Inverse**: every transformation has an inverse that also preserves the system's symmetry.

In this sense, a symmetry transformation is represented by a map that takes a state into another state within the same invariant subspace. Thus, the algebraic structure of a group provides the natural language to characterise invariance and symmetry in physical systems.

Next, we introduce the formal mathematical definition of a group, its unitary representations, and the notion of operations that remain invariant under a given symmetry. In addition, we introduce some examples of symmetry groups that will be particularly relevant to the discussions developed throughout this work.

[1] A *reference frame* is a physical system that provides a standard for interpreting relational quantities such as orientation, phase, or time. Since absolute directions or phases have no operational meaning, states related by symmetry transformations (e.g., rotations) become indistinguishable in the absence of such a system. A reference frame therefore enables the preparation, comparison, and measurement of asymmetric states, making it possible to distinguish states within a group orbit. For a detailed discussion of quantum reference frames and their role in symmetry and information, refer to [64].

4.1.1 Group of symmetry

Let's us define formally group, element of a group and how these elements act in a state of the system.

Definition 1 (Group G). *A set G, together with a binary operation $*$, is said to form a group if its elements $g \in G$ satisfy the following properties [66, 67]:*

1. ***Closure:*** *For all $g_i, g_j \in G$,*

$$g_i * g_j = g_k, \qquad g_k \in G. \tag{4.1}$$

2. ***Associativity:*** *For all $g_i, g_j, g_k \in G$,*

$$(g_i * g_j) * g_k = g_i * (g_j * g_k). \tag{4.2}$$

3. ***Identity:*** *There exists an element $e \in G$ such that for all $g \in G$,*

$$e * g = g * e = g. \tag{4.3}$$

4. ***Inverse:*** *For each $g \in G$, there exists an element $g^{-1} \in G$ such that*

$$g^{-1} * g = g * g^{-1} = e. \tag{4.4}$$

In the context of physical systems, a general symmetry is described by a group whose elements are associated with symmetry transformations. These elements act by mapping a state ρ to another state $\mathcal{U}_g(\rho)$, representing the symmetry-transformed version of the original state. In quantum theory, this transformation is represented by a unitary operator $U(g)$, in one-to-one correspondence with the group element g.

Thus, a transformation associated with an element $g \in G$ is represented by the map [20]:

$$\rho \mapsto \mathcal{U}_g(\rho) \tag{4.5}$$

where $\mathcal{U}_g(\rho) \equiv U_g \, \rho \, U_g^{\dagger}$[2] is the superoperator implementing the transformation. This map, in the context of symmetry transformations in quantum mechanics, is a *projective representation* of the group G.

[2]Here, and in several instances throughout the text, we use the equivalence $U(g) \equiv U_g$ for the sake of notational simplicity.

The set of all states transformed by the elements of G is called the *group orbit* of ρ [20]:

$$\mathcal{O}_G(\rho) = \{\, \mathcal{U}_g(\rho) = U_g \rho U_g^\dagger \mid g \in G \,\}. \tag{4.6}$$

For groups admitting linear representations, the map (4.5) associates each element $g \in G$ with a unitary operator $U(g)$ acting on the Hilbert space $\mathcal{H}$ in such a way that the group multiplication law is exactly preserved $U(g_1)U(g_2) = U(g_1 g_2)$, $\forall\, g_1, g_2 \in G$. This means that applying two successive group transformations is precisely equivalent to applying the single transformation associated with the composition $g_1 * g_2$.

However, in quantum mechanics, since two vectors differ only by a global phase $e^{i\phi}$ represent the same physical state, the state is in fact a *ray* in the Hilbert space. That is, it corresponds to the set of all vectors of the form $e^{i\phi}\,|\cdot\rangle$, which are equivalent up to a global phase.

As a result, the unitary operators associated with symmetry transformations are required to preserve the group multiplication law only up to a phase factor. This leads to the notion of a *projective representation* of the group.

Formally, a projective representation of a group G is a map

$$g \mapsto U(g), \tag{4.7}$$

such that for any pair $g_1, g_2 \in G$,

$$U(g_1)U(g_2) = \omega(g_1, g_2)\, U(g_1 g_2), \tag{4.8}$$

where $\omega(g_1, g_2)$ is called the *cocycle* of the representation and is a complex phase that satisfies $|\omega(g_1, g_2)| = 1$. If the phase factor is trivial, $\omega(g_1, g_2) = 1$ for all pairs, the representation reduces to a standard linear representation, also called *unitary representation* [63].

4.1.2 G-invariant states and G-covariant operators

Given a group of symmetry G, there may exist states that are not affected by a given transformation. That is, under the action of a unitary operator $U(g)$, one may have $\mathcal{U}_g(\rho) = \rho$. Such states are called *invariant states*. The subgroup of G with respect to which a state ρ is invariant is called the *symmetry subgroup* of the state. If all elements of G belong to the symmetry subgroup, then ρ is invariant under all symmetry transformations, that is,

$$\forall\, g \in G, \quad \mathcal{U}_g(\rho) = \rho. \tag{4.9}$$

The states satisfying Eq. (4.9) are called G-*invariant states* [23, 65].

It is worth noting that G-invariant states generate trivial group orbits, since every symmetry transformation acts trivially on the state. In other words, all elements of G map ρ to the same physical state. Consequently, G-invariant states possess no distinguishable structure with respect to the symmetry group and, therefore, occupy a single point in the space of group orbits.

In the framework of the resource theory of asymmetry, G-invariant states are identified as *free states*. These states satisfy condition (4.9), which means that they remain unchanged under the action of the symmetry group. Physically, this implies that no measurement can distinguish ρ from any of its symmetry-transformed versions $U_g \rho U_g^\dagger$, so such states carry no information about the group elements. Consequently, they cannot be used to infer or encode the value of a group parameter, such as a rotation angle in the rotational symmetry case. Within this framework, asymmetry becomes a valuable resource: states that are not G-invariant contain information about the symmetry group and can therefore be exploited to perform tasks that require a reference frame, such as parameter estimation or the implementation of symmetry-breaking operations [68, 69].

Another important concept within this framework is that of G-*covariant operations*. An operation $\mathcal{E}(\cdot)$ is said to be G-covariant, that is, covariant with respect to a symmetry group G, if it satisfies the following condition [23, 63, 68]:

$$\mathcal{E}(U_g \rho U_g^\dagger) = U_g \mathcal{E}(\rho) U_g^\dagger, \qquad \forall\, g \in G. \tag{4.10}$$

In other words, these operations commute with all the symmetry transformations of the group, meaning that they are themselves symmetric and cannot generate asymmetry. Physically, this implies that for any initial state and for any symmetry transformation, the final state is independent of the order in which the symmetry operation and the dynamical map $\mathcal{E}$ are applied. This property can be represented pictorially in Fig. 4.1.

Recalling once again the perspective of the resource theory of asymmetry, the operations that satisfy condition (4.10) are referred to as *free operations*. In this context, they are operations that cannot generate resources such as asymmetry in a quantum state. Therefore, when applied to a free (G-invariant) state, they produce another free state, that is, they map the set of free states onto itself. Moreover, when applied to non-free states, those possessing a nonzero amount of resource, they must not increase the amount of asymmetry [68, 69].

An important implication of G-invariance is that, in the absence of an external reference frame, states connected by symmetry transformations are operationally

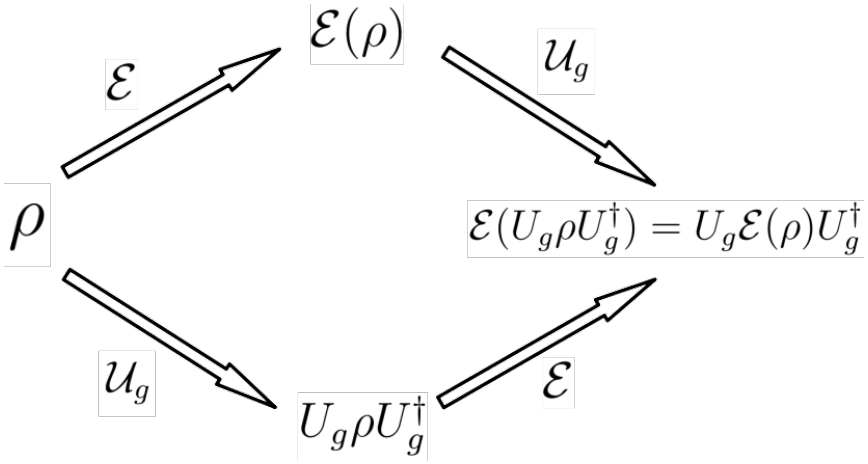

FIGURE 4.1: Schematic representation of a G-covariant operation. Figure based in ref. [63].

indistinguishable. In this case, no G-covariant operation can distinguish ρ from $U_g\rho U_g^\dagger$, since applying a symmetry transformation does not alter any physically accessible property.

From the perspective of resource theory, this indistinguishability shows that asymmetry and reference frames are deeply related [69]. A G-invariant state represents the absence of such a reference, while an asymmetric one provides it, encoding information about the symmetry group and allowing tasks such as parameter estimation or frame alignment.

4.1.3 Examples

To conclude this subsection, we briefly present a few examples of symmetry groups. We focus on the symmetry groups associated with the Lipkin–Meshkov–Glick (LMG) model, since this is the model used in our work.

Permutation symmetry

We begin with the group composed of all permutation operations, also known as the symmetric group, S_N. Given a set of N distinct objects $\{a_i\}_{i=1}^N$, there exist $N!$ distinct arrangements of these objects. Each such arrangement corresponds to a unique permutation and, therefore, to an element of the group S_N. Thus, S_N is a finite group of order $N!$ [66, 67].

As a simple example, consider the case $N = 3$, with the set $\{a, b, c\}$. A permutation can be represented by cycle notation, for instance $P = (1\,3)$, which exchanges the first and third elements while leaving the second fixed:

$$P\{a, b, c\} = \{c, b, a\}. \tag{4.11}$$

The full symmetric group on three elements is therefore

$$S_3 = \big\{(1),\ (1\,2),\ (1\,3),\ (2\,3),\ (1\,2\,3),\ (1\,3\,2)\big\}, \tag{4.12}$$

where (1) denotes the identity permutation (no reordering).

Taking into account a quantum system composed of N subsystems, a generic product state can be written as $|i_1\rangle \otimes |i_2\rangle \otimes \cdots \otimes |i_N\rangle$. The action of a permutation group element $\pi \in S_N$ is represented as:

$$U_\pi \left(|i_1\rangle \otimes |i_2\rangle \otimes \cdots \otimes |i_N\rangle \right) = \left|i_{\pi^{-1}(1)}\right\rangle \otimes \left|i_{\pi^{-1}(2)}\right\rangle \otimes \cdots \otimes \left|i_{\pi^{-1}(N)}\right\rangle, \tag{4.13}$$

where U_π is the unitary operator that implements the permutation in the quantum state.

This representation is unitary for all $\pi \in S_N$ and satisfies

$$U_{\pi_1} U_{\pi_2} = U_{\pi_1 * \pi_2}, \qquad U_{(1)} = \mathbb{I}, \qquad U_{\pi^{-1}} = U_\pi^\dagger. \tag{4.14}$$

In the context of the LMG model, which will be discussed in the next chapter, the spin sites of the chain can be regarded as permutable particles. Because all spins interact collectively and identically, the Hamiltonian is invariant under any permutation of spin indices:

$$[H_{\mathrm{LMG}},\, U_\pi] = 0 \quad ; \quad \forall\, \pi \in S_N. \tag{4.15}$$

This invariance implies that the dynamics is restricted to the fully symmetric subspace of the Hilbert space, significantly simplifying the structure of the model.

Physically, permutation symmetry reflects the fact that no spin carries an individual identity within the dynamics: exchanging two sites does not change any observable property of the system. Breaking this symmetry, on the other hand, would mean that spins no longer evolve collectively, destroying the equivalence among constituents and modifying the accessible subspace of states.

Spin–rotation symmetry

Rotations are implemented through group transformations. In 3D physical space, rotations are described by the Lie group $SO(3)$. However, when dealing with spin systems, rotational transformations are represented by the compact Lie group $SU(2)$, whose generators are the angular momentum operators (J_x, J_y, J_z) satisfying the

commutation relations [62, 66]:

$$[J_i, J_j] = i\,\epsilon_{ijk}\,J_k \quad ; \quad i,j,k = x,y,z, \tag{4.16}$$

where ϵ_{ijk} is the Levi–Civita symbol.

For a general spin state ρ, a rotation by an angle θ around an axis $\mathbf{n}$ has unitary representation

$$U(\hat{n},\theta) = e^{-i\theta\,\hat{n}\cdot\mathbf{J}}. \tag{4.17}$$

Considering a spin-$\frac{1}{2}$ system, the operators J_i are given in terms of the Pauli matrices σ_i. In this case, the unitary representation of the group takes the form:

$$U(\hat{n},\theta) = e^{-i\frac{\theta}{2}\,\hat{n}\cdot\sigma}. \tag{4.18}$$

We can see that a rotation by 2π does not act as the identity, but rather as a global phase factor equal to -1. Setting $\theta = 2\pi$ in (4.18), we obtain[3]

$$U(\hat{n},2\pi) = e^{-i\pi\,\hat{n}\cdot\sigma} = \cos(\pi)\,\mathbb{I} - i\sin(\pi)\,\hat{n}\cdot\sigma = -\mathbb{I}. \tag{4.19}$$

Equation (4.19) shows that a rotation by $\theta = 2\pi$ is equivalent to the action of the negative identity operator, meaning that it produces a state that is physically identical but with a general minus sign. This result is counterintuitive compared to classical rotations, for which a 2π rotation returns the system to its original state. In contrast, for rotations in spin systems, a 4π rotation is required for the system to return to its initial state [70].

This characteristic of rotations in spin systems is a consequence of the surjective *two-to-one* homomorphism[4] between the groups $SU(2)$ and $SO(3)$. For each rotation described by an element of $SO(3)$, there exist two corresponding elements in $SU(2)$, namely U and $-U$. This relation is known as the double covering of the group $SO(3)$ by the group $SU(2)$ [67, 70].

Once again invoking the LMG model, we note that the Hamiltonian, given in (5.11)[5], can be rewritten, in the isotropic case $\gamma = 1$, in the form:

$$\hat{H}_{\gamma=1} = -2h\,\hat{J}_x - \frac{J}{j}\left(\mathbf{J}^2 - \hat{J}_x^2\right). \tag{4.20}$$

[3]Here we use the expansion $e^{-i\frac{\theta}{2}\,\hat{n}\cdot\boldsymbol{\sigma}} = \sum_{l=0}^{\infty}\frac{\left(-i\frac{\theta}{2}\,\hat{n}\cdot\boldsymbol{\sigma}\right)^l}{l!}$ and the identities $(\hat{n}\cdot\boldsymbol{\sigma})^{2l} = \mathbb{I}$ and $(\hat{n}\cdot\boldsymbol{\sigma})^{2l+1} = \hat{n}\cdot\boldsymbol{\sigma}$. In this way, the terms with even powers combine into the cosine term of the expression, while the terms with odd powers give rise to the sine term.

[4]A homomorphism between two groups is a correspondence between their elements that preserves the group multiplication laws [66].

[5]For clarity: $\hat{H} = -2h\hat{J}_x - \frac{J}{j}\left(\hat{J}_z^2 + \gamma\hat{J}_y^2\right)$

since $\hat{J}_z^2 + \hat{J}_y^2 = \mathbf{J}^2 - \hat{J}_x^2$. As a consequence, we obtain:

$$[\hat{H}_{LMG}^{\gamma=1},\ \hat{J}_x] = 0, \tag{4.21}$$

indicating invariance under rotations around the x axis. The presence of anisotropy breaks this rotational invariance.

Parity (spin-flip) symmetry

As a final example of symmetry, we introduce the discrete symmetry group $\mathbb{Z}_2$, also known as *parity* or *spin-flip* symmetry. The group $\mathbb{Z}_2$ consisting of only two elements,

$$\mathbb{Z}_2 = \{\mathbb{I},\ p\}, \tag{4.22}$$

where $\mathbb{I}$ denotes the identity element and p is the inversion symmetry operation, satisfying $p * p = \mathbb{I}$.

In spin systems, the $\mathbb{Z}_2$ symmetry is associated with a global spin-flip transformation, which reverses the sign of certain spin components. In the context of collective spin operators, this transformation can be represented by the unitary operator [71, 72]

$$\hat{\Pi}_x = e^{i\pi(\hat{J}_x - j)}, \tag{4.23}$$

with j being the quantum number of the total angular momentum along the x direction. Therefore, $\hat{\Pi}_x$ generates a reflection with respect to the x axis in spin space.

Under this transformation, the collective spin operators transform as [73]

$$\hat{\Pi}_x \hat{J}_x \hat{\Pi}_x^\dagger = \hat{J}_x, \qquad \hat{\Pi}_x \hat{J}_y \hat{\Pi}_x^\dagger = -\hat{J}_y, \qquad \hat{\Pi}_x \hat{J}_z \hat{\Pi}_x^\dagger = -\hat{J}_z. \tag{4.24}$$

Therefore, the spin-flip operation leaves the x component invariant while reversing the sign of the transverse components.

When acting on an eigenstate of $\hat{J}_x$, denoted by $|j, m_x\rangle$, the parity operator yields

$$\hat{\Pi}_x |j, m_x\rangle = e^{i\pi(m_x - j)} |j, m_x\rangle = (-1)^{(m_x - j)} |j, m_x\rangle , \tag{4.25}$$

since $m_x = -j, -j+1, \ldots, j-1, j$, the quantity $m_x - j$ is always an integer. If $m_x - j$ is even, the action of $\hat{\Pi}_x$ yields $+|j, m_x\rangle$; otherwise, if $m_x - j$ is odd, the result of the operation is $-|j, m_x\rangle$. Therefore, when acting on an eigenstate of H, the parity operator can present eigenvalues ± 1, defining two distinct parity sectors in the Hilbert space of the system [72].

Considering again the model described by the Hamiltonian (5.11), we can see that the Hamiltonian commutes with the parity transformation operator (4.23):

$$[H_{LMG}, \Pi_x] = 0. \tag{4.26}$$

which shows that the Hamiltonian of the system is invariant under the parity operation. This can be seen straightforwardly, since the operators that are flipped under the action of $\hat{\Pi}_x$, see Eq. (4.24), appear quadratically in the Hamiltonian (5.11). Moreover, Eq. (4.26) implies that one can construct a common eigenbasis for both operators, $\{|E_{n,p}\rangle\}$, where the index p labels the parity sector such that:

$$H_{LMG}\,|E_{n,p}\rangle = E_n\,|E_{n,p}\rangle\,, \tag{4.27}$$

$$\Pi_x\,|E_{n,p}\rangle = \pm\,|E_{n,p}\rangle\,. \tag{4.28}$$

However, despite the invariance of the Hamiltonian system under the parity operator, the system may be prepared in states that are not parity invariant.

For instance, in the next chapter, where we describe the LMG model in more detail and present the DQPT in this system, we consider the dynamics starting from the ground state of H_0[6], given by the eigenstate corresponding to all spins aligned along the z direction, $|j, m_z\rangle = |j, +j\rangle$, which is one of the degenerate ground states of H_0. This state is not invariant under the action of the parity operator Π_x, since $\Pi_x\,|j, \pm m_z\rangle = |j, \mp m_z\rangle$, even though H_0 itself is invariant under parity. Therefore, we start from a state that spontaneously breaks the $\mathbb{Z}_2$ symmetry, a fact that plays a crucial role in the characterisation of both the QPT and the DQPT in this model [72, 73].

4.2 Asymmetry of Quantum States

As discussed in the previous section, the asymmetry of a quantum state can be regarded as a resource within the framework of the asymmetry resource theory. Consequently, it is of interest to quantify the amount of asymmetry a physical state possesses, that is, to measure how strongly a given state breaks the symmetry associated with a particular group.

[6] We set $h = 0$ in Eq. (5.11): $\hat{H}_0 = -\frac{J}{j}\left(\hat{J}_z^2 + \gamma \hat{J}_y^2\right)$.

4.2.1 Asymmetry Properties

A function $f(\cdot)$, defined as $f : \mathcal{D}(\mathcal{H}) \to \mathbb{R}$, that quantifies the amount of resource contained in a quantum state ρ must satisfy the following general conditions [74]:

1. $f(\rho) \geq 0$.
2. $f(\rho) = 0$ if ρ is a free state.
3. $f(\rho) \geq f(\mathcal{E}(\rho))$ if $\mathcal{E}$ is a free operation.

Since asymmetry is treated as a resource, these conditions must be satisfied by any valid asymmetry measure. The first condition guarantees the non-negativity of the measure, the second ensures that free (i.e., symmetric or G-invariant) states possess a zero resource value, and the third expresses the *monotonicity*, meaning that the amount of asymmetry cannot increase under free (i.e., G-covariant) operations, as discussed in the previous section. Together, these properties provide a consistent framework for quantifying asymmetry as a resource in quantum systems.

Moreover, the measure should also satisfy the property of *convexity*, which guarantees that statistical mixtures of states cannot increase the amount of resource. In other words, for any pair of states ρ_1 and ρ_2, and any $0 \leq p \leq 1$,

$$f\left(p\rho_1 + (1-p)\rho_2\right) \leq pf(\rho_1) + (1-p)f(\rho_2). \tag{4.29}$$

This means that random mixing of states introduces classical uncertainty, which tends to wash out information about the symmetry of the system, never increasing it. This property is therefore essential for any monotonic asymmetry [68].

An important classification to make is that of *G-equivalent states*. Considering a given symmetry group, we may have non-free states with respect to this group. As discussed previously, these states have the ability to break, to some extent, the symmetry of the group, that is, possess a certain amount of resource (asymmetry). However, within a given set of states, there are those that share the same amount of resource, and these states are called G-equivalent.

These states can be reversibly interconverted by G-covariant operations [23]. This means that, although G-equivalent states are not invariant under the symmetry transformations, they share the same amount of asymmetry or, in other words, the same "symmetry-breaking power", unlike G-invariant states, which exhibit a complete absence of the resource.

Formally, we can define the following: two states, ρ and σ, are said to be G-equivalent if and only if they can be reversibly interconverted by G-covariant operations, i.e., if there exist operations $\mathcal{E}$ and $\mathcal{F}$ such that [63]:

$$\forall\, g \in G \quad , \quad [\mathcal{E}, \mathcal{U}_g] = 0 \quad \text{with} \quad \mathcal{E}(\rho) = \sigma \tag{4.30}$$

and

$$\forall\, g \in G \quad , \quad [\mathcal{F}, \mathcal{U}_g] = 0 \quad \text{with} \quad \mathcal{F}(\sigma) = \rho. \tag{4.31}$$

The commutation conditions with the superoperator ensure that the operations are G-covariant.

As an example, consider the group $SU(2)$, presented in subsection 4.1.3. A state with a total angular momentum equal to zero is invariant under any rotation, while a state with nonzero angular momentum is not G-invariant. Nevertheless, all states resulting from rotations of a given angular momentum vector form a class of G-equivalent states, since they possess the same magnitude of angular momentum, that is, the same amount of resource associated with the breaking of rotational symmetry.

4.2.2 Informational approach

The purpose of this section is to introduce the informational perspective on symmetry. Our aim is to show that asymmetry can be interpreted as a form of information, and therefore quantities originating from information theory can be used as valid asymmetry measures. To illustrate this idea, consider the following communication task.

Suppose that the scientist A wants to communicate a spatial direction $\hat{\mathbf{n}} \in \mathbb{R}^3$ to the scientist B. To do this, A prepares a spin-j system in a coherent state whose mean spin points along that direction, and sends the state to B. Formally, a coherent spin state is obtained by rotating the maximal–weight eigenstate, $|\psi_{\hat{\mathbf{n}}}\rangle = R(\hat{\mathbf{n}})\ |j, j\rangle$, with $\langle \mathbf{J} \rangle = \hbar j\, \hat{\mathbf{n}}$. For $j = \frac{1}{2}$, a coherent state pointing in the $+x$ direction is, for example, $|+x\rangle = \frac{1}{\sqrt{2}}(|+z\rangle + |-z\rangle)$.

From the point of view of B's point of view, the information about the direction $\hat{\mathbf{n}}$ is encoded in the received quantum state. By taking measurements along different directions, B can estimate which direction was sent. If A prepared a state pointing along $\hat{z}$, measurements of $\mathbf{J} \cdot \hat{z}$ yield outcomes concentrated near $\hbar j$, while measurements along orthogonal directions give smaller expectation values. The larger the spin j, the smaller the uncertainty in the estimation, scaling as $\frac{1}{j}$ [20].

However, the ability to perform the estimation depends directly on the asymmetry of the received state. Without asymmetry, that is, if the state is G-invariant with

respect to the rotation group, B would not be able to infer any direction, because all measurement outcomes would be indistinguishable from each other. Thus, the state asymmetry is essential for the success of the task of transmitting the desired information.

Therefore, a state must break the symmetry of the group, $SU(2)$ in our example, to carry information about a spatial direction. The stronger the symmetry breaking, the greater the capacity of the state to encode such information. A purely coherent state has maximal asymmetry with respect to $SU(2)$; on the contrary, mixed states that reduce $|\langle \mathbf{J} \rangle|$ decrease both asymmetry and the amount of accessible information. The maximally mixed state, $\rho_{\text{mix}} = \mathbb{I}/(2j+1)$, is G-invariant since $U_g \rho_{\text{mix}} U_g^\dagger = \rho_{\text{mix}}$ for all $g \in SU(2)$, and therefore it does not encode any direction, making parameter communication impossible. Hence, the asymmetry of the state is the resource that enables operational inference of the direction. Then we can infer that rotational asymmetry can be quantified by the amount of information the state encodes about spatial orientation [20].

The example given above can be viewed in light of the group–theoretic concepts introduced earlier. Recalling that symmetry transformations of a system are given by the projective representation $\mathcal{U}_g(\rho) = U_g \rho U_g^\dagger$, if a physical state is non-free, then the orbit $\{\mathcal{U}_g(\rho) : g \in G\}$ is composed of physically distinguishable states. Consequently, an asymmetric state ρ can encode information about the elements of the group.

On the other hand, if ρ is a free state (G-invariant), then its orbit consists of a single element:

$$\mathcal{O}_G(\rho) = \{\rho\}, \tag{4.32}$$

in this case, it carries no information since all group transformations yield the same physical state. Thus, the state has zero asymmetry [63].

We now reach the key point of our discussion. The information–theoretic characterisation of asymmetry lies in the fact that the more distinguishable the elements of the orbit of a state are, the more information that state can encode about the group of transformations and, consequently, the more asymmetric the state is [20, 63].

Comparing the asymmetry of two states ρ and σ therefore reduces to comparing the information contained in their orbits, $\{\mathcal{U}_g(\rho) : g \in G\}$ and $\{\mathcal{U}_g(\sigma) : g \in G\}$, in such a way that the two orbits can be reversibly mapped into each other by G-covariant operations, i.e. if:

$$\rho \xleftrightarrow{G\text{-cov.}} \sigma \quad \Longleftrightarrow \quad \rho \text{ and } \sigma \text{ are } G\text{-equivalent}, \tag{4.33}$$

then the states contain the same amount of asymmetry and belong to the same G-equivalence class [23].

Therefore, given the above, we can state that the dynamical and informational viewpoints coincide:

$$\text{Asymmetry} \quad = \quad \begin{matrix}\text{Distinguishability of} \\ \text{the group orbit}\end{matrix} \quad = \quad \begin{matrix}\text{Information about} \\ \text{the symmetry}\end{matrix}$$

This equivalence justifies the use of information-theoretic quantities as valid asymmetry measures in the next section.

4.3 Asymmetry measures

Having established that asymmetry can be treated as a physical resource and that the amount of asymmetry of a state with respect to a symmetry group is closely related to the amount of information that the state can encode about that group, we may now introduce the general conditions that any asymmetry measure must satisfy.

As with any resource monotone, an asymmetry measure, also called *frameness monotone*, must be a function that does not increase under G-covariant time evolution. In other words, free operations cannot create asymmetry in a quantum state. Consequently, a valid asymmetry monotone must satisfy monotonicity: under symmetric dynamics, the asymmetry of the final state cannot exceed that of the initial state, and is strictly conserved in the case of closed, symmetry-preserving evolutions [63]. In addition to monotonicity, the asymmetry measures must be non-negative and vanish exclusively for G-invariant (free) states [21, 22, 75–77].

These conditions ensure that any quantity used to quantify the amount of asymmetry behaves consistently with the operational picture developed in the previous sections. In particular, since we have shown that asymmetry is equivalent to the ability of a state to encode information about the symmetry group, it is natural to consider measures derived from the distinguishability structure of the group orbit.

In view of the above discussion, any functional of the state that:

(i) quantifies the distinguishability structure of the group orbit $\mathcal{O}_G(\rho)$, and

(ii) satisfies the general conditions of Sec. 4.2.1

can be regarded as a valid asymmetry monotone [20, 21, 63, 76].

More generally, quantities that measure how "spread out" or distinguishable the orbit is, such as distances between elements of $\mathcal{O}_G(\rho)$ or divergences between ρ and

its symmetry-transformed versions, provide natural candidates for asymmetry measures. Information-theoretic functionals built from these distinguishability properties, such as relative entropies [75], trace distances [63], or coherence norms [24], therefore, emerge as monotone asymmetry.

Here, we focus on a specific measure used in this work, based on the ℓ_1-*norm*.

4.3.1 The ℓ_1-norm

The asymmetry monotone employed in this thesis is constructed from the ℓ_1-norm, also known as the *trace norm*. This function provides a quantifier of how strongly a quantum state fails to commute with the generators of the symmetry group, capturing the idea that asymmetry measures how strongly a state is affected by a symmetry transformation.

To define the asymmetry measure, we must first introduce the trace norm, or ℓ_1-norm. Given an operator $A \in \mathcal{L}(\mathcal{H})$, its ℓ_1-norm is defined as [57]:

$$\|A\|_1 = \mathrm{Tr}\left(\sqrt{A^\dagger A}\right), \tag{4.34}$$

which corresponds to the sum of the singular values of A[7].

Properties of the ℓ_1-norm

The ℓ_1-norm exhibits several fundamental properties that are particularly relevant for our discussion. In the following, we briefly list some of these properties. Additional examples can be found in more detail in [57].

- **Positivity.** For any operator $A \in \mathcal{L}(\mathcal{H})$,

$$\|A\|_1 \geq 0, \tag{4.35}$$

  with $\|A\|_1 = 0$ if and only if $A = 0$. This property follows directly from the fact that $A^\dagger A$ is a positive semidefinite operator, and therefore its square root $\sqrt{A^\dagger A}$ is also positive, which guarantees that its trace is non-negative. Moreover, $\mathrm{Tr}\left(\sqrt{A^\dagger A}\right) = 0$ implies that all singular values vanish, and hence $A = 0$.

[7] The singular values of an operator A are defined as the eigenvalues of the positive operator $\sqrt{A^\dagger A}$. Equivalently, in the singular value decomposition (SVD), any matrix or operator A can be written as $A = WDV^\dagger$, where W and V are unitary and $D = \mathrm{diag}(s_1, s_2, \ldots)$ is a diagonal matrix whose entries $s_i \geq 0$ are the singular values of A. The trace norm is then given by $\|A\|_1 = \mathrm{Tr}\left(\sqrt{A^\dagger A}\right) = \sum_i s_i$, that is, the sum of all singular values of A [78].

- **Homogeneity.** For any $c \in \mathbb{C}$,

$$\|cA\|_1 = |c| \, \|A\|_1. \tag{4.36}$$

We obtain (4.36) noting that $(cA)^\dagger(cA) = |c|^2 A^\dagger A$. Thus,

$$\|cA\|_1 = \mathrm{Tr}\left(\sqrt{|c|^2 A^\dagger A}\right) = |c| \ \mathrm{Tr}\left(\sqrt{A^\dagger A}\right) = |c| \, \|A\|_1.$$

- **Variational characterization.** For any operator $A \in \mathcal{L}(\mathcal{H})$, the ℓ_1-norm admits the characterisation

$$\|A\|_1 = \max_U \, |\mathrm{Tr}(AU)|, \tag{4.37}$$

where the maximum is taken over all unitary operators U in the Hilbert space.

To obtain (4.37), let us consider the singular value decomposition $A = WDV^\dagger$, with unitary W and V and $D = \mathrm{diag}(s_1, \ldots, s_n)$ containing the singular values of A. Then

$$\mathrm{Tr}(AU) = \mathrm{Tr}\big(WDV^\dagger U\big) = \mathrm{Tr}\big(D\, V^\dagger UW\big).$$

Since $V^\dagger UW$ is unitary for any unitary U, optimising over U is equivalent to optimising over an arbitrarily unitary $U' = V^\dagger UW$. Thus,

$$\max_U |\,\mathrm{Tr}(AU)| = \max_{U'} |\,\mathrm{Tr}(DU')| = \sum_i s_i = \|A\|_1.$$

- **Triangle inequality.** For any operator $A, B \in \mathcal{L}(\mathcal{H})$,

$$\|A + B\|_1 \leq \|A\|_1 + \|B\|_1. \tag{4.38}$$

Here, we may use the variational characterisation of the norm. For the operator $(A + B)$ we have

$$\|A + B\|_1 = \max_U |\,\mathrm{Tr}[(A + B)U]|.$$

Using the linearity of the trace, $\mathrm{Tr}[(A + B)U] = \mathrm{Tr}(AU) + \mathrm{Tr}(BU)$, and applying the triangle inequality for complex numbers, $|\,\mathrm{Tr}(AU) + \mathrm{Tr}(BU)| \leq |\,\mathrm{Tr}(AU)| + |\,\mathrm{Tr}(BU)|$, we can write

$$\|A + B\|_1 \leq \max_U \left(|\,\mathrm{Tr}(AU)| + |\,\mathrm{Tr}(BU)|\right).$$

Finally, since $\max_U (|\operatorname{Tr}(AU)| + |\operatorname{Tr}(BU)|) \leq \max_U |\operatorname{Tr}(AU)| + \max_U |\operatorname{Tr}(BU)|$, we obtain

$$\begin{aligned} \|A+B\|_1 &\leq \max_U |\operatorname{Tr}(AU)| + \max_U |\operatorname{Tr}(BU)|, \\ &\leq \|A\|_1 + \|B_1\|. \end{aligned}$$

- **Convexity.** Let $\{A_i\}$ be a collection of operators, $A_i \in \mathcal{L}(\mathcal{H})$, and let $\{p_i\}$ be probabilities with $p_i \geq 0$ and $\sum_i p_i = 1$. Then

$$\Big\| \sum_i p_i A_i \Big\|_1 \leq \sum_i p_i \|A_i\|_1. \tag{4.39}$$

This property follows directly from homogeneity and the triangle inequality:

$$\Big\| \sum_i p_i A_i \Big\|_1 \leq \sum_i \|p_i A_i\|_1 = \sum_i p_i \|A_i\|_1. \tag{4.40}$$

Let us note that some of these properties are precisely the ones required for an asymmetry monotone. We now proceed to define the asymmetry monotone based on the ℓ_1-norm.

4.3.2 The ℓ_1-norm based asymmetry monotone

Given a generator L of the symmetry group G, the ℓ_1-norm asymmetry measure is defined as [20, 63]:

$$F_L(\rho) = \|[\rho,\, L]\|_1. \tag{4.41}$$

This quantity is defined in terms of the commutator between the density operator and the generator of the symmetry group. It can be understood as a quantification of how much the state of the system does not commute with the group generator. To provide a clearer understanding of the meaning of $F_L(\rho)$, we follow the reasoning presented in [63].

Consider an infinitesimal group transformation generated by L:

$$U(g) = e^{-i\theta L}, \qquad \theta \ll 1. \tag{4.42}$$

Expanding to first order, $e^{-i\theta L} = \mathbb{I} - i\theta L - \mathcal{O}(\theta^2)$, we obtain the transformed state:

$$\begin{aligned} U_g\, \rho\, U_g^\dagger &= \left(\mathbb{I} - i\theta L - \mathcal{O}(\theta^2)\right) \rho \left(\mathbb{I} + i\theta L + \mathcal{O}(\theta^2)\right), \\ &= \rho - i\theta[L,\rho] + \mathcal{O}(\theta^2). \end{aligned} \tag{4.43}$$

Since $\|\rho - \sigma\|_1$ is the trace distance between two quantum states, providing a measure of how distinguishable they are [57], the trace distance between ρ and its symmetry-transformed version $U_g \rho U_g^\dagger$, for a group element $g \in G$, is:

$$\|\rho - U_g \rho U_g^\dagger\|_1 = \theta \, \|[\rho, L]\|_1 + \mathcal{O}(\theta^2). \tag{4.44}$$

In this way, the asymmetry monotone defined in (4.41) is simply the first-order term of Eq. (4.44), which makes the meaning of the measure clear: we are quantifying how much the symmetry transformation $U(g)$ makes the transformed state distinguishable from the initial one, that is, how strongly the state responds to the infinitesimal action of the group. This quantification, as we have seen, is determined by the commutator between the state and the symmetry generator. The less the state commutes with the generator, the more distinguishable the initial and transformed states become, and consequently the more asymmetric the state is with respect to the group.

In addition to the interpretation discussed above, we may understand (4.41) in terms of the coherence between the eigenvalues of the operator L. The monotone $F_L(\rho)$ can be viewed as a quantification of the coherent spread over the eigenvalues of L [20].

To visualise this, let us consider the spectral decomposition of L in the form $L = \sum_i l_i \, |l_i\rangle\langle l_i|$, where $\{|l_i\rangle\}$ is the set of orthonormal eigenstates of L and l_i are the corresponding eigenvalues. The matrix elements of the operator $[\rho, L]$ in the eigenbasis of L are given by:

$$\begin{aligned}
\langle l| \, [\rho, L] \, |l'\rangle &= \langle l| \, (\rho L - L\rho) \, |l'\rangle \, , \\
&= \langle l| \, \rho L \, |l'\rangle - \langle l| \, L\rho \, |l'\rangle \\
&= \langle l| \, \rho \sum_i l_i \, |l_i\rangle \, \langle l_i|l'\rangle - \langle l| \sum_j l_j \, |l_j\rangle\langle l_j| \, \rho \, |l'\rangle \\
&= \sum_i l_i \delta_{l_i,l'} \, \langle l| \, \rho \, |l_i\rangle - \sum_j l_j \delta_{l_j,l} \, \langle l_j| \, \rho \, |l'\rangle \\
&= (l' - l) \, \langle l| \, \rho \, |l'\rangle \, .
\end{aligned} \tag{4.45}$$

Equation (4.45) presents the matrix elements of the commutator $[\rho, L]$ in the eigenbasis of L as the product of the difference between the eigenvalues and the corresponding density-matrix element. We now analyse this expression in two distinct situations.

The first situation corresponds to the case in which the state ρ is diagonal in the eigenbasis of L. In this case, $\langle l| \, \rho \, |l'\rangle = 0$ for all $l \neq l'$, so that only the terms with $l = l'$ contribute. However, under this condition, the multiplicative factor $(l' - l)$

vanishes, cancelling all elements of the commutator $[\rho, L]$, implying that

$$[\rho, L] = 0. \tag{4.46}$$

As a result, we see that states that are diagonal in the basis of L are invariant under the transformation generated by L, characterising symmetric states ($F_L(\rho) = 0$) with respect to this generator.

In the second case, where ρ exhibits off-diagonal elements based on L, that is, when $\langle l| \rho |l'\rangle \neq 0$ for $l \neq l'$, the commutator may be nonzero, provided that these elements connect distinct eigenvalues of L. In this case, both the factor $(l' - l)$ and the matrix elements $\langle l| \rho |l'\rangle$ do not disappear, resulting in

$$[\rho, L] \neq 0. \tag{4.47}$$

Therefore, the existence of coherence between different eigenvalues of L (coherence necessarily between l's such that $l_i \neq l$, with coherences between states sharing the same eigenvalue not being taken into account) implies that the commutator does not vanish, which corresponds to a nonzero asymmetry measure. In this way, the quantity $F_L(\rho)$ quantifies how much the state spreads over different eigenvalues of the generator.

This "coherent spreading" over the spectrum of L characterises the breaking of the symmetry associated with the generator and justifies interpreting $F_L(\rho)$ as a measure of asymmetry or, equivalently, as a quantifier of the sensitivity of the state to the symmetry transformation generated by L [20].

It is important to note that the quantity defined in Eq. (4.41) satisfies the axioms presented in Sec. 4.2.1 for resource measures and therefore qualifies as a valid asymmetry monotone:

- **Vanishing on free states**: If ρ is G-invariant (a free state), then $U_g \rho U_g^\dagger = \rho \ \forall g$, which implies $[\rho, L] = 0$. Hence, since the ℓ_1-norm vanishes only for the zero operator,
$$F_L(\rho) = 0.$$

- **Non-negativity**: this condition follows directly from the positivity property of the ℓ_1-norm, namely $\|A\|_1 \geq 0$, with equality holding only in the case discussed above [57].

- **Monotonicity**: if there exists a G-covariant transformation Λ such that $\rho \xrightarrow{\Lambda} \sigma$, then $\Lambda(U_g \rho U_g^\dagger) = U_g \Lambda(\rho) U_g^\dagger = U_g \sigma U_g^\dagger$. Moreover, the trace norm is contractive under any completely positive trace-preserving map, as is the case

for G-covariant operations. That is, for any Hermitian operator A we have $\|A\|_1 \geq \|\Lambda(A)\|_1$ [63]. Therefore, taking $A = \rho - U_g \rho U_g^\dagger$, we obtain

$$\begin{aligned} \|\rho - U_g \rho U_g^\dagger\|_1 &\geq \|\Lambda(\rho) - \Lambda(U_g \rho U_g^\dagger)\|_1 \\ &\geq \|\sigma - U_g \sigma U_g^\dagger\|_1. \end{aligned} \tag{4.48}$$

From (4.44), we can conclude:

$$\begin{aligned} \|[\rho, L]\|_1 &\geq \|[\sigma, L]\|_1, \\ F_L(\rho) &\geq F_L(\sigma), \end{aligned} \tag{4.49}$$

ensuring that the distinguishability of the orbit cannot increase under free operations, or, in other words, that G-covariant operations cannot increase the distinguishability between a state and its symmetry-transformed version [63].

- **Convexity**: Given an ensemble $\{p_i, \rho_i\}$, the convexity of $F_L(\rho)$ follows directly from the convexity of the ℓ_1-norm:

$$F_L\left(\sum_i p_i \rho_i\right) \leq \sum_i p_i F_L(\rho_i).$$

Let us see this explicitly. Let

$$\begin{aligned} F_L\left(\sum_i p_i \rho_i\right) &= \left\| \left[\sum_i p_i \rho_i, L \right] \right\|_1, \\ &\leq \sum_i p_i \|[\rho_i, L]\|_1 \\ &\leq \sum_i p_i F_L(\rho_i). \end{aligned} \tag{4.50}$$

where we used again the triangle inequality and the homogeneity of the ℓ_1-norm.

We may interpret convexity as expressing the fact that statistical uncertainty about the state only degrades the information about the symmetry. Therefore, it is not possible to increase the system's sensitivity to symmetry transformations (its asymmetry) by statistical mixing.

To conclude, let us view $F_L(\rho)$ in terms of the geometry of the orbit generated by the group action. If the state is G-invariant, then $U_g \rho U_g^\dagger = \rho \,;\, \forall\, g \in G$, which implies $[\rho, L] = 0$. In this case, the orbit $\mathcal{O}_G(\rho) = \{\rho\}$ contains a single point, and no symmetry transformation produces a state distinguishable from ρ.

The "distance" along the orbit is therefore zero for any transformation, reflecting the complete absence of asymmetry.

If, on the contrary, $[\rho, L] \neq 0$, the state "moves" along its group orbit: small transformations generate physically distinct states $U_g \rho U_g^\dagger = \rho - i\theta[L, \rho] + O(\theta^2)$, so the orbit contains a continuum of distinguishable points. The trace distance between ρ and its infinitesimally transformed version behaves as

$$\|\rho - U_g \rho U_g^\dagger\|_1 = \theta \, \|[\rho, L]\|_1 + O(\theta^2), \tag{4.51}$$

which shows that $\|[\rho, L]\|_1$ quantifies the initial rate at which the state departs from itself along the orbit. Thus, $F_L(\rho)$ measures the distinguishability generated by the group action and provides a geometric characterisation of asymmetry, which is perfectly in line with the informational interpretation developed in the previous section.

Thus, the ℓ_1-norm of the commutator provides a fully operational information-theoretic measure of asymmetry. It quantifies how distinguishable the neighbourhood of ρ is within its group orbit, matches the intuitive idea that asymmetry reflects the failure of a state to respect a symmetry generator, and satisfies all requirements expected of a monotone resource.

Example: rotation asymmetry

As an example, again, let us consider the group $SU(2)$, presented in subsection 4.1.3, whose generators are the spin operators J_x, J_y, and J_z. If we choose $L = J_z$, the monotone

$$F_{J_z}(\rho) = \|[\rho, J_z]\|_1 \tag{4.52}$$

measures the amount of asymmetry of ρ with respect to rotations around the z-axis.

Analysing this from the perspective of coherence, as discussed previously, we can interpret $F_{J_z}(\rho)$ as a measure of the amount of coherence of the state across different eigenvalues of J_z. Indeed, writing the eigenstates of J_z as $\{|j, m_z\rangle\}$, with $m_z = -j, -j+1, \ldots, j$, the matrix elements of the commutator in this basis, given in Eq. (4.45), are

$$\langle j, m_z| \, [\rho, J_z] \, |j, m_z'\rangle = (m_z' - m_z) \, \langle j, m_z| \, \rho \, |j, m_z'\rangle \, . \tag{4.53}$$

Therefore, only matrix elements of ρ that connect states with different magnetic quantum numbers $m_z \neq m_z'$ contribute to the asymmetry. Coherences between states with the same eigenvalue of J_z do not contribute, since $(m_z' - m_z)$ vanishes.

For example, a state that is diagonal in the basis J_z, such as $\rho = \sum_{m_z} p_{m_z} |j, m_z\rangle\langle j, m_z|$. has all non-diagonal elements $\langle j, m_z| \rho |j, m'_z\rangle$ with $m_z \neq m'_z$ equal to zero, implying $[\rho, J_z] = 0$ and hence $F_{J_z}(\rho) = 0$. Such states are invariant under rotations generated by J_z and therefore do not encode any information about rotations around the z axis.

In contrast, consider a coherent spin state that points in a direction not parallel to $\hat{z}$. When expressed in the J_z basis, this state is a superposition of several $|j, m_z\rangle$ eigenstates,

$$|\psi\rangle = \sum_{m_z} c_{m_z} |j, m_z\rangle , \tag{4.54}$$

leading to a density operator $\rho = |\psi\rangle\langle\psi|$ with nonvanishing off-diagonal elements $\langle m_z| \rho |m'_z\rangle$ for $m_z \neq m'_z$. These terms correspond to coherences between different eigenvalues of J_z and generate a $[\rho, J_z] \neq 0$, resulting in a finite value of $F_{J_z}(\rho)$.

This reflects the fact that such a state is not invariant under rotations around the z axis, that is, an infinitesimal rotation changes the state in an operationally distinguishable way, generating a nontrivial group orbit. The larger the coherent spread of ρ over distinct J_z eigenvalues, the greater the distinguishability between ρ and its symmetry-transformed versions, and hence the greater the asymmetry monotone $F_{J_z}(\rho)$.

In this sense, $F_{J_z}(\rho)$ provides a clear geometric and physical interpretation: it quantifies how strongly the state is delocalised across different J_z eigenvalues and therefore how sensitive it is to symmetry transformations generated by J_z. This aligns with the interpretation of asymmetry as a resource for encoding directional information in the transverse plane [20].

Chapter 5

Lipkin-Meshkov-Glick Model

The Lipkin–Meshkov–Glick (LMG) model was originally proposed in [32–34] in the context of nuclear physics as a model to study many-fermion systems. The construction considers N fermions distributed across two energy levels, each with an N-fold degeneracy, allowing each level to accommodate multiple states. The model includes pair scattering interactions, in which two fermions can be simultaneously transferred from the lower level to the upper one (or vice versa).

The originally proposed Hamiltonian has the form [32]:

$$H = \frac{\epsilon}{2}\sum_{p,\sigma}\sigma a^{\dagger}_{p\sigma}a_{p\sigma} + \frac{V}{2}\sum_{p,p',\sigma} a^{\dagger}_{p\sigma}a^{\dagger}_{p'\sigma}a_{p'-\sigma}a_{p-\sigma} + \frac{W}{2}\sum_{p,p',\sigma} a^{\dagger}_{p\sigma}a^{\dagger}_{p'-\sigma}a_{p'\sigma}a_{p-\sigma}. \quad (5.1)$$

where ϵ is the energy gap between the two levels, V and W are the interaction strengths, with V associated with the scattering of a pair of particles within the same level and W associated with the exchange of particles between energy levels, σ denotes the energy level and can take values $+1$ (for the upper level) and -1 (for the lower level), and p is the quantum number specifying the state of a fermion in level σ.

Despite its initial proposal, the LMG model is widely used to describe a chain of N spin-$\frac{1}{2}$ particles with global interaction, subjected to an external transverse magnetic field [71, 72, 79, 80]:

$$\hat{H} = -\frac{J}{N}\sum_{i<j}\left(\sigma^i_z\sigma^j_z + \gamma\sigma^i_y\sigma^j_y\right) - h\sum_i \sigma^i_x, \quad (5.2)$$

where J is the spin coupling term in the zy direction, h is the transverse magnetic field applied along the x direction, the matrices σ_l, with $l = x, y, z$, are the Pauli spin operators, and γ is an anisotropy parameter. This Hamiltonian, described by Eq. (5.2), will be used throughout this thesis.

5.1 Symmetries

The model exhibits two important symmetries: the *permutation symmetry*, associated with the permutation group S_N, and the *parity symmetry*, also known as the $\mathbb{Z}_2$ symmetry or spin-flip symmetry.

The first is associated with the fact that the spin interactions have the same intensity for any pair of spins. Thus, the permutation of a pair of particles does not change the Hamiltonian of the system, making it invariant under the action of elements of the group S_N [81]. This symmetry allows us to classify the state of the system into distinct sectors, each associated with a total spin value J. Since the Hamiltonian of the model preserves J^2, it does not mix states with different values of J, enabling the decomposition of the Hilbert space into independent subspaces.

Among these sectors, the totally symmetric sector (TSS) corresponds to the subspace where $J = N/2$, containing states that are symmetric under permutation of any pair of spins. Because the Hamiltonian of the model does not couple states from different sectors, if the initial state belongs to the sector $J = N/2$, it will remain in that sector throughout the evolution. Restricting the analysis to this sector reduces the Hilbert space dimension from 2^N to only $N + 1$ [32].

This property allows reformulating the problem in the totally symmetric sector in terms of collective spin operators $J_l = \sum_i \frac{\sigma_l^i}{2}$, with $l = x, y, z$, enabling the system's dynamics to be equivalently described as the dynamics of a single spin of magnitude $J = \frac{N}{2}$.

On the other hand, the $\mathbb{Z}_2$ symmetry, or spin-flip symmetry, is associated with the invariance of the Hamiltonian under the global transformation that inverts the sign of the transverse spin components, i.e.,

$$\sigma_z^i \to -\sigma_z^i, \quad \sigma_y^i \to -\sigma_y^i, \quad \sigma_x^i \to \sigma_x^i. \tag{5.3}$$

This symmetry arises from the spin interactions in the LMG model's Hamiltonian (5.2), where the interaction terms in the zy plane always appear as quadratic products, ensuring that the Hamiltonian remains invariant under this global inversion. Meanwhile, the external field term in the x-direction, $h \sum_i \sigma_x^i$, remains unchanged, meaning the $\mathbb{Z}_2$ symmetry is restricted to the transverse plane.

Its role in characterising the phases of the system is crucial. In the paramagnetic phase ($h \gg J$), the spins are forced into alignment. The term associated with the external field dominates the energy of the system, aligning the spins in its direction, ensuring a unique ground state. In this case, the $\mathbb{Z}_2$ symmetry is preserved because both the Hamiltonian and the ground state remain symmetric [35].

On the other hand, in the ferromagnetic phase ($h \ll J$), the spin interaction term becomes dominant. In this situation, the system spontaneously chooses one of the two possible spin alignment directions in the zy plane, resulting in ground state degeneracy. Since the two degenerate states do not exhibit spin-flip symmetry even though the Hamiltonian remains symmetric, we say that this symmetry is spontaneously broken in the ferromagnetic phase [35].

The spontaneous breaking of $\mathbb{Z}_2$ symmetry is explored in the context of quantum phase transitions in the LMG model, with a critical external magnetic field given by $h_c = J$, in references [35, 72, 82]. Later, we will discuss the relationship between these phases and DQPT.

The fact that the model possesses permutation symmetry allows us to treat the system in the collective spin regime, providing a very useful simplification that enables computational simulation at a lower cost. We will now rewrite the Hamiltonian (5.2) using this approach.

First, we rewrite the interaction terms $\sigma_z^i\sigma_z^j$ and $\sigma_y^i\sigma_y^j$ using the collective spin operators. Note that

$$\sum_{i<j} \sigma_l^i\sigma_l^j = \frac{1}{2}\left(\sum_{i,j} \sigma_l^i\sigma_l^j - \sum_i \sigma_l^i\sigma_l^i\right). \tag{5.4}$$

Since $\sigma_l^i\sigma_l^i = I$ for any i, we obtain:

$$\sum_{i<j} \sigma_l^i\sigma_l^j = \frac{1}{2}\left(\sum_{i,j} \sigma_l^i\sigma_l^j - NI\right). \tag{5.5}$$

Using the collective spin operators:

$$\sum_{i,j} \sigma_l^i\sigma_l^j = \left(\sum_i \sigma_l^i\right)\left(\sum_j \sigma_l^j\right) = 4\hat{J}_l^2. \tag{5.6}$$

Thus,

$$\sum_{i<j} \sigma_l^i\sigma_l^j = \frac{1}{2}\left(4\hat{J}_l^2 - NI\right). \tag{5.7}$$

Moreover,

$$\sum_i \sigma_x^i = 2\hat{J}_x. \tag{5.8}$$

Using (5.7) and (5.8) in (5.2), we obtain the following:

$$\begin{aligned}\hat{H} &= -\frac{J}{N}\sum_{i<j}\left(\sigma_z^i\sigma_z^j+\gamma\sigma_y^i\sigma_y^j\right)-h\sum_i\sigma_x^i \\ &= -\frac{J}{N}\left[\frac{1}{2}\left(4\hat{J}_z^2-NI\right)+\gamma\frac{1}{2}\left(4\hat{J}_y^2-NI\right)\right]-2h\hat{J}_z. \end{aligned} \tag{5.9}$$

Rearranging,

$$\hat{H}=-2h\hat{J}_x-\frac{J}{N}\left(2\hat{J}_z^2+2\gamma\hat{J}_y^2-\frac{N}{2}(1+\gamma)I\right). \tag{5.10}$$

The term proportional to $\frac{N}{2}(1+\gamma)I$ represents only a global energy shift and can be ignored. Additionally, we can define $j=\frac{N}{2}$. Thus, we obtain:

$$\hat{H}=-2h\hat{J}_x-\frac{J}{j}\left(\hat{J}_z^2+\gamma\hat{J}_y^2\right). \tag{5.11}$$

The LMG model, represented in terms of collective spin operators, can be described by the Hamiltonian in Eq. (5.11) with a dimension of $N+1$, instead of Eq. (5.2) with a dimension of 2^N [72]. For the main results of this thesis, we set $J=1$, which does not lead to any loss of generality in our results, as J only rescales the interaction energy. The anisotropy parameter γ will be analysed in two situations: first, we will consider a fixed value of γ to identify the role of DQPT in the entropy production of the model; second, we allow γ to vary within the interval $\gamma\in[0,1]$ to study the behaviour of symmetry under DQPT.

5.2 DQPT in LMG model

The LMG model exhibits dynamical behaviour with critical features that can be analysed in two complementary ways: through a dynamical order parameter, also called DPT-I, and through nonanalyticities in the rate function, called DPT-II or simply DQPT. These two approaches to identifying dynamical phase transitions were introduced in Chapter 2 and have been investigated in several works, including [4, 7, 27, 28, 37, 53, 82, 83].

In this section, we discuss both approaches in the context of the LMG model, presenting the behaviour of the Loschmidt amplitude, Loschmidt echo, rate function, and dynamical order parameter. In addition, we address the validity of the transition markers observed in our calculations, considering both finite-size chains and systems described by mixed states.

5.2.1 Loschmidt Echo and Rate Function

Starting with the DPT-II, which is the dynamic transitions related to the Loschmidt echo and rate function, as discussed in Section 2.3.

We focus on this type of transition motivated by the possibility of relating the Loschmidt echo to the Bures angle when dealing with pure states, since, for two pure states $\rho_0 = |\psi_0\rangle\langle\psi_0|$ and $\rho_t = |\psi(t)\rangle\langle\psi(t)|$, Uhlmann fidelity takes the form (6.7), and the Loschmidt echo is given by (2.46). In this case, we can write:

$$\mathcal{F}(|\psi_0\rangle, |\psi_t\rangle) = \mathcal{L}_e(t), \tag{5.12}$$

thus, the Bures angle between ρ_0 and ρ_t can be expressed in terms of $\mathcal{L}_e(t)$:

$$\mathcal{L}(\rho_0, \rho_t) = \arccos\sqrt{\mathcal{L}_e(t)}. \tag{5.13}$$

Equation (5.13) suggests that the dynamic behaviour of $\mathcal{L}_e$ directly influences the behaviour of $\mathcal{L}$ for pure states. Since the Bures angle is closely related to the lower bound of entropy production via (6.17), we can infer that the behaviour of the Loschmidt echo, including its behaviour during criticalities, will influence the behaviour of this bound.

The LMG model has a dynamic critical point given by $h_c^d = \frac{h_0+J}{2}$ [84], where h_0 is the initial value of the transverse magnetic field and J is the coupling parameter in the zy direction. It is important to mention that this critical point differs from the QPT critical point given by $h_c^{QPT} = J$ [79, 82].

This point separates two distinct dynamical regimes in the LMG model. For quenches leading to $h < h_c^d$, the system remains in the symmetry-broken phase, where the final state exhibits spontaneous magnetization in the zy plane, maintaining the degeneracy of the ground states. On the other hand, for quenches with $h > h_c^d$, the system evolves into a phase where the $\mathbb{Z}_2$ symmetry is dynamically restored, resulting in a state without transverse magnetization. This phase difference can be captured by the behaviour of the rate function, with the emergence of non-analyticities in $\lambda(t)$ for quenches to $h > h_c^d$, signalling the occurrence of a DQPT [27, 82].

In our calculations, we will consider quenches starting from $h_0 = 0$. Furthermore, as mentioned earlier, we will set $J = 1$. Therefore, the dynamic critical point for our considerations will be $h_c^d = \frac{1}{2}$.

Before proceeding to the results of our work, two discussions are necessary. The system we consider has two characteristics that require attention. The first arises

from the impossibility of treating the system in the thermodynamic limit both experimentally and computationally. The second is associated with the calculation of the entropy production bound, which will use the framework presented in subsection 6.1.2, where the bound is expressed in terms of mixed states. Therefore, it is necessary to discuss the validity of identifying DQPTs both for finite systems and for systems represented by mixed states.

5.2.2 DQPT in finite-size systems

DQPT is defined for systems in the thermodynamic limit, as we saw in section 2.3. However, several works [7, 8, 27, 29] have shown that it is possible to identify DQPT signatures with high precision even in systems with a small number of components.

In systems that exhibit spontaneous $\mathbb{Z}_2$ symmetry breaking and ground state degeneracy, such as Ising chain models [8, 27], XXZ [29], and LMG, the characteristics of DQPT can be observed even for relatively small N.

The degeneracy of the ground state is essential in this scenario because, in phases with broken symmetry, the rate function $\lambda(t)$ can be expressed in terms of contributions from different symmetry sectors, $\lambda_\eta(t)$, which represent the probability of return to each of the degenerate ground states.

The total return probability to the ground state manifold, in such cases, can be written as [29]:

$$P(t) = \sum_\eta P_\eta(t), \tag{5.14}$$

where $P_\eta(t) = |\langle\eta|\psi_0(t)\rangle|^2$ represents the probability that the system returns to one of the ground states $|\eta\rangle$, and the sum runs through all system degeneracies.

For large systems $N \gg 1$, each of these probabilities follows a large deviation behavior.

$$P_\eta(t) = e^{-N\lambda_\eta(t)}. \tag{5.15}$$

As time t evolves, a transition occurs between regimes in which different $P_\eta(t)$ are more probable, meaning that over time, one of the ground states ceases to be the most probable and another of the system's degenerate ground states takes over.

In terms of the rate function, where the highest probability is associated with the smallest value of λ_η, this corresponds to one λ_η dominating the dynamics at a given moment, and at a critical time, another λ_η takes over. This happens because the rate functions $\lambda_\eta(t)$ have different regions of validity as the smallest contributions to the effective rate function. In the thermodynamic limit ($N \to \infty$), this transition

becomes increasingly abrupt, and the global rate function is defined as [8]:

$$\lambda(t) = \min_{\eta} \lambda_{\eta}(t), \tag{5.16}$$

which implies that only one of the probabilities associated with ground state degeneracies dominates the system's behavior, allowing the return probability to be written as:

$$P(t) = e^{-N\lambda(t)} \equiv \mathcal{L}_e(t), \tag{5.17}$$

where $\mathcal{L}_e(t)$ is the Loschmidt echo, defined in (2.46).

The transition in probability dominance and, consequently, in rate functions occurs at the critical time t_c. This switching leads to a discontinuity in $\lambda(t)$, signalling a DQPT[1]. Although this change occurs regardless of N, increasing the size of the system sharpens the transition, making it closer to a actual discontinuity.

The non-analytic behaviour of $\lambda(t)$ for finite N was experimentally demonstrated in [8], with measurements for systems of $N = 6, 8$ and 10 atoms, and numerically in [29], where rate functions were calculated for systems of $N = 16$ and 24. In both cases, discontinuities in the effective rate function characterise DQPTs.

Thus, following this approach, we assume that, although the thermodynamic limit provides a rigorous description of DQPTs, the essential characteristics of these transitions emerge even in finite systems.

5.2.3 DQPT in mixed systems

In references [31, 85], the behaviour of both the Loschmidt echo and the rate function was analysed in the context of mixed states. For this analysis, the authors considered thermal states at finite temperatures and demonstrated that the effects of DQPT can still be observed in such situations. In other words, it is possible to identify DQPTs via the non-analyticity of the rate function even in cases where the system is represented by mixed states.

To perform these analyses, [31, 85] defined a generalised form of the Loschmidt amplitude, given in terms of a state ρ_0^p:

$$\mathcal{G} = \mathrm{Tr}\{\rho_0^p U_t\}, \tag{5.18}$$

[1] This non-analyticity arises similarly to the non-analyticities in Gibbs free energy, presented in figure 2.5.

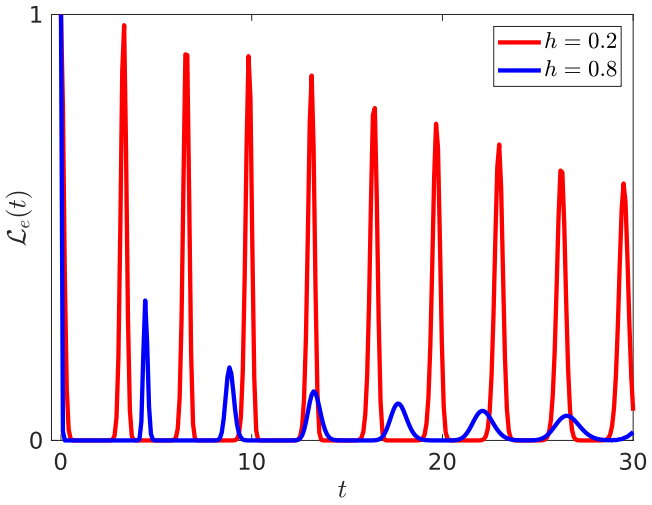

FIGURE 5.1: Behaviour of the Loschmidt echo for the LMG model under two distinct quenches: one crossing the dynamical critical point (blue lines) and the other not (red lines).

where U_t is the unitary evolution operator. The state $\rho_0^p = |w(0)\rangle\langle w(0)|$ represents the purified density matrix, with

$$|w(0)\rangle = \sum_i \sqrt{p_i}\, |\psi_i^s(0)\rangle \otimes |\psi_i^a\rangle \tag{5.19}$$

being the normalised initial state acting in the enlarged Hilbert space $\mathcal{H}_p = \mathcal{H}_s \otimes \mathcal{H}_a$ (system s and ancilla a).

With these considerations, both works showed that the rate function associated with the generalised Loschmidt amplitude can exhibit non-analyticities even for thermal states at finite temperatures. This indicates that DQPTs can be identified in systems described by mixed states while maintaining the usual interpretation based on discontinuities or singularities in the rate function.

5.2.4 Rate function and Loschmidt echo

Here, we analyse the dynamical transition in terms of the Loschmidt echo, defined in section 2.3. To compute $\mathcal{L}_e(t)$ and $\lambda(t)$ at each time instant, we start from the ground state of the Hamiltonian model LMG (5.11) with $h_0 = 0$, $J = 1$, and $\gamma = 0$.

We numerically compute the evolutions $|\psi(t)\rangle \equiv e^{iHt}|\psi_0\rangle$, governed by the post-quench Hamiltonian H. Thus, we obtain the Loschmidt echo, given by (2.46), shown in Fig. 5.1, and the rate function, given by (2.52), shown in Fig. 5.2, for the

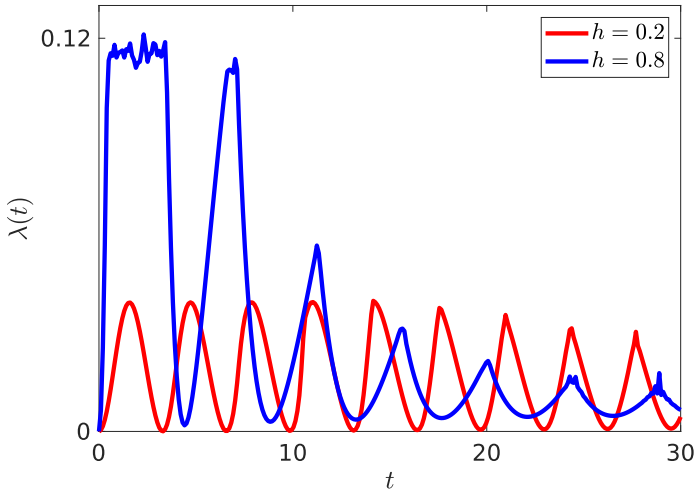

FIGURE 5.2: Behavior of the rate function for the LMG model under two distinct quenches: one crossing the dynamical critical point (blue lines) and the other not (red lines).

interval $t \in [0, 30]$ and for two different quench values $h = 0.2$ and 0.8. In both cases, we adopt $j = 300$.

It is clear that for a quench from $h_0 = 0$ to $h < h_c^d$ – Fig. 5.2 (blue line) – the rate function exhibits a smooth behaviour, with no non-analytic points. This regime is associated with the symmetry-broken phase of the model, in which longitudinal magnetization remains nonzero, and ground state degeneracy is preserved.

On the other hand, when the quench is performed from $h_0 = 0$ to $h > h_c^d$, the rate function exhibits non-analytic points at specific time instants – figure 5.2 (red line). These non-analyticities are associated with the points where the Loschmidt echo vanishes, indicating that the system's state at that moment has zero probability of returning to the ground state, characterising the transition to the phase where the $\mathbb{Z}_2$ symmetry is dynamically restored. Thus, the presence of these non-analyticities provides clear evidence of the occurrence of DQPT in this model.

5.3 DPT-I in the LMG Model

The other way of characterising DQPT, as discussed in Chapter 2, often referred to as DPT-I, relies on the long-time behaviour of a parameter of dynamical order. In summary, the dynamical order parameter takes nonzero values in the dynamically ordered phase, where the $\mathbb{Z}_2$ symmetry is broken, and vanishes in the disordered phase, where the symmetry is restored.

In this section, we revisit this characterisation in the context of the LMG model. For our analysis, we set $J = 1$, $h_0 = 0$, and consider different values of the transverse field after the challenge h and the size of the system j. The anisotropy parameter is fixed again at $\gamma = 0$.

5.3.1 Time evolution of the dynamical order parameter

Given the chosen parameters, the dynamical order parameter of our model (see Eq. 5.11) is magnetisation along the z-axis. We therefore begin by analysing the time evolution of $\langle J_z \rangle(t)$ for different quenches, with fixed $j = 300$.

The expectation value of J_z is calculated with respect to the time-evolved state $|\psi(t)\rangle = e^{-iHt} |\psi_0\rangle$, where H is the post-quench Hamiltonian and $|\psi_0\rangle$ is the ground state of the initial Hamiltonian. We choose as the initial state the fully polarised state along the positive z-axis, which is one of the two degenerate ground states of H_0. In the collective spin framework, this corresponds to a single global spin pointing in the z-direction, whose dynamics can be represented as the trajectory of a spin on the Bloch sphere [27].

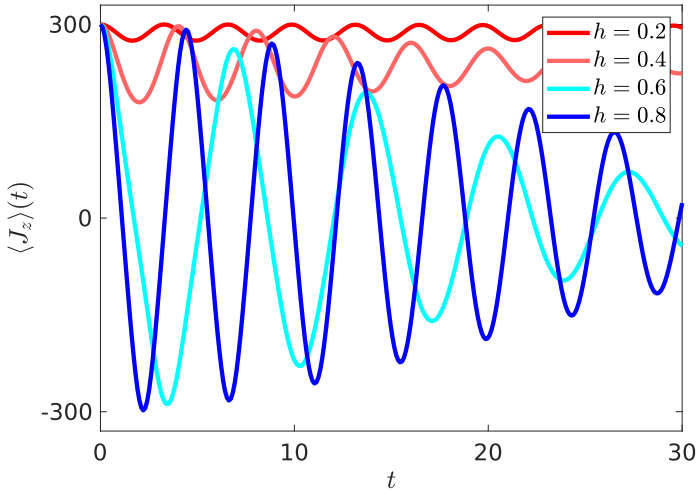

FIGURE 5.3: Time evolution of the magnetization $\langle J_z \rangle(t)$ for the LMG model with $j = 300$ under four quenches: $h = 0.2$ (red line), $h = 0.4$ (pink line), $h = 0.6$ (light-blue line) and $h = 0.8$ (blue line).

In Fig. 5.3, we show the time evolution of magnetisation in the LMG model for four different quenches: two noncritical, $h = 0.2$ and $h = 0.4$, and two critical, $h = 0.6$ and $h = 0.8$. A clear qualitative difference can be observed between the two regimes.

For the noncritical quenches, $\langle J_z \rangle(t)$ oscillates around a nonzero value (around 300 in our case), indicating the stabilization of the magnetization along the initial

direction. These oscillations can be viewed as the precession of the collective spin around its initial orientation on the Bloch sphere, which does not characterise a phase transition, since the system remains in the phase with $\mathbb{Z}_2$ symmetry-broken.

On the other hand, for critical quenches, the magnetization oscillates around zero, indicating that the system evolves to a state without a preferential spin direction. On the Bloch sphere, this can be viewed as a trajectory spreading over both hemispheres, exploring different magnetization values and stabilising around zero. In this regime, the time-evolved state recovers the symmetry $\mathbb{Z}_2$, thus characterising the restoration of dynamical symmetry and the occurrence of a DQPT.

5.3.2 Finite-size effects

To analyse the effects and behaviour of finite-size in a long-time evolution, we plot $\langle J_z \rangle(t)$ in the interval $t \in (0, 100)$ for quenches in $h = 0.2$ (Fig. 5.4) and $h = 0.8$ (Fig. 5.5), considering three system sizes: $j = 50$, $j = 100$ and $j = 300$.

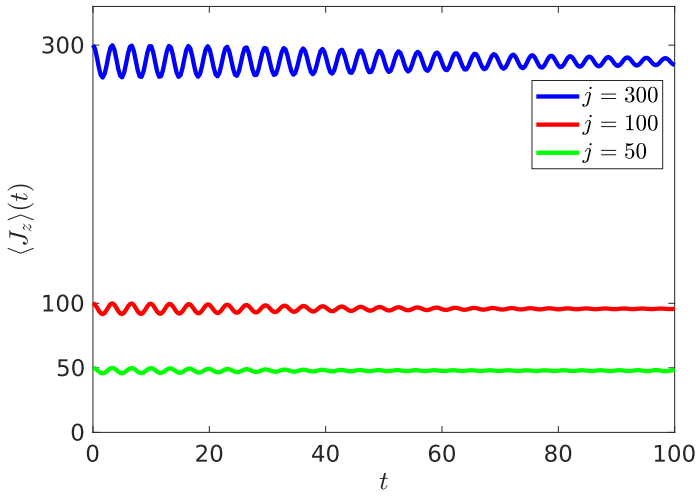

FIGURE 5.4: Time evolution of $\langle J_z \rangle(t)$ for different system sizes: $j = 50, 100, 300$, under a noncritical quench $h = 0.2$.

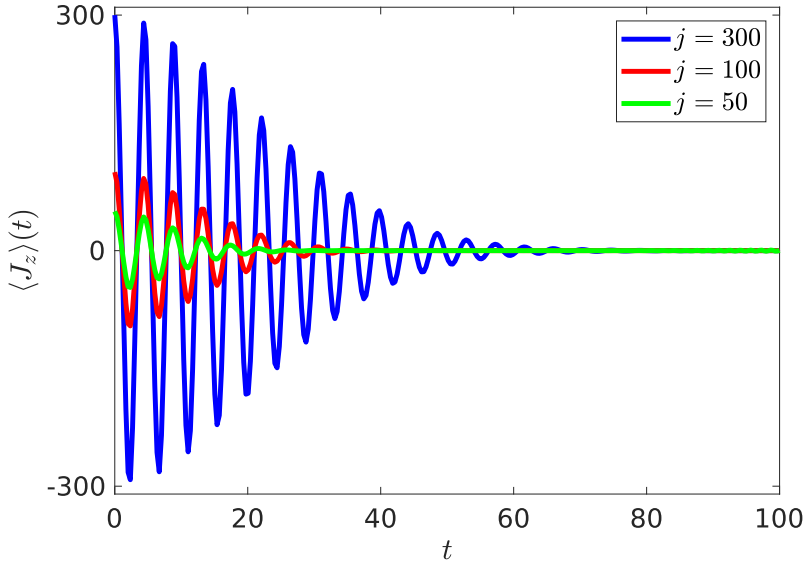

FIGURE 5.5: Time evolution of $\langle J_z \rangle(t)$ for different system sizes: $j = 50, 100, 300$, under a critical quench $h = 0.8$.

In both graphs, Figs. 5.4 and 5.5, we observe that the qualitative behaviour presented in Fig. 5.3 remains, regardless of the size of the system. In addition, the magnetization exhibits a decay with time, indicating the stabilization of the system after the post-quench evolution.

For noncritical quenches, the stabilization occurs around a nonzero value that depends on the system size, while for critical quenches the stabilization occurs around zero.

5.3.3 Long-time average as dynamical order parameter

To conclude the analysis of the spontaneous magnetisation behaviour in our model, we present in Fig. 5.6 the long-term average of this quantity for different values of h. The average was calculated over a long evolution time $t = 500$.

In Fig. 5.6, the behaviour of the dynamical order parameter $\overline{\langle J_z \rangle}$ is clearly displayed. For quenches with $h < h_c^d$, the order parameter remains finite, indicating that the evolution preserves the order of the initial state, i.e., the system remains in a symmetry-broken phase. In contrast, for quenches with $h > h_c^d$, the long-term average tends to zero, in agreement with the results shown in Fig. 5.5.

The disappearance of the magnetization average indicates that the initial order of the state is lost and that the $\mathbb{Z}_2$ symmetry is dynamically restored. This behaviour characterises the appearance of DPT-I in the LMG model, with the critical quench point at $h_c^d = \frac{1}{2}$.

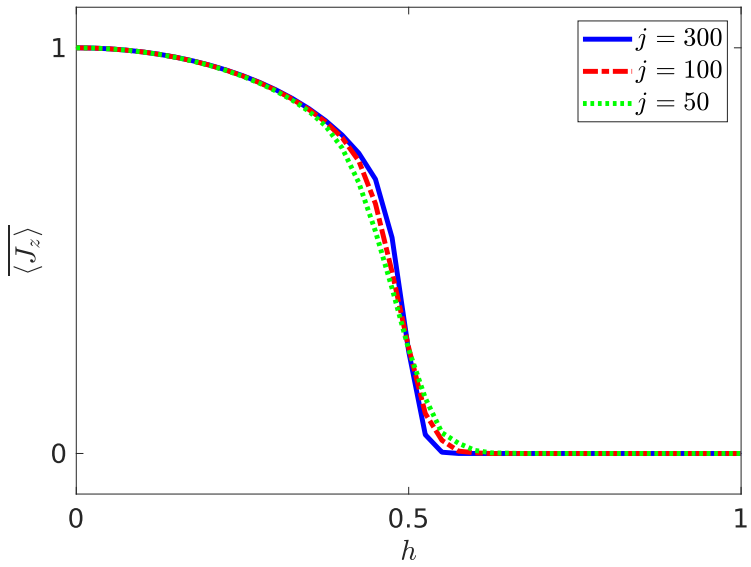

FIGURE 5.6: Dynamical order parameter $\overline{\langle J_z \rangle}$ as a function of the transverse field h, for quenches from $h_0 = 0$ and different system sizes. The parameter vanishes at the critical point, marking the dynamical transition.

These results are not new. Reference [37] analyses the LMG model in this context and obtains results consistent with those presented here. Similarly, Ref. [27] investigates a spin-chain model with long-range interactions, reporting oscillations of the magnetization and the corresponding behaviour of the dynamical order parameter analogous to those obtained in our study.

Chapter 6

Quantum Dynamical Criticality: Entropy and Symmetry Effects in the LMG Model

In this chapter, we present the results obtained and the analyses concerning the quantities introduced in the previous chapters: entropy production (Chapter 3) and asymmetry (Chapter 4), for the LMG model under dynamical quantum phase transitions. These results were published during the PhD in two articles: *Speedup of thermodynamic entropy production via quantum dynamical criticality* [38] and *Asymmetry and dynamical criticality* [39].

In Part I, we present the results of [38]. In Chapter 3, we obtained the average entropy production in out-of-equilibrium systems in terms of relative entropies, in a more general case. In this situation, we see that this relation satisfies the Clausius inequality $\langle \Sigma \rangle \geq 0$. However, as an improvement over the Clausius expression, Eq. (3.119), as well as the expression for the particular case of closed systems (3.127), incorporates the contribution of the system's deviation from equilibrium during its evolution.

Although we already have an expression that takes into account the out-of-equilibrium evolution, it is expressed in terms of relative entropies between the density matrices representing the system. However, relative entropy cannot be considered a metric in the space of these matrices. It is therefore interesting to seek a formulation in terms of a truly metric quantity. This formulation was developed in work [18, 19], where the Bures angle between the thermal states of the system is used as a lower bound for the production of entropies.

In this first part, we examine how this construction was made. We will begin by introducing the concept of the Bures metric and distances, then we will discuss the lower bound for entropy production in terms of this quantity, and finally we apply this bound to the LMG model and present the results obtained in our calculations.

In Part II of this chapter, we present the results of [39]. We investigate DQPT from the perspective of symmetry, focussing on how the symmetry properties of the quantum state evolve under nonequilibrium dynamics. The analysis is based on the asymmetry framework introduced in Chapter 4, which provides quantitative tools to characterise the symmetry-related features of quantum states.

Since DQPTs in the LMG model are associated with the dynamical restoration of parity, this part is devoted to exploring how such symmetry-related phenomena manifest themselves within an asymmetry-based description. In this context, we analyse the behaviour of the asymmetry measure, defined by Eq. (4.41), under sudden quenches and examine their relation to dynamical criticality.

This approach allows us to establish a complementary viewpoint to the thermodynamic analysis presented in Part I, providing further insight into the interplay between dynamical criticality and symmetry in the LMG model.

Part I: Entropy Production

6.1 Entropy production and thermodynamic distances

In the context of classical thermodynamics, a geometric bound for entropy production was derived based on a Riemannian metric in the space of statistical distributions. This bound establishes that the mean entropy production is, at minimum, proportional to the square of the thermodynamic length ℓ between the initial and final states [19]:

$$\langle \Sigma \rangle \gtrsim \ell^2 \tag{6.1}$$

The thermodynamic length ℓ can be understood as a measure of the number of distinguishable states between two probability distributions. This quantity is equivalent to the Wootters statistical distance between two state vectors in Hilbert space, as defined in [16]:

$$\ell(p_a, p_b) = \arccos\left(\int dx \sqrt{p_a(x) p_b(x)}\right) \tag{6.2}$$

Eq (6.2) can be interpreted as a measure of the angle between the probability distributions p_a and p_b in the phase space of states [18].

With the aim of generalising the above result to the case of mixed quantum states, a first lower bound for entropy production in out-of-equilibrium quantum systems was proposed in [18], and this relation was later refined in [19]. These approaches introduce the *Bures angle* $\mathcal{L}$ as a fundamental metric to characterise the deviation from equilibrium in the quantum context.

6.1.1 Bures distance, angle, and metric

The Bures metric is a natural extension of the notion of distance in the space of normalised density matrices. As a Riemannian metric, it allows for the definition of geodesic distances between these matrices within this space, providing a geometric description of the distinction between different mixed states.

We will briefly discuss how these quantities are defined. For more details on the Bures metric and the distances introduced in this subsection, we refer the reader to [17].

Bures Distance and Bures Angle

Given a density matrix ρ_1 acting on a Hilbert space $\mathcal{H}_1$, it is always possible to associate it with a pure state acting on a larger Hilbert space $\mathcal{H}_{12}$. This procedure is known as *state purification* and is of great importance for understanding the geometric distances between density operators.

Formally, we can describe purification as follows:

Given ρ_1 acting on $\mathcal{H}_1$, there exists a pure state ρ_{12} acting on $\mathcal{H}_{12} \equiv \mathcal{H}_1 \otimes \mathcal{H}_2$, such that its partial trace recovers the original state: $\rho_1 = \mathrm{Tr}_2\, \rho_{12}$.

This procedure allows rewriting any density matrix as an operator of the form:

$$\rho = AA^\dagger, \tag{6.3}$$

where A is an operator that belongs to the Hilbert-Schmidt space $\mathcal{HS}$ and acts on the Hilbert space $\mathcal{H}$.

The set of operators $A \in \mathcal{HS}$ that project onto the same operator $\rho \in \mathcal{M}$[1], which constitutes a *fiber*. In other words, a fibre represents the set of all possible purifications of a mixed state ρ in $\mathcal{HS}$. The set of all fibres associated with density matrices defines a *fiber bundle* structure[2].

Purification therefore provides a geometric interpretation for the set of density matrices, establishing a direct relationship between the operators $A \in \mathcal{HS}$ and the mixed states in the subspace of normalised density matrices $\mathcal{M}$. Thus, the space $\mathcal{HS}$ can be viewed as a principal manifold, where $\mathcal{M}$ acts as the base of the associated fibre bundle.

The fibre bundle definition allows us to write distances in this space. Two quantities can be defined in this geometric structure: the Bures distance and the Bures angle.

The **Bures distance** quantifies the separation between two density matrices ρ_1 and ρ_2. It is defined as the shortest geodesic length in the space of normalised density matrices $\mathcal{M}$, i.e. the shortest distance within the Riemannian structure induced by the Bures metric. This distance is obtained by considering the smallest separation between all possible purifications of ρ_1 and ρ_2, which means between the elements of their respective fibres in the purification fibre bundle [17].

It can be expressed as:

$$D_B^2(\rho_1, \rho_2) = \mathrm{Tr}\rho_1 + \mathrm{Tr}\rho_2 - 2\sqrt{\mathcal{F}}(\rho_1, \rho_2), \tag{6.4}$$

[1] $\mathcal{M}$ is the subspace of $\mathcal{HS}$ containing the positive-definite and normalised density matrices ρ.

[2] Here, we consider operators A with $\ker A = 0$, a necessary condition for the different fibres of the bundle to be isomorphic and thus form a fibre bundle [17].

However, the **Bures angle**, which is also a measure of separation between two density matrices, instead of measuring lengths, quantifies the geometric angle between their respective purifications in the Hilbert-Schmidt space. It is defined as:

$$\mathcal{L}(\rho_1, \rho_2) = \arccos \sqrt{\mathcal{F}}(\rho_1, \rho_2). \tag{6.5}$$

Thus, the Bures angle $\mathcal{L}$ can be interpreted as the geodesic angle connecting the fibres corresponding to the density matrices in the purification fibre bundle. Characterises how density matrices differ in terms of their representation in the space of purifications, being a natural generalisation of the concept of angle between states for the case of mixed states [17].

Note that both are defined in terms of the Uhlmann fidelity $\mathcal{F}(\rho_1, \rho_2)$, given by [86]:

$$\mathcal{F}(\rho_1, \rho_2) = \left(\mathrm{Tr} \sqrt{\sqrt{\rho_1}\rho_2\sqrt{\rho_1}} \right)^2, \tag{6.6}$$

which is a measure of similarity between two density matrices. Fidelity is symmetric, non-negative and unitary invariant, equal to 0 for completely orthogonal states, and 1 for $\rho_1 = \rho_2$ [87]. It can be interpreted as the maximum overlap between the purifications of ρ_1 and ρ_2, considering all possible choices of the auxiliary space in the purification. This result is a direct consequence of Uhlmann's theorem [86].

Additionally, fidelity reduces to the projection of one state onto the other in the case of pure density matrices, $\rho_1 = |\psi_1\rangle\langle\psi_1|$ and $\rho_2 = |\psi_2\rangle\langle\psi_2|$:

$$\begin{aligned}
\mathcal{F}(\rho_1, \rho_2) &= \left(\mathrm{Tr} \sqrt{\sqrt{|\psi_1\rangle\langle\psi_1|}\, |\psi_2\rangle\langle\psi_2|\, \sqrt{|\psi_1\rangle\langle\psi_1|}} \right)^2, \\
&= \left(\mathrm{Tr} \sqrt{|\psi_1\rangle\langle\psi_1|\, |\psi_2\rangle\langle\psi_2|\, |\psi_1\rangle\langle\psi_1|} \right)^2, \\
&= \left(\mathrm{Tr}(|\langle\psi_1|\psi_2\rangle|\, |\psi_1\rangle\langle\psi_1|) \right)^2, \\
&= |\langle\psi_1|\psi_2\rangle|^2.
\end{aligned} \tag{6.7}$$

In this case, the Bures angle reduces to $\mathcal{L}(\rho_1, \rho_2) = \arccos \langle\psi_1|\psi_2\rangle$, which is known as the Fubini-Study distance, and quantifies the geometric angle between two pure states, $|\psi_1\rangle$ and $|\psi_2\rangle$, in the Hilbert space $\mathcal{H}$ [17].

Bures Metric

Both methods of quantifying distances in the purification space $\mathcal{HS}$ are considered Riemannian distances, given that they derive from a more fundamental metric in the space of normalised density matrices $\mathcal{M}$, which is Riemannian [17]. The

Bures metric emerges from the construction of the fibre bundle associated with purifications as a measure of the infinitesimal distance between two density operators in the space $\mathcal{M}$.

For conciseness, we will describe how this quantity is obtained. For more details, see Chapter 9 of reference [17].

Consider a tangent vector dA in the purification fibre bundle[3]. This vector, when projected onto the space $\mathcal{M}$, corresponds to a tangent vector $d\rho$. The Bures metric is obtained by minimising the Hilbert-Schmidt norm[4] of the operator dA:

$$d_B^2(\rho + d\rho, \rho) = \min \mathrm{Tr}\big(dA\, dA^\dagger\big). \tag{6.8}$$

The minimisation in (6.8) is performed to find the smallest possible variation $dA \in \mathcal{HS}$ that results in $d\rho \in \mathcal{M}$. The condition for dA to be an orthogonal vector of the fibre is: $dA = GA$, with G being a Hermitian matrix [17].

Here, a brief comment is warranted. Taking into account the variation $dA = X + AU$, where X is the component tangent to the fibre and AU is the parallel component (resulting from a linear transformation of A: AU) to the fibre, we can impose that dA has no vertical component by setting $\langle dA, AU\rangle = 0$. This leads to $\langle dA, AU\rangle = \frac{1}{2}\left[\mathrm{Tr}\big(dA^\dagger AU\big) + \mathrm{Tr}\big((AU)^\dagger dA\big)\right] = 0$. This constraint results in $dA^\dagger A = A^\dagger dA$, which is only satisfied when $dA = GA$, with G being a Hermitian matrix [17].

Since $\rho = AA^\dagger$, we can write:

$$\begin{aligned} d\rho &= d(AA^\dagger) = dA\, A^\dagger + A dA^\dagger, \\ &= GAA^\dagger + AA^\dagger G, \\ &= G\rho + \rho G. \end{aligned} \tag{6.9}$$

The operator G is uniquely determined due to the positivity of ρ [17][5].

Rewriting (6.8) using $dA = GA$, we obtain:

$$\begin{aligned} d_B^2(\rho + d\rho, \rho) &= \mathrm{Tr}\big(GA\, A^\dagger G\big), \\ &= \mathrm{Tr}(G\rho G), \\ &= \frac{1}{2}\mathrm{Tr}(Gd\rho). \end{aligned} \tag{6.10}$$

[3] Displacements along the fibre are not considered as they do not cause variations in the projected state in $\mathcal{M}$.

[4] The Hilbert-Schmidt norm is defined as: $|O|^2 = \mathrm{Tr}\big(OO^\dagger\big)$ [17]

[5] The positivity of ρ implies that Eq. (6.9) can be uniquely solved for G, since we are dealing with a system of linear equations over a space of positive operators [17].

In obtaining (6.10), the minimisation was omitted since the operator G is uniquely determined, making the minimisation operation unnecessary. Additionally, in the final equality, we used $\mathrm{Tr}(Gd\rho) = \mathrm{Tr}(GG\rho) + \mathrm{Tr}(\rho GG) = 2\,\mathrm{Tr}(G\rho G)$.

Thus, we have obtained the Bures metric, which defines the metric in the space of normalised density matrices $\mathcal{M}$, providing a quantification of the infinitesimal distance between density operators. It arises from the geometric structure of the purification space and serves as a foundation for defining the Bures distances and angles previously discussed.

6.1.2 Entropy production bound and Bures Angle

In Section 3.3.7, we derived an exact expression for the average entropy production in an open system that evolves arbitrarily far from equilibrium, driven by an external parameter. Eq. (3.119) provides this quantification for the general scenario, where a system starts from an arbitrary state, ρ_i, evolves out of equilibrium, and reaches ρ_f. This allows entropy production to be determined in terms of three contributions: two associated with the "distances" between the initial and final states and their corresponding equilibrium states with the reservoir, and a third term due to the nonequilibrium dynamics to which the system was subjected.

By restricting the system to be closed and initially in thermal equilibrium with the reservoir, $\rho_i = \rho_0^{th}$, we obtain Eq. (3.127). In this case, only the final state and its equivalent thermal state contribute to entropy production. The resulting equation is as follows:

$$\langle \Sigma \rangle = S(\rho_\tau \parallel \rho_\tau^{th}) \geq 0. \tag{6.11}$$

Note that this equation expresses the entropy production in terms of relative entropy. Although relative entropy can be interpreted as a measure of distinction between states, it cannot be considered a strict metric, as it is neither symmetric nor satisfies the triangle inequality [19].

To establish a relationship between entropy production and a measure of geometric distance, it was proposed to rewrite Eq. (6.11) as an inequality in terms of the Bures angle, thus generalising the known result for classical entropy production in terms of Wootters distance. In two studies [18, 19], a lower bound for entropy production in terms of this quantity was proposed. The next section presents the bound developed in these works.

Considering a unitarily invariant norm $D(\rho_1, \rho_2)$, we can write a lower bound for relative entropy [88]:

$$S(\rho_1 \parallel \rho_2) \geq s\left(\frac{D(\rho_1, \rho_2)}{D_\perp}\right) \tag{6.12}$$

where $D_\perp$ is a scaling factor, given by the maximum possible value for $D(\rho_1, \rho_2)$, ensuring that the argument of s remains within the interval $[0, 1]$.

Taking into account the Bures angle (6.5) and the fact that the Bures metric is unitarily invariant, we can rewrite (6.12) as:

$$S(\rho_1 \parallel \rho_2) \geq s\left(\frac{2}{\pi}\mathcal{L}(\rho_1, \rho_2)\right) \tag{6.13}$$

since the maximum possible value for the Bures angle, reached when $\rho_1 \perp \rho_2$, is $D_\perp = \frac{\pi}{2}$ [19].

The function $s(x)$, for $0 \leq x < 1$, is obtained by minimising the relative entropy[6] [88]:

$$\begin{aligned} s(x) &= \min_{x \leq r < 1} S((r - x, 1 - r + x) \parallel (r, 1 - r)), \\ s(x) &= \min_{x \leq r < 1} \left[(r - x) \ln \frac{r - x}{r} + (1 - r + x) \ln \frac{1 - r + x}{1 - r}\right]. \end{aligned} \tag{6.14}$$

Expanding $s(x)$ around $x = 0$, we obtain:

$$s(x) = 2x^2 + \frac{4}{9}x^4 + \frac{32}{135}x^6 + O(x^8), \tag{6.15}$$

For small values of x, the first term of (6.15) provides a good approximation, carrying an error that is negligible compared to the exact value obtained using (6.14). Thus, the first term can be considered a lower bound for (6.14). However, for larger values of x, additional terms in the expansion are necessary, and for x close to 1, the function approaches its upper bound, given by $-\ln(1 - x)$. When $x = 1$, the function $s(x)$ diverges to infinity [88]. We can then write:

$$2x^2 \leq s(x) < -\ln(1 - x). \tag{6.16}$$

A graphical representation of the exact function and its lower and upper bounds is shown in Fig. 6.1.

Thus, considering the average entropy production written in the form (3.103), we can express it in terms of the Bures angle through a lower bound:

$$\langle \Sigma \rangle \geq s\left(\frac{2}{\pi}\mathcal{L}(\rho_\tau, \rho_\tau^{th})\right) \geq \frac{8}{\pi^2}\mathcal{L}^2(\rho_\tau, \rho_\tau^{th}) \tag{6.17}$$

This relation was obtained by Sebastian Deffner and Eric Lutz in two studies. In the first, Ref. [18], the authors presented the lower bound $\frac{8}{\pi^2}\mathcal{L}^2(\rho_\tau, \rho_\tau^{th})$ for entropy

[6] The relative entropy between two distributions is given by: $S(p \parallel q) = \sum_i p_i \ln \frac{p_i}{q_i}$.

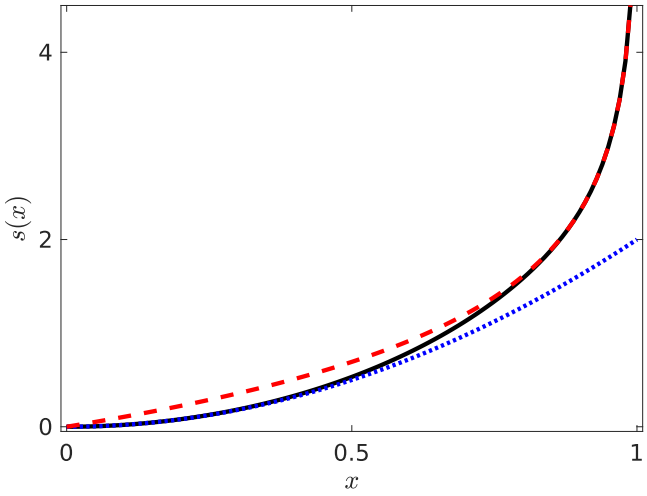

FIGURE 6.1: The red solid line shows the exact function $s(x)$, while the black dashed and blue dashed-dotted lines show the upper and lower bounds on $s(x)$, respectively. The variables on the axes are dimensionless.

production in a closed system subjected to an arbitrarily far-from-equilibrium evolution, which is associated with the first term of expansion (6.15). Shortly afterward, they refined the result, presenting the first inequality of Eq. (6.17) [19]. This provided a more precise lower bound for the average entropy production, valid over the entire range of the function argument, which corresponds to the interval $0 \leq \mathcal{L}(\rho_\tau, \rho_\tau^{th}) < \frac{\pi}{2}$.

The more general bound is particularly useful for our work, as we will deal with a system that is undergoing a DQPT, traversing a critical regime. Under this condition, the function argument reaches the upper limit of $s\left(\frac{2}{\pi}\mathcal{L}\right)$, with $\mathcal{L} \to \frac{\pi}{2}$, making it impractical to use only the first term of the expansion (6.15).

The results presented here provide a way to quantify the irreversibility of a process the system undergoes in terms of a purely geometric measure between the system's final states, given the conditions discussed in Section 3.3.8. We will use this result as a tool to quantify the average entropy production LMG model, subjected to a DQPT.

6.2 Entropy production in LMG model

We will calculate the lower bound of the average entropy production in the system using Eq. (3.127),in terms of the Bures angle, as derived in section 6.1.2. Since this relation is based on the Bures angle between the system's evolved state and the final thermal state, with evolution governed by a post-quench Hamiltonian, analysing the behaviour of the Bures angle for quenches that do or do not cross the

dynamical critical point may provide some insight into the behaviour of this lower bound. Let us proceed with this analysis.

Bures Angle

To compute the Bures angle, we consider that the system is initially in thermal equilibrium with the reservoir, i.e. the initial state of the system is:

$$\rho_0 = \frac{e^{-\beta H_0}}{Z_0}, \tag{6.18}$$

where $Z_0 = \mathrm{Tr}(e^{-\beta H_0})$ is the partition function.

Thus, the evolved state at each time instant is given by $\rho_t = U\rho_0^{th}U^\dagger$, with $U = e^{-iHt}$. Additionally, the thermal state at time t is given by $\rho_t^{th} = \frac{e^{-\beta H}}{Z_t}$. For calculations, we consider $\beta = 1$.

The evolution of the Bures angle over time for two different quenches is presented in Fig. 6.2. We observe that the behaviour of the Bures angle qualitatively resembles the behaviour exhibited by the Loschmidt echo (Fig. 5.1). The distinction between behaviours in different dynamical phases of the model is clear. Note that there is a decrease in the amplitude of the oscillation in both cases; however, in the restored symmetry phase, for $h > h_c^d$, the decay occurs more rapidly compared to the decay in the broken symmetry phase.

From a state distance perspective, the more rapid attenuation indicates that ρ_t moves away more quickly from the corresponding thermal state when a DQPT occurs. This behaviour suggests a significant role for dynamical criticality in the evolution of the system. We will further explore this in the context of entropy production.

The same calculation was performed to analyse the effects of increasing temperature β^{-1} on the Bures angle dynamics. In Fig. 6.3, we present the behaviour of the Bures angle for three different values of the inverse temperature: $\beta = 1$, $\beta = 0.1$, and $\beta = 0.01$.

We observe that increasing temperature (decreasing β) leads to stabilisation of the Bures angle. This indicates that thermal fluctuations begin to dominate the dynamics, suppressing the quantum contributions associated with dynamical criticality in the model. Thus, analysis at low temperatures becomes essential to capture the purely quantum effects of the dynamical transition. Therefore, for the calculation of the lower bound of entropy production, we adopt $\beta = 1$.

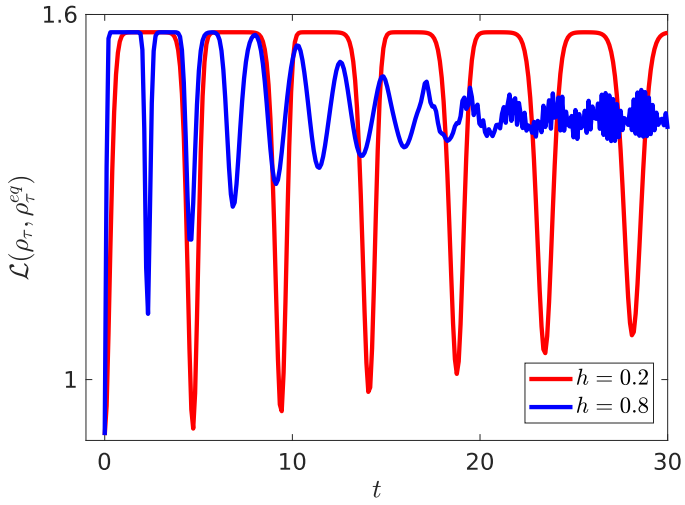

FIGURE 6.2: The graph shows the dynamics of the Bures angle for two distinct quenches, $h = 0.2$ and 0.8, for $j = 300$.

Entropy production $\langle\Sigma\rangle$

Based on the results presented in the previous section, we can now compute the lower bound for the entropy production in the system, given by Eq. (3.127). The validity conditions for our calculation are:

(i) Approximately low temperature.

(ii) Initial state in thermal equilibrium with the reservoir $\rho_0 = \rho_0^{th}$.

(iii) Closed system.

Condition (i) ensures that the effects associated with criticality, as shown in the results, are of purely quantum origin, as discussed in section 6.2. Conditions (ii) and (iii) were adopted in deriving Eq. (3.127).

Using the same considerations applied in the computation of the Bures angle, we calculate the lower bound of the average entropy production, given by (6.17), with the function $s(\frac{2}{\pi}\mathcal{L})$ defined by the expression (6.14). The dynamical behaviour of $s(\frac{2}{\pi}\mathcal{L})$ is presented in Fig. 6.4.

Once again, the difference in behaviour in the dynamical evolution of the lower bound becomes evident. This quantity tends to stabilize more quickly for evolutions governed by post-quench Hamiltonians with values of $h > h_c^d$. In other words, when the system undergoes a DQPT, the lower bound of entropy production stabilizes more rapidly, in contrast to the behaviour of this quantity for cases where the system does not exhibit a DQPT.

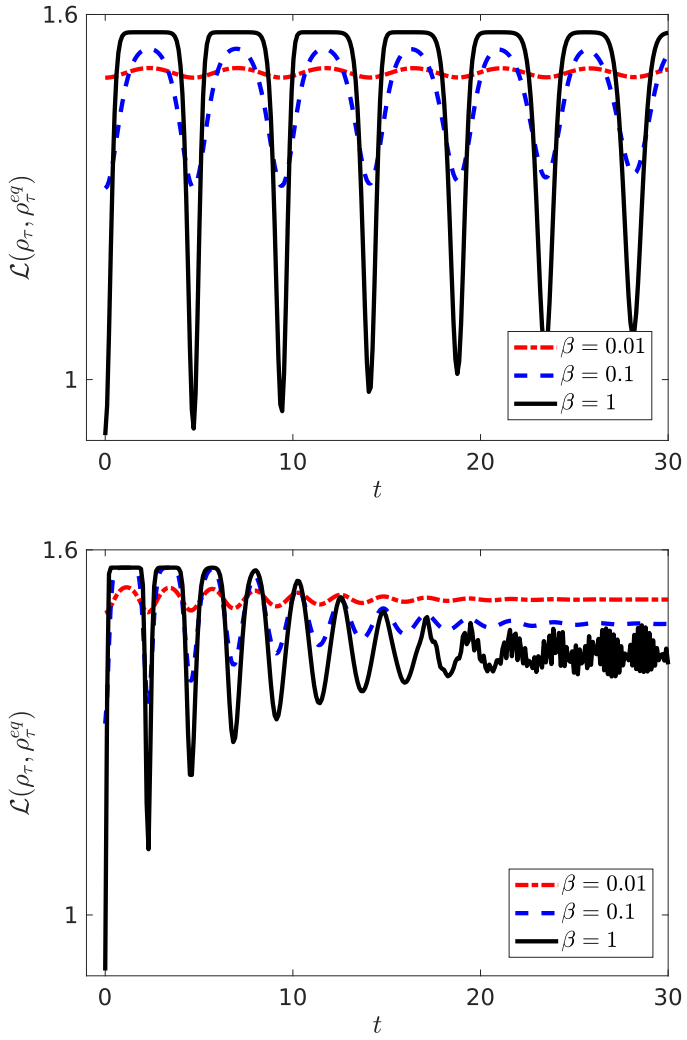

FIGURE 6.3: The top panel shows the effect of temperature when the quench does not cross the critical point ($h = 0.2$), while the bottom panel shows the same behavior when crossing the critical point ($h = 0.8$). In both plots, we consider $j = 300$.

The behaviour of $s(\frac{2}{\pi}\mathcal{L})$ suggests that the system reaches equilibrium more quickly when the quench crosses the critical point of the model. It is worth emphasising here that the entire development carried out is independent of the characteristics of the model since the derivation of the lower bound is formulated in terms of the Bures angle. The relationship with DQPT is established through the behaviour of this quantity under a critical or non-critical quench.

It is also possible to analyse the result in terms of the distance between states from the perspective of entropy production. The initially higher entropy production, combined with the faster attenuation of $s(\frac{2}{\pi}\mathcal{L})$ in the case of a DQPT, indicates

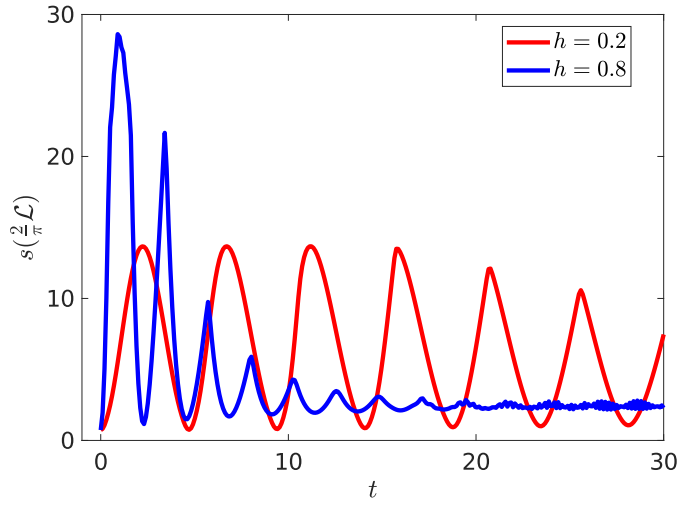

FIGURE 6.4: Lower bound on the entropy production. The blue line shows the case $h = 0.8$ (crossing the critical point), while the red line represents the case $h = 0.2$ (not crossing the critical point). We considered $j = 300$ and $\beta = 1$.

that the system moves away from equilibrium more rapidly when subjected to criticality. In terms of distance, we can say that ρ_t moves further away from the corresponding thermal state more quickly when a DQPT occurs. This behaviour directly reflects a higher rate of entropy production compared to non-critical evolution.

Time Average Entropy Production $\overline{\langle\Sigma\rangle}$

Finally, we investigate the production of entropy based on time to analyse the behaviour of the production of entropy in terms of the quench parameter h. The time average is given by:

$$\overline{\langle\Sigma\rangle} = \lim_{T\to\infty} \frac{1}{T} \int_0^T \mathrm{d}t \langle\Sigma\rangle. \tag{6.19}$$

In figure 6.5, we present $\overline{\langle\Sigma\rangle}$ as a function of the quench parameter h. Here, we vary the system size, adopting $j = 100, 200$ and 500.

It is evident that the production of time-averaged entropy exhibits a clear distinction in behaviour when the quench parameter crosses the critical value, represented by the dashed vertical line in Fig. 6.5. There is a stabilization of this quantity for quench values $h > h_c^d$, indicating an acceleration in entropy production in such situations, with entropy reaching a constant average value more quickly, as also shown in Fig. 6.4.

Furthermore, it is clear that $\overline{\langle\Sigma\rangle}$ as a function of h can be used as an indicator of the occurrence of DQPT. In addition to displaying different behaviours for each dynamical phase, it exhibits a peak around the system's critical point, a behaviour

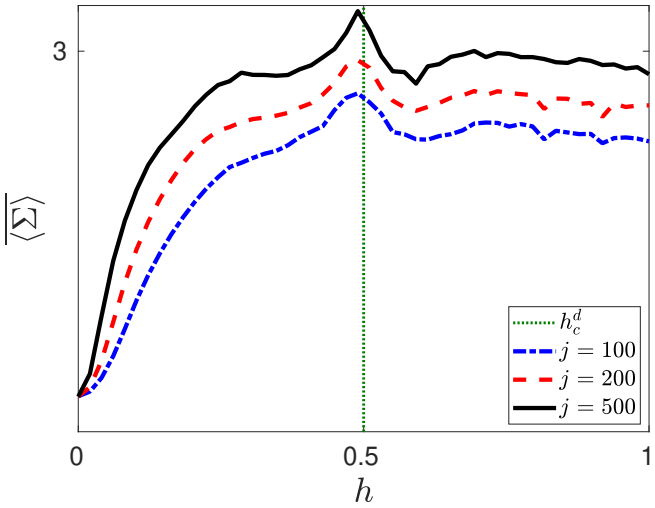

FIGURE 6.5: The plot illustrates the h-dependent behaviour of the time-averaged entropy production for three spin chain sizes: $j = 100$ (blue dashed-dotted line), $j = 200$ (red dashed line), and $j = 500$ (black solid line). We considered $T = 10^3$ to perform the calculation of the time average presented in the graph.

that becomes even more pronounced as the system size increases, suggesting that in the thermodynamic limit, the transition becomes more well-defined.

We emphasise once again that the entire construction presented, from the definitions of the Loschmidt echo and Bures angle to the derivation of entropy production and its lower bounds in terms of geometric quantities, was carried out independently of the model. Therefore, our results are not specific to the adopted model, but are valid for any system that exhibits similar dynamical behaviour, given that the origin of the behavioural differences in the calculated quantities lies in the criticality observed in the Loschmidt echo and the rate function.

In this first part, we show that DQPT in the LMG model can be identified from the perspective of irreversibility. By analysing entropy production and its geometric lower bounds, we demonstrated that the emergence of dynamical criticality is accompanied by an accelerated departure from equilibrium and by a rapid stabilization of quantities associated with irreversible dynamics. Within this framework, the DQPT manifests itself as a qualitative change in the dynamical regime of the system, reflecting a reorganisation of evolution in the space of quantum states.

In the second part of this chapter, we turn to a complementary viewpoint and analyse the same dynamical phenomenon from the perspective of symmetry. The focus is placed on how the symmetry properties of the quantum state evolve under critical dynamics. This change of perspective provides a different geometric view of DQPT, based on the symmetry properties of the evolving quantum state.

Part II: Asymmetry Measure

As discussed in Chapter 5, the dynamical restoration of the symmetry of $\mathbb{Z}_2$ parity constitutes a central hallmark of DQPTs in the LMG model. Motivated by this, the question arises as to how this symmetry restoration can be captured within a quantitative framework based on asymmetry. However, the asymmetry measure employed in this work, $F_L(\rho)$ (see Section 4.3), is defined with respect to generators of continuous symmetry groups, namely Lie groups, and is not directly applicable to discrete symmetries such as $\mathbb{Z}_2$.

For the model adopted in our work, presented in Chapter 5, the parity symmetry is associated with the operator J_x, as discussed in Section 4.1.3. Therefore, to overcome the limitation related to the definition of $F_L(\rho)$, we exploit the fact that the parity operation can be interpreted as a discrete rotation by an angle π around the x axis, corresponding to a finite element of the rotation subgroup $U(1) \subset SU(2)$ generated by J_x.

This motivates our choice of the collective spin operators J_x, J_y, and J_z, which generate the rotation group $SU(2)$, as symmetry generators. By analysing the asymmetry associated with rotations around these three Cartesian axes, we are able to analyse how the dynamical restoration of parity manifests itself within a framework based on continuous generators, while simultaneously comparing its behaviour with that of other rotational directions that are not directly related to the underlying symmetry $\mathbb{Z}_2$.

6.3 Behavior of Asymmetry Measures $F_L(\rho)$

6.3.1 Time evolution of asymmetry measure

Our investigation is focused on the dynamical behaviour of the asymmetry measure of the system and on the possibility of identifying a clear signature of a dynamical quantum phase transition through this quantity. With this goal in mind, we begin our analysis by considering the asymmetry measure $F_L(\rho)$, defined in Eq. (4.41):

$$F_L(\rho) = \|[\rho, L]\|_1. \tag{6.20}$$

The dynamical evolution analysed here takes place after a sudden quench in the transverse field h, in the same spirit as in Part I of this chapter, and may correspond to a critical or noncritical quench in the LMG model.

We begin by considering quenches from $h_0 = 0$ to two values of the transverse field: $h = 0.2$, which does not cross the dynamical critical point, and $h = 0.8$, which

does cross it. Moreover, unlike the results presented in Part I, where a single value of the anisotropy parameter was considered, here we initially analyse two different anisotropy values, $\gamma = 0.2$ (strongly anisotropic) and $\gamma = 0.8$ (nearly isotropic), to investigate the influence of this parameter on the dynamical behaviour of the system. Throughout this analysis, we set $J = 1$ and work in the fully symmetric subspace with fixed $j = 100$.

The dynamics of $F_L(\rho)$ for $L = J_x$, J_y, and J_z are shown in Fig. 6.6. As a first feature, we can clearly observe that, for critical quenches (blue dotted lines), regardless of the anisotropy parameter or the generator L, the oscillatory dynamics of $F_L(\rho)$ tends to be damped more rapidly, leading to an earlier approach to a plateau-like regime. This indicates that the critical nature of the quench accelerates the stabilization of the model's dynamics. However, for noncritical quenches (red solid lines), the oscillations persist longer times, and the growth of asymmetry is slower. In this case, one may interpret that the dynamics remains closer to the initial symmetry structure of the state.

We can interpret this behaviour as a first indication that the asymmetry monotone provides relevant information about the critical behaviour of the model. Nevertheless, it is worth examining in more detail the specific features displayed in the plots shown in Fig. 6.6.

For $L = J_y$ (Figs. 6.6 (b) and (e)) and $L = J_z$ (Figs. 6.6 (c) and (f)), the qualitative behaviour is very similar. In both and for both $\gamma = 0.2$ and $\gamma = 0.8$, the critical quench (blue dotted lines) produces a rapid initial increase of $F_L(\rho)$ followed by a stabilisation at long times. This behaviour parallels the pattern observed for the entropy production bound (Fig. 6.4) in the same model: dynamical criticality initially accelerates the dynamical response, while subsequently driving the quantity toward rapid saturation.

In the context of asymmetries, the rapid increase indicates that the post-quench dynamics quickly generates coherence across different eigenspaces of J_y or J_z, thereby increasing the degree of asymmetry of the state in these bases, whereas the subsequent stabilization suggests that the generation of additional asymmetry becomes progressively less effective after the transient regime.

The generator $L = J_x$ (Figs. 6.6 (a) and (d)) is particularly relevant for our analysis for two reasons. First, the Hamiltonian (5.11) contains the linear term $-hJ_x$, which directly links the transverse field to this generator. Second, and more importantly, the parity symmetry, whose unitary operator is given by Eq. (4.23), is expressed in terms of J_x, thus directly associating this generator with the symmetry that is dynamically restored in the model at the occurrence of a DQPT.

Interestingly, a distinct behaviour emerges for $L = J_x$ compared to the other

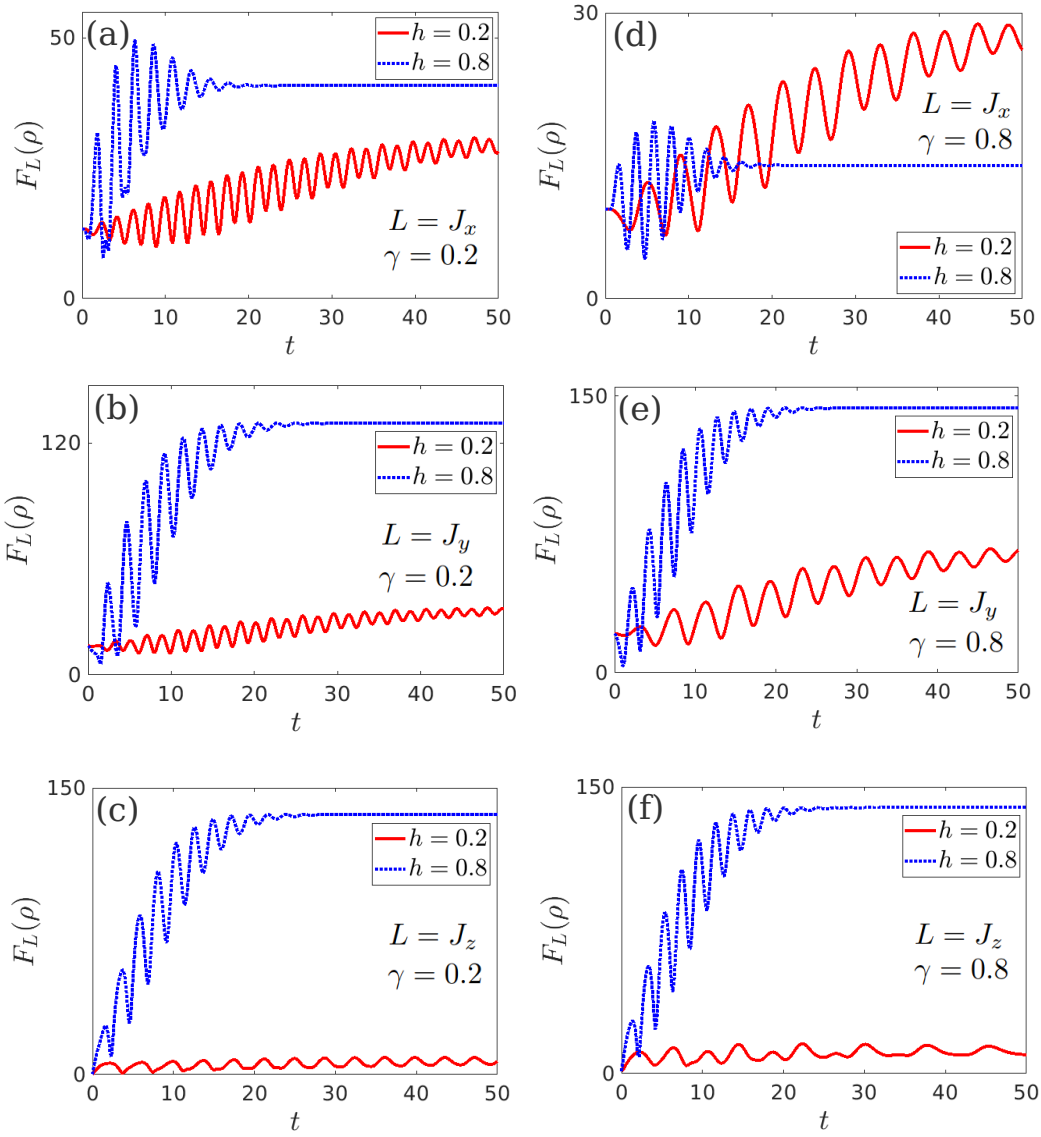

FIGURE 6.6: Time evolution of the asymmetry measure $F_L(\rho)$, for the generators $L = J_x$, J_y, and J_z. The first, second, and third rows correspond to the generators J_x, J_y, and J_z, respectively. Results are shown for two values of the anisotropy parameter: $\gamma = 0.2$ (left column) and $\gamma = 0.8$ (right column). In each panel, two quench protocols are considered: a noncritical quench to $h = 0.2 < h_c^d$ (red solid line) and a critical quench to $h = 0.8 > h_c^d$ (blue dashed line).

generators considered. Two aspects should be highlighted. First, the dependence on the anisotropy parameter becomes more pronounced: while for $\gamma = 0.2$ the behaviour under a critical quench closely resembles that observed for J_y and J_z, for $\gamma = 0.8$ the critical quench leads to lower asymmetry values when compared to the noncritical quench. Second, independently of the value of γ, the quantitative separation between the two quench protocols is less pronounced for J_x than for the other generators.

This is consistent with the fact that, as $\gamma \to 1$ (isotropic limit), the model approaches a regime in which the Hamiltonian becomes closer to a J_x-symmetric structure. Thus, increasing the weight of the term J_x, via h, does not necessarily enhance coherence in the eigenbasis J_x. In this near-isotropic regime, the post-quench evolution tends to preserve the symmetry sector associated with J_x more efficiently, limiting the generation of J_x-asymmetry even when the quench is critical.

Therefore, from Fig. 6.6, we can conclude that $F_L(\rho)$ is sensitive to whether the quench crosses the dynamical critical region, showing a systematic tendency toward faster damping and earlier stabilization in the critical case. In addition, the response depends on the choice of generator: while J_y and J_z display a more uniform enhancement of asymmetry under critical quenches, the J_x case reveals a stronger interplay with anisotropy and with the symmetry structure associated with parity.

The temporal behaviour of $F_L(\rho)$ therefore provides interesting insights into the relationship between asymmetry and the model parameters, indicating that both h and γ play an important role in characterising the behaviour of this quantity. Based on this and on the fact that the asymmetry monotone exhibits a strongly oscillatory behaviour, we now turn our attention to the long-term average of $F_L(\rho)$, which will be presented in the following section.

6.3.2 Time-Averaged Asymmetry and Critical Regions

The time evolution of the asymmetry measures discussed in the previous sections is characterised by strong oscillations, which are typical of unitary dynamics following a sudden quench. In order to extract more information about the long-time behaviour of the system and its relation to dynamical criticality, in the same spirit adopted for the lower bound of entropy production in Part I, we now consider time-averaged quantities. In this section, we analyse the time-averaged asymmetry measure

$$\overline{F_L(\rho)} = \frac{1}{T}\int_0^T dt\, F_L(\rho), \tag{6.21}$$

investigate how it behaves as a function of the quench strength h and the anisotropy parameter γ.

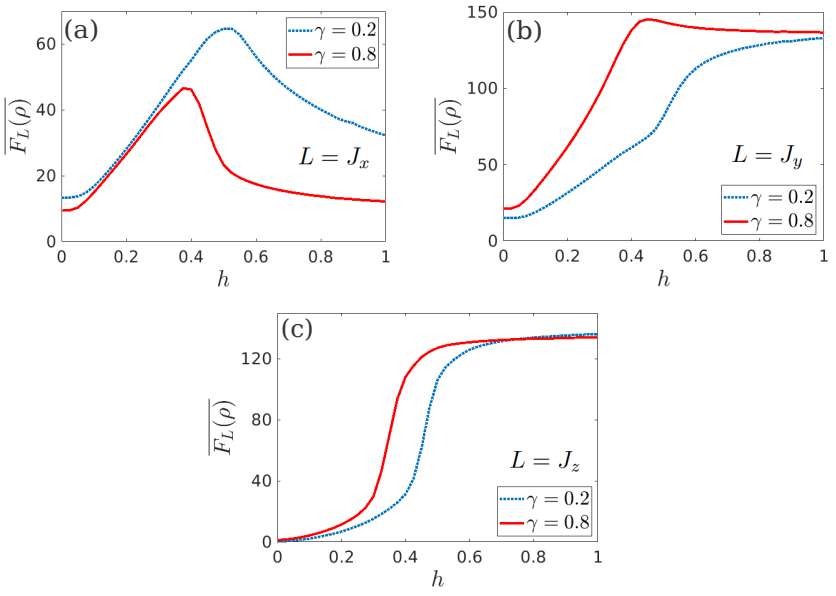

FIGURE 6.7: Time-averaged asymmetry measure $\overline{F_L(\rho)}$ as a function of the transverse field h for the three generators (a) $L = J_x$, (b) $L = J_y$, and (c) $L = J_z$. Results are shown for two values of the anisotropy parameter: $\gamma = 0.2$ (blue dotted lines) and $\gamma = 0.8$ (red solid lines). The abrupt changes in the behaviour of $\overline{F_L(\rho)}$ signal the dynamical critical region of the model, whose location shifts with increasing anisotropy.

Time-averaged of asymmetry measure for fixed anisotropy

We begin by considering the results for the two values of γ discussed in the previous section, $\gamma = 0.2$ and $\gamma = 0.8$. In Fig. 6.7, we present the behaviour of $\overline{F_L(\rho)}$ as a function of the transverse field h for the generators of the $SU(2)$ group.

We first emphasise that, independent of the choice of L, $\overline{F_L(\rho)}$ exhibits a clear change in behaviour as the transverse field h increases. This change takes place within a well-defined region of h and manifests itself as an abrupt growth of $\overline{F_L(\rho)}$, followed by a saturation or a reduction at larger values of h, depending on the generator considered. From this behaviour, we can infer that the time-averaged asymmetry is able to capture relevant information about the dynamical reorganisation of the system as a function of the quench strength. In addition, γ induces a clear shift in the location of this change in behaviour, reinforcing the idea that anisotropy directly influences the dynamical properties of the model and the occurrence of DQPTs. Beyond this global behaviour, it is instructive to analyse the results shown in Fig. 6.7 separately for each generator.

Starting with the case $L = J_z$, Fig. 6.7 (c), we observe that $\overline{F_{J_z}(\rho)}$ remains small for weak quenches, independent of the value of the anisotropy parameter γ. In this regime, the system dynamics remains close to the initial structure of the state, and the coherence between different eigenstates of J_z increases only very weakly. However, as h increases, a pronounced growth of the time-averaged asymmetry

occurs, indicating that the dynamics begins to explore more extensively the state space associated with different values of m_z.

This increase occurs around $h \approx 0.5$ for $\gamma = 0.2$ (blue dotted line) and $h \approx 0.4$ for $\gamma = 0.8$ (red solid line). After this initial growth, the curve tends to stabilize, suggesting that the state reaches a regime in which the asymmetry structure with respect to J_z is essentially established and the subsequent evolution does not significantly modify this content. This behaviour is consistent with the interpretation that critical dynamics promotes a rapid spreading of the state in Hilbert space, followed by a stabilization associated with the post-critical regime.

Another interesting aspect of the result for $L = J_z$ is that, up to a horizontal shift, the curves corresponding to the two values of the anisotropy parameter exhibit very similar numerical values. This feature is observed exclusively for this generator.

Taking into account $L = J_y$, Fig. 6.7 (b), we observe a behaviour similar to that found in the previous case. The time-averaged asymmetry exhibits a pronounced growth within a well-defined region of the transverse field h, coinciding with the region identified for J_z. For $\gamma = 0.2$ (blue dotted line), $\overline{F_{J_y}(\rho)}$ increases rapidly as the system approaches the critical region and tends to stabilize for $h \gtrsim 0.5$. In contrast, for $\gamma = 0.8$ (red solid line), the quantity reaches a maximum around $h \approx 0.4$ and shows a slight decay as h increases further. This decay suggests a gradual reduction of the relevant coherence in the basis J_y in the nearly isotropic regime, as the dynamics becomes increasingly dominated by the transverse-field term.

Finally, $\overline{F_{J_x}(\rho)}$, shown in Fig. 6.7 (a), exhibits distinct features and therefore deserves a separate analysis. Unlike the previous cases, the smallest values of the asymmetry averaged over time occur for $\gamma = 0.8$, that is, when the system approaches the isotropic limit. This difference can be understood from the structure of the model Hamiltonian, which explicitly contains the linear term $-hJ_x$. As γ increases, the Hamiltonian becomes closer to a form that is symmetric with respect to J_x, so that increasing the transverse field effectively reduces the asymmetry along this direction, leading to the decay observed in the figure.

Despite these quantitative differences, the position of the inflexion point of $\overline{F_{J_x}(\rho)}$ occurs around the same critical region identified for the other generators. This indicates that, although the asymmetry associated with J_x does not provide the most pronounced signal in terms of magnitude, it still responds sensitively to the change in the dynamical regime associated with the DQPT.

In general, the results presented in Fig. 6.7 show that the time-averaged asymmetry clearly captures the presence of a region in which the characteristics of the

system undergo qualitative changes, its location depends on the anisotropy parameter γ. The displacement of this region as γ increased leads us to infer that anisotropy plays an active role in determining the dynamical critical point of the model. In view of this, we next analyze the same quantity over the interval $\gamma \in (0, 1)$, which spans the regime from the maximally anisotropic model ($\gamma = 0$) to the isotropic limit ($\gamma = 1$).

Time-averaged of asymmetry measure in the (h, γ) Plane

The Fig. 6.8 shows the time-averaged asymmetry $\overline{F_L(\rho)}$ as a function of the transverse field h and the anisotropy parameter γ, both varied within the interval $(0, 1)$, for the three generators $L = J_x$ (Fig. 6.8 (a)), J_y (Fig. 6.8 (b)), and J_z (Fig. 6.8 (c)). This plot allows us to visualise how the asymmetry responds to simultaneous variations of the quench strength and of the intrinsic anisotropy of the model.

As a key characteristic, shared by all generators, is the presence of a well-defined region in the (h, γ) plane where $\overline{F_L(\rho)}$ undergoes a pronounced change in behaviour. This region forms a line separating regimes of low- and high time-averaged asymmetry in cases (b) and (c), while giving rise to a pronounced peak in the observed quantity in case (a). In addition, we observe a clear shift in the values of h at which these behaviours occur as γ is varied. This shift confirms that the location of the dynamical critical region is not fixed but is controlled by the anisotropy parameter. Moreover, as $\gamma \to 1$, this line gradually weakens and eventually disappears, consistently with the absence of DQPTs in the isotropic limit.

Once again, the behaviours for $L = J_y$ and $L = J_z$ are very similar. The corresponding surfaces display features consistent with those discussed in the previous section, with a clear increase of $\overline{F_L(\rho)}$ along a well-defined line in the (h, γ) plane. Once the critical region is crossed, the asymmetry remains finite over a broad range of parameters, indicating that the post-quench dynamics promotes a persistent redistribution of coherence among different eigenstates of these operators.

Again, as in the previous section, Fig. 6.8 (a) shows that the behaviour associated with $L = J_x$ is qualitatively different from that observed for the other generators. Although a well-defined critical region is still present, the surface of $\overline{F_{J_x}(\rho)}$ is characterised by a pronounced peak followed by a reduction, rather than by a monotonic increase. This behaviour is associated with the special role played by J_x in the LMG model, since this operator is directly involved both in the transverse-field term of the Hamiltonian and in the definition of the $\mathbb{Z}_2$ parity symmetry.

In this way, the results shown in Fig. 6.8 confirm that the time-averaged asymmetry provides a description of how both the anisotropy parameter and the quench

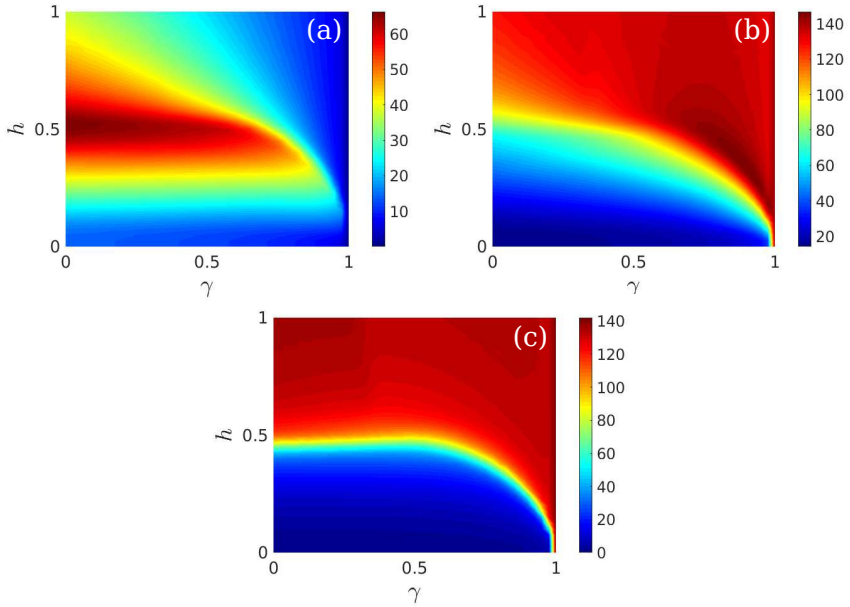

FIGURE 6.8: Time-averaged asymmetry measure $\overline{F_L(\rho)}$ in the (h, γ) plane for the three generators of the $SU(2)$ group: (a) $L = J_x$, (b) $L = J_y$, and (c) $L = J_z$. The surfaces reveal well-defined regions where $\overline{F_L(\rho)}$ undergoes abrupt changes, signaling the occurrence of dynamical quantum phase transitions.

strength affect the dynamical behaviour of the model. In particular, the distinct behaviour observed for $L = J_x$ already indicates that the dynamical critical region is accompanied by qualitative changes in the way the system redistributes coherence among states related by the $\mathbb{Z}_2$ parity symmetry in the J_x eigenbasis.

We note that, at the dynamical critical point, the post-quench dynamics undergoes a qualitative reorganisation, which is reflected in how coherence is dynamically generated and redistributed. Critical quenches improve the generation of coherence between different m_x eigenspaces, leading to an increased spreading of the state in the J_x eigenbasis when compared to noncritical dynamics. This increased coherence production naturally explains the pronounced peak observed in $\overline{F_{J_x}(\rho)}$. For higher values of the transverse field, the $-hJ_x$ term increasingly dominates the dynamics, progressively suppressing the generation of additional coherence in this basis and leading to the observed reduction of $\overline{F_{J_x}(\rho)}$.

At the same time, these results raise a central question: to what extent can the features identified by $\overline{F_L(\rho)}$ be directly associated with the appearance of a DQPT? In other words, can we claim that the asymmetry monotone acts as a marker of dynamical phase transitions in the LMG model, in the same sense as established indicators of dynamical criticality? To address this point, in the next section we directly compare the asymmetry results with two independent diagnostics of DQPTs: the time-averaged entropy production and the dynamical order parameter.

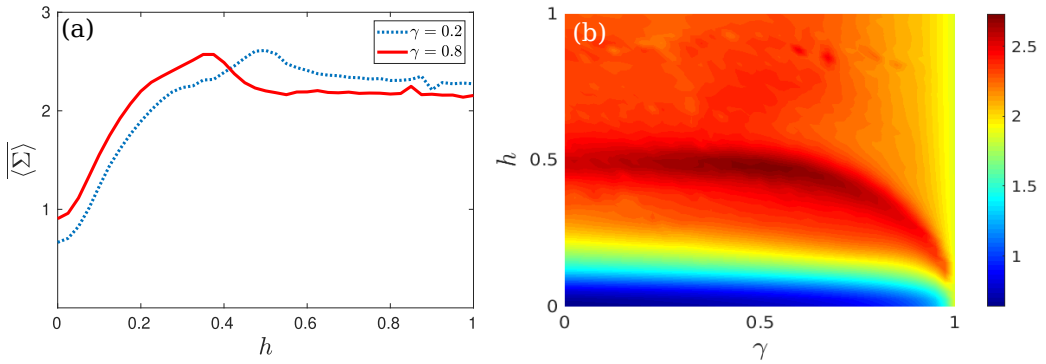

FIGURE 6.9: Time-averaged entropy production $\overline{\langle\Sigma\rangle}$ in the LMG model for $j = 100$. Panel (a) shows $\overline{\langle\Sigma\rangle}$ as a function of the transverse field h for two representative values of the anisotropy parameter: $\gamma = 0.2$ (blue dotted line) and $\gamma = 0.8$ (red solid line). Panel (b) displays the same quantity in the (h, γ) plane, with both parameters varied within the interval $(0, 1)$.

6.4 Connecting Asymmetry with DQPT

In Part I and in Ref. [38], we show that the time-averaged entropy production $\overline{\langle\Sigma\rangle}$ exhibits a pronounced peak at the dynamical critical point of the LMG model. We associated this peak directly with the occurrence of a DQPT, characterising the emergence of dynamical criticality through a quantity linked to irreversibility.

Motivated by the results obtained for $\overline{F_L(\rho)}$, presented in Figs. 6.7 and 6.8, we now compute the lower bound on the entropy production, following the same procedure adopted in Part I, for the same parameter values used in the analysis of the asymmetry measure.

In Fig. 6.9 we present the results for the time-averaged entropy production $\overline{\langle\Sigma\rangle}$, computed for $j = 100$. In Fig. 6.9 (a), we consider two values of the anisotropy parameter, $\gamma = 0.2$ (blue dotted line) and $\gamma = 0.8$ (red solid line), in direct analogy with the analysis performed in the first part of Section 6.3.2. Figure 6.9 (b), in turn, shows the behaviour of the same quantity when the anisotropy parameter is continuously varied within the interval $\gamma \in (0, 1)$.

Interestingly, the characteristic features highlighted in the discussion of the results shown in Fig. 6.7 also appear in the behaviour of the time-averaged entropy production $\overline{\langle\Sigma\rangle}$. As can be seen in Fig. 6.9 (a), a change in the anisotropy parameter leads to a clear shift in the position of the peak of $\overline{\langle\Sigma\rangle}$, which closely mirrors the shift observed in the points where the behaviour of the functions $\overline{F_L(\rho)}$ changes, for all generators L considered in the previous section.

Similarly, when we consider the full range of values of the anisotropy parameter, the behaviour of entropy production shown in Fig. 6.9 (b) exhibits a strong resemblance to that obtained for $\overline{F_L(\rho)}$ under the same conditions, as displayed in

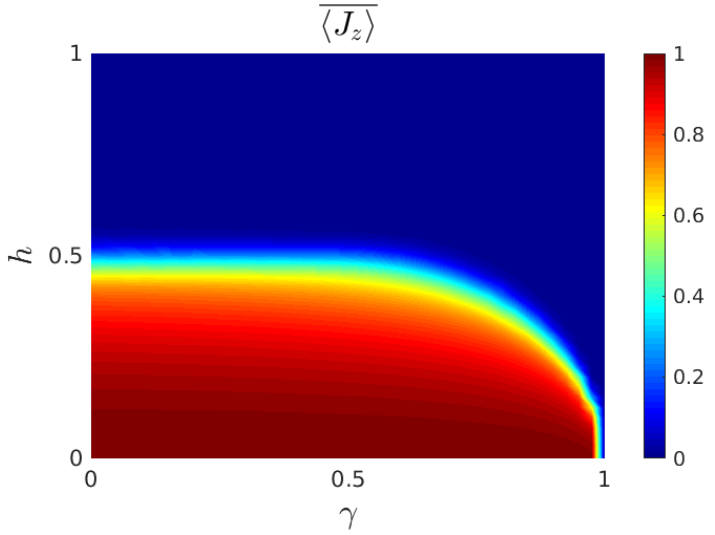

FIGURE 6.10: Dynamic order parameter $\overline{\langle J_z \rangle}$ in terms of quench parameter h and anisotropy parameter γ. We use the same range that in Figs. 6.8 and 6.9: $\gamma \in (0, 1)$ and $h \in (0, 1)$ and fixed $j = 100$.

Fig. 6.8. This similarity is particularly evident for the case $L = J_x$, which presents a pronounced peak in the same parameter region where the lower bound of the entropy production also attains its maximum.

To complement our analysis, we present the dynamical order parameter of the model, which is defined in terms of the collective magnetization along the z direction, $\langle J_z \rangle$, and is computed for the same set of parameters used in the results of this section. As shown in Fig. 6.10, a clear dynamical transition line emerges in the (h, γ) plane, along which the order parameter rapidly decays to zero. In particular, this line coincides with regions where significant changes occur in the behaviour of both time-averaged entropy production $\overline{\langle \Sigma \rangle}$ and time-averaged asymmetry $\overline{F_L(\rho)}$, confirming the direct connection between these behaviours and the occurrence of a DQPT.

It is worth highlighting the close correspondence between the behaviour of the dynamical order parameter and that of $\overline{F_{J_z}(\rho)}$, which indicates that the asymmetry along the z direction is particularly sensitive to the redistribution of populations that governs the decay of the order parameter, and therefore acts as a highly effective marker of the DQPT.

In contrast, the asymmetry associated with J_x plays a conceptually distinct role. Although it does not produce the largest numerical signal, its behaviour is directly connected to the dynamical restoration of the $\mathbb{Z}_2$ parity symmetry that characterises the DQPT in the LMG model.

Across the dynamical critical point, the system transitions from a regime in which the dynamics remains confined to a symmetry-broken region of phase space

to one in which the evolution dynamically explores parity-related configurations in a balanced way. This does not imply that the instantaneous quantum state becomes parity symmetric; rather parity is restored at the level of long-time, time-averaged quantities.

As a consequence, the dynamical critical region is accompanied by a pronounced improvement in coherence between different m_x eigenspaces, leading to a maximal spread of the state in the J_x eigenbasis. This mechanism provides a natural explanation for the sharp peak observed in $\overline{F_{J_x}(\rho)}$, which occurs in the same parameter region where the dynamical order parameter vanishes and where the entropy production is maximised.

For higher values of the transverse field, the $-hJ_x$ term increasingly dominates the dynamics, progressively reducing the generation of additional coherence in the J_x basis and leading to the subsequent reduction of $\overline{F_{J_x}(\rho)}$. In this sense, the behaviour of $\overline{F_{J_x}(\rho)}$ identifies a critical dynamical regime and can be associated with the dynamical restoration of parity and with qualitative changes in the coherence properties of the system.

Therefore, the results presented here allow us to state that asymmetry measures provide reliable indicators of DQPTs in the LMG model, exhibiting distinct behaviours across different dynamical phases. In particular, the asymmetry associated with the operator J_x displays especially interesting features due to its close similarity to an established indicator of criticality, the production of entropy on time average, and its direct connection to the symmetry that is dynamically restored when a DQPT occurs in the LMG model.

Chapter 7

Conclusion

In this work, we investigate how dynamical criticality manifests itself in the LMG model through two independent physical quantities: entropy production and the asymmetry of the quantum state. These quantities provide distinct perspectives on nonequilibrium behaviour. While entropy production is associated with the degree of irreversibility of the dynamical process, asymmetry allows one to characterise how the symmetry properties of the system evolve and are dynamically restored throughout the temporal evolution. The central objective was to evaluate the ability of these quantities to identify and characterise the occurrence of DQPTs in the model.

We began in Chapter 2 by introducing phase transitions, starting from classical transitions, moving through quantum phase transitions, and finally arriving at DQPTs. The fundamental concept of non-analyticity in thermodynamic functions, which characterises classical phase transitions, finds a direct analogue in the Loschmidt echo and in the associated rate function throughout the temporal evolution of the system. In the same spirit, we also introduced a dynamical order parameter, establishing a parallel with the Landau order parameter used in classical phase transitions. Within this framework, the DQPT phenomenon was defined, with dynamical criticality characterised both by the appearance of critical times at which the rate function becomes non-analytic and by the vanishing of the dynamical order parameter.

Chapter 3 was dedicated to developing the concept of entropy production. We highlighted its role as an indicator of irreversibility in out-of-equilibrium thermodynamic processes. We began with a review of the entropy concept in both the classical formulation and quantum information theory. Then, we addressed how entropy production can be extended to irreversible processes in quantum regimes, even when the system is strongly coupled to finite reservoirs or simply evolves unitarily, as in the case of a closed system.

Subsequently, in Chapter 4, the focus shifted to asymmetry as a tool to characterise symmetry properties in quantum states. The fundamental concepts of group

theory and symmetry transformations were introduced, providing the basis for the definition and interpretation of asymmetry in quantum systems. At the end of the chapter, the asymmetry monotone adopted in this work was defined and discussed, which is then employed in the analysis of the results presented in the following chapters.

In Chapter 5, we devoted ourselves to presenting the LMG model. We emphasise its symmetry properties and the occurrence of dynamical quantum phase transitions in this model. The characterisation of the DQPT was presented both through the non-analyticities of the rate function, associated with the zeros of the Loschmidt echo, and through the behaviour of the dynamical order parameter, which vanishes for evolutions resulting from critical quenches.

Finally, the numerical results are presented in Chapter 6, which is divided into two parts encompassing the results of two works published during the development of this thesis [38, 39].

In Part I, we analyse the role of dynamical criticality in the behaviour of entropy production. We observed that, when crossing the dynamical critical point, there is a significant acceleration in the entropy production rate, indicating that the system departs from its thermal reference state more rapidly. This behaviour highlights the direct connection between DQPTs and the irreversibility of the dynamical process.

Moreover, we showed that this effect is independent of specific details of the model. Even for finite systems, the presence of non-analyticities in the rate function, and thus of dynamical phase transitions, is sufficient to distinguish different dynamical regimes through entropy production. We also investigated the role of temperature and verified that, in high-temperature regimes, the effects associated with criticality are progressively suppressed, making the identification of DQPTs increasingly difficult.

The relation between entropy production and the Bures angle, which introduces a geometric character into the analysis, allowed us to quantify the "distance" between the evolved state and the thermal state associated with the post-quench Hamiltonian. In this context, quenches that cross the dynamical critical point lead to a more pronounced growth of the lower bound of the average entropy production, reflecting a faster departure in the space of states. These results establish entropy production as a clear indicator of the occurrence of DQPTs associated with the dynamical reorganisation of the system and the increase of irreversibility in the process.

Part II is devoted to the characterisation of the evolution of asymmetry in the system during the post-quench dynamics. The fact that the LMG model displays a dynamical restoration of the discrete $\mathbb{Z}_2$ symmetry when subjected to critical

quenches motivated the investigation of how the asymmetry of the quantum state behaves along the temporal evolution and how this quantity responds to the appearance of a DQPT.

The first results obtained, concerning the asymmetry monotone based on the ℓ_1 norm, $F_L(\rho)$, indicated that the behaviour of this quantity is directly influenced by the regime in which the dynamics takes place, that is, whether the quench crosses the critical region of the model or not. Clear distinctions were observed between the dynamics of the asymmetry monotone for evolutions associated with critical and noncritical quenches, independently of the choice of the symmetry generator considered. These initial results highlighted the sensitivity of asymmetry to dynamical criticality and motivated a more refined analysis of this quantity.

Analysis of the time average of $F_L(\rho)$ confirmed this sensitivity and also revealed a direct relation between the position of the dynamical critical point and the degree of anisotropy of the model. From the results, one observes a well-defined change in the behaviour of the time-averaged asymmetry around the critical value of the transverse magnetic field, again for all generators analysed. In addition, variations in the anisotropy parameter were shown to be responsible for shifts in the critical point h_c^d, indicating that anisotropy plays an important role in determining the critical region of the model.

The central result here consists of the analysis of the monotone time-averaged asymmetry in the (h, γ) plane, considering the interval $(0, 1)$ for both the transverse field and the anisotropy parameter. In this representation, a critical line dependent on γ clearly emerges, separating dynamically distinct regions. This result allows us to conclude that the asymmetry measure is indeed sensitive to the occurrence of DQPTs in the LMG model and that anisotropy directly influences the position of the dynamical critical point.

In order to reinforce this interpretation, we analysed, under the same conditions, both the time average of the lower bound of entropy production and the dynamical order parameter of the model. Both quantities are recognised as independent diagnostics of DQPTs and exhibit critical regions that coincide with those identified through the asymmetry measures, including the shift of the critical point as a function of anisotropy. This agreement ensures that asymmetry measures can be regarded consistent and reliable markers of DQPTs in the model under study.

Due to its relationship with symmetry $\mathbb{Z}_2$, the analysis of the asymmetry associated with the generator J_x becomes particularly relevant. Unlike the other generators considered, J_x plays a special role in the LMG model, since it is directly related both to the transverse-field term of the Hamiltonian and to the definition of the $\mathbb{Z}_2$ parity symmetry, which is dynamically restored during the occurrence of a DQPT.

As a consequence, the asymmetry with respect to J_x exhibits a qualitatively distinct behaviour, directly reflecting the structural changes associated with the restoration of symmetry. Although $F_{J_x}(\rho)$ does not directly quantify parity, its evolution is sensitive to dynamical reorganisation that occurs at the critical dynamical point.

In particular, when the system undergoes a DQPT, the long-time dynamics allows for a more balanced exploration of configurations related to the parity transformation, which is accompanied by a transient enhancement of coherence between different m_x eigenspaces. This mechanism provides a natural explanation for the pronounced peak observed in the asymmetry on time average $\overline{F_{J_x}(\rho)}$, whose behaviour closely resembles that found for the production of entropy.

In this sense, the asymmetry associated with J_x captures qualitative changes in the dynamical regime of the system that are consistently associated with the dynamical restoration of the symmetry $\mathbb{Z}_2$.

In summary, we conclude that the two independent quantities adopted to analyse DQPTs in the LMG model, the lower bound of entropy production and the asymmetry measure, despite probing different physical aspects, are both effective indicators of dynamical criticality. They consistently display different behaviours across different dynamical phases of the model. Moreover, the anisotropy parameter plays a fundamental role in determining the value of the critical quench.

As a perspective for future work, it would be particularly interesting to extend this analysis to alternative asymmetry measures, especially those based on information-theoretic quantities such as Holevo-type measures, which have been connected to thermodynamic entropy [89]. Such extensions could further deepen the connection between symmetry, information, and thermodynamics in nonequilibrium quantum systems, and potentially reveal new universal aspects of dynamical quantum phase transitions.

Bibliography

[1] M. Heyl, "Dynamical quantum phase transitions: a review", Rep. Prog. Phys. **81**, 054001 (2018).

[2] M. Heyl, "Dynamical quantum phase transitions: a brief survey", EPL **125**, 26001 (2019).

[3] M. Heyl, A. Polkovnikov, and S. Kehrein, "Dynamical quantum phase transitions in the transverse-field ising model", Physical Review Letters **110**, 135704 (2013).

[4] B. Sciolla and G. Biroli, "Quantum quench, dynamical transition, and off-equilibrium quantum criticality", Physical Review B **88**, 201110(R) (2013).

[5] P. Smacchia, M. Knap, E. Demler, and A. Silva, "Exploring dynamical phase transitions and prethermalization with quantum noise of excitations", Physical Review B **91**, 205136 (2015).

[6] J. C. Halimeh, V. Zauner-Stauber, I. P. McCulloch, I. de Vega, U. Schollwöck, and M. Kastner, "Prethermalization and persistent order in the absence of a thermal phase transition", Physical Review B **95**, 024302 (2017).

[7] J. A. Muniz, D. Barberena, R. J. Lewis-Swan, D. J. Young, J. R. K. Cline, A. M. Rey, and J. K. Thompson, "Exploring dynamical phase transitions with cold atoms in an optical cavity", Nature **580**, 602 (2020).

[8] P. Jurcevic, H. Shen, P. Hauke, C. Maier, T. Brydges, C. Hempel, B. P. Lanyon, M. Heyl, R. Blatt, and C. F. Roos, "Direct observation of dynamical quantum phase transitions in an interacting many-body system", Physical Review Letters **119**, 080501 (2017).

[9] N. Fläschner, D. Vogel, M. Tarnowski, B. S. Rem, D.-S. Lühmann, M. Heyl, J. C. Budich, L. Mathey, K. Sengstock, and C. Weitenberg, "Observation of dynamical vortices after quenches in a system with topology", Nature Physics **14**, 265–268 (2018).

[10] B. O. Goes, G. T. Landi, E. Solano, M. Sanz, and L. C. Céleri, "Wehrl entropy production rate across a dynamical quantum phase transition", Physical Review Research **2**, 033419 (2020).

[11] M. Esposito, K. Lindenberg, and C. V. den Broeck, "Entropy production as correlation between system and reservoir", New Journal of Physics **12**, 013013 (2010).

[12] J. P. Santos, L. C. Céleri, F. Brito, G. T. Landi, and M. Paternostro, "Spin-phase-space-entropy production", Physical Review A **97**, 052123 (2018).

[13] B. Leggio, A. Napoli, A. Messina, and H.-P. Breuer, "Entropy production and information fluctuations along quantum trajectories", Physical Review A **88**, 042111 (2013).

[14] C. Cafaro and P. M. Alsing, "Information geometry aspects of minimum entropy production paths from quantum mechanical evolutions", Physical Review E **101**, 022110 (2020).

[15] G. Ruppeiner, "Riemannian geometry in thermodynamic fluctuation theory", Reviews of Modern Physics **67**, 605 (1995).

[16] W. K. Wootters, "Statistical distance and hilbert space", Physical Review D **23**, 357 (1981).

[17] I. Bengtsson and K. Życzkowski, *Geometry of quantum states* (Cambridge University Press, Cambridge, 2006).

[18] S. Deffner and E. Lutz, "Generalized clausius inequality for equilibrium quantum processes", Physical Review Letters **105**, 170402 (2010).

[19] S. Deffner and E. Lutz, "Thermodynamic length for far-from-equilibrium quantum systems", Physical Review E **87**, 022143 (2013).

[20] I. Marvian and R. W. Spekkens, "Extending noether's theorem by quantifying the asymmetry of quantum states", Nature Communications **5**, 3821 (2014).

[21] G. Gour and R. W. Spekkens, "The resource theory of quantum reference frames: manipulations and monotones", New Journal of Physics **10**, 033023 (2008).

[22] G. Gour, I. Marvian, and R. W. Spekkens, "Measuring the quality of a quantum reference frame: the relative entropy of frameness", Physical Review A **80**, 012307 (2009).

[23] I. Marvian and R. W. Spekkens, "The theory of manipulations of pure state asymmetry: i. basic tools, equivalence classes and single copy transformations", New Journal of Physics **15**, 033001 (2013).

[24] I. Marvian and R. W. Spekkens, "Modes of asymmetry: the application of harmonic analysis to symmetric quantum dynamics and quantum reference frames", Phys. Rev. A **90**, 062110 (2014).

[25] I. Marvian, R. W. Spekkens, and P. Zanardi, "Quantum speed limits, coherence and asymmetry", Physical Review A **93**, 052331 (2016).

[26] I. Marvian and R. W. Spekkens, "How to quantify coherence: distinguishing speakable and unspeakable notions", Physical Review A **94**, 052324 (2016).

[27] B. Žunkovič, M. Heyl, M. Knap, and A. Silva, "Dynamical quantum phase transitions in spin chains with long-range interactions: merging different concepts of equilibrium criticality", Physical Review Letters **120**, 130601 (2018).

[28] A. Sehrawat, C. Srivastava, and U. Sen, "Dynamical phase transitions in the fully connected quantum ising model: time period and critical time", Phys. Rev. B **104**, 085105 (2021).

[29] M. Heyl, "Dynamical quantum phase transitions in systems with broken-symmetry phases", Physical Review Letters **113**, 205701 (2014).

[30] S. Vajna and B. Dóra, "Topological classification of dynamical phase transitions", Physical Review B **91**, 155127 (2015).

[31] U. Bhattacharya, S. Bandyopadhyay, and A. Dutta, "Mixed state dynamical quantum phase transitions", Physical Review B **96**, 180303 (2017).

[32] H. Lipkin and N. M. an d A. Glick, "Validity of many-body aproximation methods foa a solvable model: (i). exact solutions and perturbation theory", Nucl. Phys. **62**, 188 (1965).

[33] N. Meshkov, A. Glick, and H. Lipkin, "Validity of many-body approximation methods for a solvable model: (ii). linearization procedures", Nucl. Phys. **62**, 199 (1965).

[34] A. Glick, H. Lipkin, and N. Meshkov, "Validity of many-body approximation methods for a solvable model: (iii). diagram summations", Nucl. Phys. **62**, 211 (1965).

[35] P. Ribeiro, J. Vidal, and R. Mosseri, "Exact spectrum of the lipkin-meshkov-glick model in the thermodynamic limit and finite-size corrections", Physical Review E **78**, 021106 (2008).

[36] O. Castaños, R. López-Peãa, J. G. Hirsch, and E. López-Moreno, "Classical and quantum phase transitions in the lipkin-meshkov-glick model", Physical Review B **74**, 104118 (2006).

[37] P. H. S. Bento, A. del Campo, and L. C. Céleri, "Krylov complexity and dynamical phase transition in the quenched lipkin-meshkov-glick model", Physical Review B **109**, 224304 (2024).

[38] A. B. Nascimento and L. C. Céleri, "Speedup of thermodynamic entropy production via quantum dynamical criticality", Phys. Rev. A **110**, 052223 (2024).

[39] A. B. Nascimento and L. C. Céleri, "Asymmetry and dynamical criticality", ArXiv, 2602.00900 (2026).

[40] S. R. A. Salinas, *Introdução à física estatística*, 2nd ed. (Editora EdUSP, 2005).

[41] H. B. Callen, *Thermodynamics and an introduction to thermostatics*, 2nd (John Wiley & Sons, Inc., 1985).

[42] K. Huang, *Introduction to statistical physics*, 2nd (CRC Press, 2009).

[43] L. D. Landau and E. M. Lifshitz, *Statistical physics, vol. 5, part 1*, 3nd (Pergamon Press, 1980).

[44] L. A. da S. Mól, "Transições de fase em modelos magnéticos bi-dimensionais com interações dipolares", Thesis (Phd) (Universidade Federal de Minas Gerais, Belo Horizonte, Brasil, 2009).

[45] K. Huang, *Statistical mechanics*, 2nd ed. (John Wiley and Sons, 2000).

[46] S. Sachdev, *Quantum phase transitions* (Cambridge University Press, 2011).

[47] T. D. Lee and C. N. Yang, "Statistical theory of equations of state and phase transitions. ii. lattice gas and ising model", Physical Review **87**, 410–419 (1952).

[48] R. G. M. Rodrigues, "Sobre o uso dos zeros da função de partição no estudo de transições de fase", Thesis (Universidade Federal de Minas Gerais, Departamento de Física, Brasil, 2017).

[49] J. S. M. Fonseca, "Zeros de fisher e aspectos críticos do modelo de ising dipolar", Dissertação de Mestrado, orientador: Prof. Dr. Nelson Augusto Alves, Thesis (Universidade de São Paulo, Faculdade de Filosofia, Ciências e Letras de Ribeirão Preto, Ribeirão Preto, Brasil, 2011).

[50] M. Vojta, "Quantum phase transitions", Reports on Progress in Physics **66**, 2069–2110 (2003).

[51] S. L. Sondhi, S. M. Girvin, J. P. Carini, and D. Shahar, "Continuous quantum phase transitions", Reviews of Modern Physics **69**, 315 (1997).

[52] M. P. L. Heyl, "Nonequilibrium phenomena in many-body quantum systems: dynamics, thermodynamics, and dynamical phase transitions", Thesis (Ludwig-Maximilians-Universität München, München, 2012).

[53] A. Lerose, B. Žunkovič, J. Marino, A. Gambassi, and A. Silva, "Impact of nonequilibrium fluctuations on prethermal dynamical phase transitions in long-range interacting spin chains", Phys. Rev. B **99**, 045128 (2019).

[54] G. T. Landi and M. Paternostro, "Irreversible entropy production: from classical to quantum", Rev. Mod. Phys. **93**, 035008 (2021).

[55] R. Clausius, "Über verschiedene für die anwendung bequeme formen der hauptgleichungen der mechanischen wärmetheorie", Annalen der Physik **201**, 353 (1865).

[56] C. E. Shannon, "A mathematical theory of communication", The Bell System Technical Journal **27**, 379–423 (1948).

[57] M. M. Wilde, *From classical to quantum shannon theory*, arXiv:1106.1445 [quant-ph] (July 2019).

[58] M. Nielsen and I. Chuang, *Quantum computation and quantum information*, Cambridge Series on Information and the Natural Sciences (Cambridge University Press, 2000).

[59] S. Heusler, W. Dür, M. S. Ubben, and A. Hartmann, "Aspects of entropy in classical and in quantum physics", Journal of Physics A: Mathematical and Theoretical **55**, 404006 (2022).

[60] S. Deffner and E. Lutz, "Equilibrium entropy production for open quantum systems", Physical Review Letters **107**, 140404 (2011).

[61] R. Alicki, "The quantum open system as a model of the heat engine", Journal of Physics A: Mathematical and General **12**, L103 (1979).

[62] H. Steinacker, *Lie groups and lie algebras for physicists: lecture notes*, Unpublished lecture notes, Lecture notes, University of Vienna, Spring 2023, Vienna, Austria, 2023.

[63] I. M. Mashhad, "Symmetry, asymmetry and quantum information", Thesis (University of Waterloo, Canada, 2012).

[64] S. D. Bartlett, T. Rudolph, and R. W. Spekkens, "Reference frames, superselection rules, and quantum information", Reviews of Modern Physics **79**, 555–609 (2007).

[65] L. R. da Silva Mendes, "Page-wootters mechanism: the role of coherence and finite sized clocks", Thesis (Instituto de Física de São Carlos, Universidade de São Paulo, São Carlos, 2021).

[66] J. M. F. Bassalo and M. S. D. Cattani, *Teoria de grupos para físicos*, Publicação IF - E-BOOK 1661/2011. Disponível em: https://www.if.usp.br, Acesso em: 23 out. 2025 (Instituto de Física, Universidade de São Paulo, São Paulo, Brasil, 2011).

[67] A. Das and S. Okubo, *Lie groups and lie algebras for physicists* (World Scientific Publishing Company, 2014).

[68] M. Piani, M. Cianciaruso, T. R. Bromley, C. Napoli, N. Johnston, and G. Adesso, "Robustness of asymmetry and coherence of quantum states", Physical Review A **93**, 042107 (2016).

[69] K. Yamaguchi and H. Tajima, "Beyond i.i.d. in the resource theory of asymmetry: an information-spectrum approach for quantum fisher information", Physical Review Letters **131**, 200203 (2023).

[70] J. Sakurai and J. Napolitano, *Modern quantum mechanics* (Cambridge University Press, 2017).

[71] P. Ribeiro, J. Vidal, and R. Mosseri, "Thermodynamical limit of the lipkin-meshkov-glick model", Physical Review Letters **99**, 050402 (2007).

[72] Z. Mzaouali, R. Puebla, J. Goold, M. E. Baz, and S. Campbell, "Work statistics and symmetry breaking in an excited-state quantum phase transition", Physical Review E **103**, 032145 (2021).

[73] Á. L. Corps and A. Relaño, "Dynamical and excited-state quantum phase transitions in collective systems", Physical Review B **106**, 024311 (2022).

[74] D. Kudo and H. Tajima, "Fisher information matrix as a resource measure in the resource theory of asymmetry with general connected-lie-group symmetry", Phys. Rev. A **107**, 062418 (2023).

[75] M. Skotiniotis and G. Gour, "Alignment of reference frames and an operational interpretation for the G-asymmetry", New Journal of Physics **14**, 073022 (2012).

[76] B. Toloui, G. Gour, and B. C. Sanders, "Constructing monotones for quantum phase references in totally dephasing channels", Physical Review A **84**, 022322 (2011).

[77] J. A. Vaccaro, F. Anselmi, H. M. Wiseman, and K. Jacobs, "Tradeoff between extractable mechanical work, accessible entanglement, and ability to act as a reference system, under arbitrary superselection rules", Physical Review A **77**, 032114 (2008).

[78] M. Dahleh, M. A. Dahleh, and G. Verghese, *Lectures on dynamic systems and control*, https://ocw.mit.edu/, Lecture notes, 2000.

[79] S. Dusuel and J. Vidal, "Continuous unitary transformations and finite-size scaling exponents in the lipkin-meshkov-glick model", Physical Review B **71**, 224420 (2005).

[80] S. Campbell, "Criticality revealed through quench dynamics in the lipkin-meshkov-glick model", Physical Review B **94**, 184403 (2016).

[81] B. Sciolla and G. Biroli, "Dynamical transitions and quantum quenches in mean-field models", Journal of Statistical Mechanics: Theory and Experiment **2011**, P11003 (2011).

[82] M. Heyl, F. Pollmann, and B. Dóra, "Detecting equilibrium and dynamical quantum phase transitions in ising chains via out-of-time-ordered correlators", Physical Review Letters **121**, 016801 (2018).

[83] B. Žunkovič, A. Silva, and M. Fabrizio, "Dynamical phase transitions and loschmidt echo in the infinite-range xy model", Philosophical Transactions of the Royal Society A **374**, 20150160 (2016).

[84] N. Defenu, A. Lerose, and S. Pappalardi, "Out-of-equilibrium dynamics of quantum many-body systems with long-range interactions", arXiv (2023).

[85] M. Heyl and J. C. Budich, "Dynamical topological quantum phase transitions for mixed states", Physical Review B **96**, 180304 (2017).

[86] A. Uhlmann, "The "transition probability" in the state space of a $*$-algebra", Reports on Mathematical Physics **9**, 273 (1976).

[87] Y.-C. Liang, Y.-H. Yeh, P. E. M. F. Mendonça, R. Y. Teh, M. D. Reid, and P. D. Drummond, "Quantum fidelity measures for mixed states", Reports on Progress in Physics **82**, 076001 (2019).

[88] K. M. R. Audenaert and J. Eisert, "Continuity bounds on the quantum relative entropy", Journal of Mathematical Physics **46**, 102104 (2005).

[89] G. F. Ferrari, Ł. Rudnicki, and L. C. Céleri, "Quantum thermodynamics as a gauge theory", Physical Review A **111**, 052209 (2025).